Development of a V5-tag-directed nanobody and its implementation as an intracellular biosensor of GPCR signaling

Kevin Matte

A dissertation submitted in partial fulfillment.

of the requirements for the degree of

Master of Science

Department of Biochemistry, Microbiology and Immunology

Faculty of Medicine

University of Ottawa

Abstracts

G protein-coupled receptors (GPCRs) are an important class of drug targets due to their involvement in various signaling pathways. GPCRs transmit signals from the extracellular environment to the interior of cells, regulating numerous physiological processes. GPCRs are known to engage in protein-protein interactions (PPIs) with a variety of intracellular signaling molecules, including G proteins, β-arrestins, and other adaptor proteins. Understanding these interactions is crucial for unraveling the complex signaling networks mediated by GPCRs and developing targeted therapeutics. Assay development plays a pivotal role in studying GPCR PPIs, allowing researchers to investigate the binding partners, functional consequences, and dynamics of these interactions. Developing assays for GPCR PPIs requires careful consideration of the specific interaction being studied, the choice of experimental techniques, and the suitability for the desired readout. These assays provide valuable insights into the molecular mechanisms underlying GPCR signaling and can aid in the discovery and development of novel therapeutic strategies targeting GPCR-associated diseases. Considering that PPIs are highly dynamic processes, cellular assays are often essential for their study because they closely mimic the biological complexities of cellular environments. The present thesis aimed to develop an *in cellulo* proteomic assay by developing an intracellular nanobody targeting the V5-peptide tag. Functionalizing this anti-V5 intrabody would allow it to be implemented in various cell-based assays with any protein carrying the V5-tag. Therefore, the NbV5:V5 tag system presents itself as a versatile tool for live-cell imaging and a befitting adaptation to existing cellular assays dedicated to probing PPIs. The NbV5:V5 tag system has been applied to interrogate G protein-coupled receptor

signaling with the ultimate goal of performing cellular studies of a broader and systematic nature using the genome-wide V5-tagged ORF library.

Table of contents

CHAPTER I: INTRODUCTION 1
1.1 Generality 1
1.2 GPCR Classification 5
1.3 GPCR structure 9
1.3.1 Class A structure: 11
1.3.2 Class B structure: 11
1.3.3 Class C structure: 12
1.3.4 Class F structure: 12
1.4 GPCR Signaling 13
1.4.1 G protein-dependent signaling 14
1.4.2 β-arrestin signaling pathway 20
1.4.3 Biased agonism/functional selectivity 21
1.5 Pain and opioid crisis 25
1.5.1 Opioid receptors 29
1.5.2 Mu-opioid receptor 32
1.5.3 Opioid interactomes. 33
1.6 Most common protein-protein assay 34
1.6.1 Presto-Tango 34
1.6.2 BRET 38
1.6.3 NanoBit 42
1.7 Nanobodies 45
1.7.1 Nanobody in GPCRs' studies 48
1.7.1.1 Nanobody in structural biology 48
1.7.1.2 Nanobody as intracellular allosteric modulator of GPCR 49
1.7.2 Nanobody as intracellular biosensor 50
1.8 Significances of our system (libraryV5) 51
1.9 Hypotheses and Aims 54
CHAPTER II: MATERIALS AND METHODS 55
2.1 Cell culture 55
2.2 Plasmids and cloning 55
2.3 Nanobody development 56

2.4 Protein purification 57
2.5 Crystallization, data collection and structure determination 58
2.6 Isothermal titration calorimetry (ITC) 59
2.7 Nanobody maturation 59
2.8 BRET^2 assay 60
2.9 NanoBiT assay 61
2.10 TANGO assay 62
2.11 Immunofluorescence 63
CHAPTER III: RESULTS 64
CHAPTER IV: PRELIMINARY DATA 92
CHAPTER V: DISCUSSION 96

List of Abbreviation

GPCRs - G protein-coupled receptors

cAMP - cyclic adenosine monophosphate

PLC - phospholipase C

MAPK - mitogen-activated protein kinase

ECL – extracellular loop

ICL – intracellular loop

LCP - lipidic cubic phase

β_2AR - beta-adrenergic receptor

cryo-EM - cryo-electron microscopy

TM, TMH - transmembrane helices

G proteins - guanine nucleotide-binding proteins

GxX – different G proteins

GDP - Guanosine diphosphate

GTP - Guanosine triphosphate

GIRK - G protein-coupled inwardly rectifying potassium

VGCC - voltage-gated calcium channels

AC - adenylate cyclase

GRK - G protein receptor kinases

PKA - protein kinase A

PIP2 - phosphatidylinositol 4,5-bisphosphate

IP3 - inositol trisphosphate

DAG – diacylglycerol

PKC – protein kinase C

GEFs - guanine nucleotide exchange factors

AT1R - angiotensin II type 1 receptor

PTH1R - type 1 parathyroid hormone receptor

CNS - central nervous system

UOD - opioid use disorder

CDC - Centers for Disease Control and Prevention

MOP, MOR, μ-OR - mu-opioid receptor

KOP, KOR - kappa-opioid receptor

DOP, DOR - delta-opioid receptor

HTS - high-throughput assays

TEVcs - TEV cutting site

tTA - the transcriptase activator

BRET - Bioluminescence Resonance Energy Transfer

Rluc - Renilla luciferases

NanoLuc – NanoLuciferase

LgBiT - large subunit

SmBiT – small subunit

scFvs - single-chain variable fragments

Nbx – nanobodies

CDRs - complementarity-determining regions

XTAL - X-ray crystallography

HEK293T - Human embryonic kidney 293T

ATCC - American Type Culture Collection

DMEM - Dulbecco’s modified Eagle’s medium

ITC – Isothermal titration calorimetry

FLIPR - Fluorescent Imaging Plate Reader

RLU - relative luminescence signals

HBSS - Hanks’ balanced salt solution

DTT – Dithiothreitol

Y2H - yeast two-hybrid

PPI – protein-protein interaction

BiFc - bimolecular fluorescence complementation

List of Figures

Figure 1 Schematic Representation of the General Structure of GPCRs. 4
Figure 2 Phylogenetic Tree of the GPCR Superfamily. 8
Figure 3 Pathways Involved in GPCR Signaling. 19
Figure 4 Bias signaling at GPCRs. 24
Figure 5 The State of the Opioid Crisis. 28
Figure 6 Resolved Crystal Structures of Opioid Receptors. 31
Figure 7 Principle of the Tango 2.0 Assay. 37
Figure 8 Principle of the TRUPATH BRET2 Assay. 41
Figure 9 Monitoring G Protein Coupling to the MOR via the NanoBiT Assay. 44
Figure 10 Overview of the selection of a synthetic nanobody interacting with the V5-tag. 67
Table 1 Data collection and refinement statistics for NbA1 in complex with the V5 peptide. 70
Figure 11 Structure of the NbA1 bound to the V5 peptide. 72
Figure 12 Effect of mutations on NbA1. 75
Figure 13 NbV5 as a versatile nanobody-based biosensor: application in protease-dependent cell-based assay (TANGO). 78
Figure 14 NbV5 as a versatile nanobody-based biosensor: application in Bioluminescence Resonance Energy Transfer (BRET2). 81
Figure 15 NbV5 as a versatile nanobody-based biosensor: application in *Nano*luciferase *Bi*nary *T*echnology (NanoBiT). 84
Figure 16 Effect of tag size on β-arrestin recruitment in BRET2 and NanoBiT assays. 88
Figure 17 NbV5-based detection of V5-tagged proteins by cell imaging. 91
Figure 18 Interaction level of G protein with the inactive receptor. 95

Acknowledgements

I am grateful to all who supported and guided me through this thesis journey. Their encouragement, insights, and assistance made this work possible. Firstly, to my supervisor, Dr. Patrick Giguère for giving me the opportunity of starting research with his group in January 2020 as 3rd year student. I will forever be grateful for the opportunity and continuous support during that time and will cherish these beautiful years forever.

To Gen, I don't know where to start to thank you since your continuous support and guidance made this thesis possible, from showing me techniques to helping to maintain a viable lab. I just want to say an enormous thank you to the best lab mom in the world.

To my thesis advisory committee members, Dr. Jean-François Couture and Dr. Maxime Rousseaux, I would like to express my gratitude for your time and helpful comments on my research progress.

To all the students I had the chance to work with and spend an amazing time with, I would like to thank all of you: Manel Zeghal, Shivani Patel, Julia Douglas Freitas, Rayan Ramdani, Isaac Kuk, Sarah Alsayadi, Marissa Hamlin, Ciara Heffernan, Abdulhamid Mohamud, and Kirsten Chua. I will always remember the time spent together in the lab.

An enormous thanks to a very special person, Angelica Venes, who is always there to brighten my days. Your encouragement and faith make me a better person. Pour terminer, j'aimerais remercier ma famille pour le support constant et l'amour qu'ils m'offrent : Maman, Papa, Ced et Mimi. Merci!

CHAPTER I: INTRODUCTION

1.1 Generality

G protein-coupled receptors (GPCRs) constitute one of mammals' largest superfamilies of membrane proteins (1). GPCRs are ubiquitously expressed and can be found in virtually all cell and tissue types(2). They are the target of a wide variety of extracellular ligands, such as photons, ions, small molecules, peptides, and hormones(3). They are characterized by a seven-transmembrane domain structure and are involved in the transmission of signals from the extracellular environment to the interior of cells. GPCRs participate in diverse physiological processes, such as vision, olfaction, taste, and regulation of cardiovascular and immune systems. GPCRs are also linked to many pathological conditions such as pain, Alzheimer's disease, type 2 diabetes, and depression (4). The structure of GPCRs consists of seven transmembrane helices connected by three intracellular loops and three extracellular loops (5). These receptors span the cell membrane, with an extracellular domain for ligand recognition and an intracellular domain for interaction with intracellular signaling proteins (4). GPCRs undergo conformational changes upon ligand binding, allowing them to interact with and activate specific heterotrimeric G proteins. These G proteins comprise α, β, and γ subunits and act as mediators between GPCRs and downstream signaling pathways. Upon activation, the Gα subunit exchanges GDP for GTP, dissociating from the βγ subunits and activating downstream effector molecules. GPCR signaling can modulate various intracellular pathways, including the cyclic adenosine monophosphate (cAMP) pathway, phospholipase C (PLC) pathway, and mitogen-activated protein kinase (MAPK) pathway. These pathways regulate cellular

responses such as gene expression, ion channel activity, neurotransmitter release, and cell proliferation. The importance of GPCRs in cellular signaling makes them attractive targets for therapeutic intervention. Many drugs currently on the market target GPCRs, including medications for hypertension, asthma, allergies, and psychiatric disorders (6). By modulating GPCR activity, these drugs can regulate abnormal signaling pathways and restore cellular homeostasis. Studies have also unveiled the complexity of GPCR signaling. Depending on which ligand activates a receptor, it can engage different intracellular transducers. This ‘biased signaling’ paradigm requires that we now characterize physiological signaling not just by receptors but by ligand-receptor pairs. In addition to ligand bias, a receptor's response is also determined by system bias, which encompasses all non-ligand molecules involved in signaling. The combined effect of ligand and system bias leads to functional selectivity and provides opportunities to elicit the predominantly therapeutically relevant effect of a receptor activation (7).

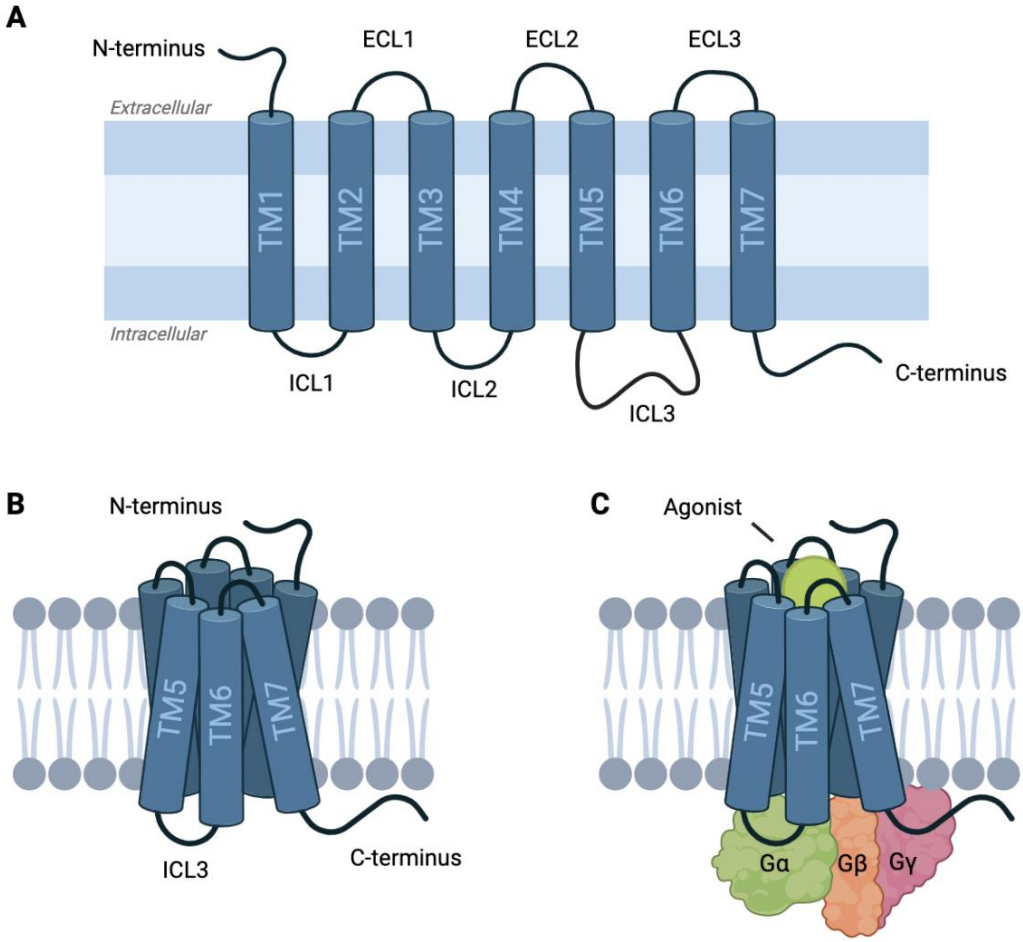
A
N-terminus
ECL1
ECL2
ECL3
Extracellular
TM1
TM2
TM3
TM4
TM5
TM6
TM7
Intracellular
ICL1
ICL2
ICL3
C-terminus
B
N-terminus
TM5
TM6
TM7
ICL3
C-terminus
C
Agonist
TM5
TM6
TM7
Gα
Gβ
Gγ

Figure 1 Schematic Representation of the General Structure of GPCRs. (A) GPCRs are membrane proteins that consist of seven transmembrane (TM) helices connected by three extracellular (ECL1-3) and three intracellular loops (ICL1-3). Their N- and C-terminus are found in the extracellular and intracellular regions, respectively. (B) The assembly of a typical GPCR is done in a counter-clockwise manner to form a functional receptor. (C) Upon agonist binding, the receptor is activated and recruits the heterotrimeric G proteins. These proteins bind to the ICL3 and C-terminus of the receptor. Figure made on Biorender

1.2 GPCR Classification

This seven-transmembrane protein family comprises 826 members encoded in the human genome and is divided into different classes. Different sorting systems have been proposed to classify GPCRs. The first proposed by L.F. Kolakowski Jr is based on the sequence homology between receptors to divide them into seven classes (A-F)(8). Another classification system based on phylogenetic studies divides GPCRs into five classes: Glutamate, Rhodopsin, Adhesion, Frizzled/Taste2, and Secretin (GRAFS)(9). The Kolakowski classification (A-F) is the basis for the widely used GPCR database (GPCRdb) built on receptor sequence homology(10). Class A, or rhodopsin-like family, is the most prominent family of GPCRs (over 80% of all GPCRs) and includes most sensory receptors. Non-sensory class A receptors bind small ligands like small molecules, neurotransmitters, peptides, and hormones. They possess common structural characteristics: a short N-terminal domain, a conserved cysteine bridge, E/DRY, NPxxY, CWxP, PIF, and Na^{+}-lock motifs(11). Non-sensory class A receptors represent the main research focus of the Giguere lab.

Orphan GPCRs, also known as orphan receptors, are a subset of G protein-coupled receptors (GPCRs) identified through genomic sequencing but have unknown endogenous ligands or functional roles. These receptors are called "orphans" because they lack identified ligands or known physiological functions (12).

Orphan GPCRs represents a significant portion of the GPCR family, with estimates suggesting that approximately one-third of the GPCRs in the human genome are still

considered orphan receptors(12). Despite their unknown ligands and functions, orphan GPCRs are believed to have important roles in various physiological processes and hold potential as therapeutic targets (6). Research efforts are focused on elucidating the ligands and functions of orphan GPCRs. Different approaches are employed to discover the ligands for orphan GPCRs, including screening compound libraries, mining databases for potential ligand-receptor interactions, and using functional assays to identify ligand-induced responses (2). Once the ligands for orphan GPCRs are identified, their functional roles can be investigated through studies involving knockout or overexpression models and selective agonists or antagonists (3). Understanding the functions of orphan GPCRs can provide insights into their involvement in physiological processes, such as sensory perception, immune response, and neuronal signaling (13). Orphan GPCRs also present opportunities for drug discovery and development. Once the ligands and functions of these receptors are elucidated, they can be targeted with selective agonists or antagonists to modulate their activity and potentially treat various diseases (14). Several orphan GPCRs have been successfully deorphanized in recent years, leading to the development of new therapeutics targeting these receptors (15).

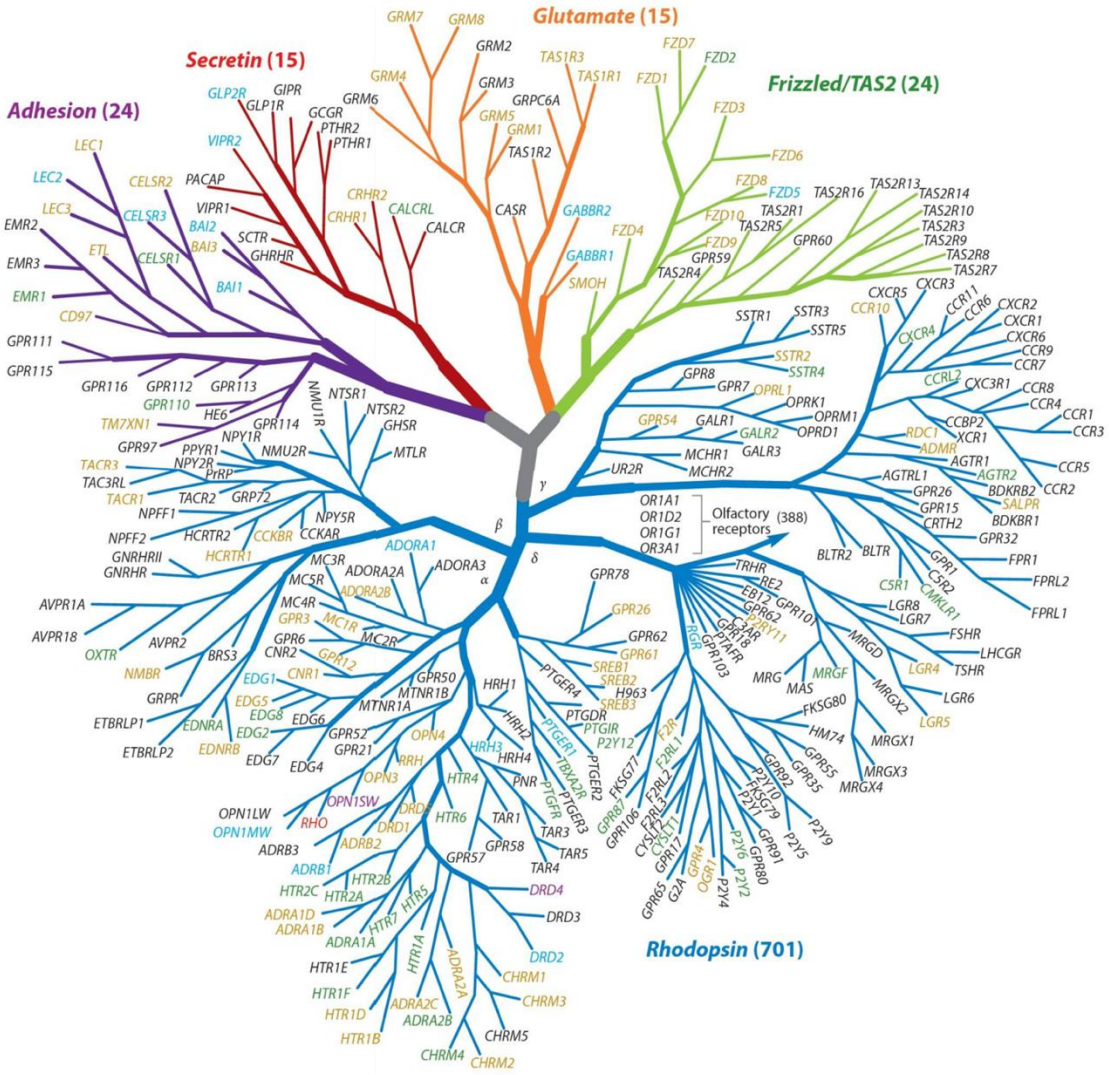
Glutamate (15)
Secretin (15)
Frizzled/TAS2 (24)
Adhesion (24)
Olfactory (388) receptors
Rhodopsin (701)
α
β
γ
δ

Figure 2 Phylogenetic Tree of the GPCR Superfamily. Having over 800 types found in humans, the family of GPCRs is very abundant and diverse. The opioid receptors (OPRM1: μ-opioid receptor, OPRD1: δ-opioid receptor, OPRK1: κ-opioid receptor) are part of the largest subfamily of GPCRs, the Rhodopsin family. Other major branches, such as Adhesion, Secretin, Glutamate, and Frizzed receptors, are also labeled. The classifications are made based on sequence similarity. The image was modified from Chen et al. (16) with permission from Annual Reviews via the Copyright Clearance Centre.

1.3 GPCR structure

GPCR structural biology is a field of research focused on elucidating the three-dimensional structures of GPCRs. Determining GPCR structures is essential for understanding their molecular mechanisms of action, ligand recognition, and signal transduction pathways. Structural information provides valuable insights into the function and pharmacology of GPCRs and aids in designing drugs targeting these receptors. Historically, GPCRs have been challenging to study structurally due to their inherent flexibility, membrane-bound nature, and difficulty obtaining purified and stable protein samples. However, significant advancements in technology and methodologies have led to notable breakthroughs in GPCR structural biology in recent years.

One of the most significant achievements in GPCR structural biology was the determination, in 2000, of the crystal structure of rhodopsin, a GPCR involved in vision, which brought the foundation necessary for drug discovery. GPCR structures are complicated to obtain due to many barriers, including difficulties in extraction, highly flexible conformations, and low expression levels. To counter these barriers, several methods were developed to solve the structure of these seven-transmembrane proteins more efficiently. One such example is lipidic cubic phase (LCP) crystallization. Other technological innovations in protein expression and purification (17, 18), GPCR crystallization (19), and the application of nanobodies led to the fantastic growth of the field's knowledge base. The first structure solved where the receptor interacts with a G protein was that of the beta-adrenergic receptor (β_2AR) in complex with G_s in 2011 (20). On the other hand, the first structure where the

receptor interacts with an arrestin was rhodopsin bound to the visual arrestin in 2015 (21). These two structures revealed important insights into the molecular mechanism of the GPCR interacting with G proteins and arrestins.

This groundbreaking work paved the way for studying other GPCRs and revealed a common seven-transmembrane helical fold characteristic of GPCRs. Since then, the field has seen remarkable progress in obtaining structures of diverse GPCRs through X-ray crystallography and, more recently, cryo-electron microscopy (cryo-EM). X-ray crystallography has successfully determined high-resolution structures of several GPCRs, providing atomic-level details of their ligand-binding pockets and interaction sites with downstream signaling molecules. Cryo-EM has emerged as a powerful technique for studying GPCRs, particularly for those that are challenging to crystallize. Cryo-EM allows for determining GPCR structures in their native lipid environment, providing more physiological relevance. Around 90% of GPCR complex structures were solved using this method (22). It has contributed to the structural understanding of GPCRs in complex with various ligands, G proteins, β-arrestins, and other regulatory proteins. Structural studies have revealed important insights into GPCR activation and signaling mechanisms, allosteric modulation, ligand binding, and receptor-ligand interactions. They have also facilitated structure-based drug design and the development of GPCR-targeted therapeutics. Furthermore, recent advances in computational modeling and molecular dynamics simulations have complemented experimental approaches, enabling the prediction of GPCR structures and exploring dynamic processes not captured by a static structure alone.

Although GPCRs have differences in their sequences, they share general aspects in their structure that distinguish them from other types of receptors. GPCRs comprise seven transmembrane helices (TM), essential for transmitting signals in cells. They are linked by three extracellular loops (ECLs) and three intracellular loops (ICLs). Most of the GPCRs are similar, but some differences depend on the classes.

1.3.1 Class A structure:

Several ligands of GPCR class A bind directly to the helix bundle. Therefore, it is not surprising that changes in the structure of ECLs, helices, and more will affect the ligand binding pocket and, at the same time, change the mechanism of ligand recognition. Most of the GPCR structures were solved in antagonist mode, but in recent years, more structures have increasingly been resolved in agonist mode via cryo-EM (23–25). GPCRs of class A are activated via micro-switches, including CWxP, PIF, Na+ pocket, NPxxY, and DRY, which link the ligand pocket and the G protein-coupling region. For example, the binding of an agonist to a GPCR of class A will cause changes in the conformation of the Na+ pocket. These changes will have an impact on TM 6 and TM3. One of the most conserved mechanisms is a salt bridge between TM3 and TM6, broken after an agonist's binding, facilitating the coupling of G protein to the receptor.

1.3.2 Class B structure:

The main attribute of the class B structure is the large extracellular domain and the large transmembrane domain (12). The major difference with class A is that the binding area of class B is more accessible compared to the more restrictive binding

pocket of class A. The activation mechanism of class B will cause a change in the orientation of TM6, breaking the previous interactions formed with TM2 and TM7, creating a pocket for the binding of the G protein.

1.3.3 Class C structure:

The structures of class C GPCRs are known to have a large extracellular domain, forming a dimer distal from the transmembrane domain. When the agonist binds to the receptor, it stabilizes the extracellular domain leading to a rearrangement in the transmembrane domain via ECL2 (26) Another possible modification of class C could be found on GABA receptors. The binding of the ligand will lead to conformational changes to TM3, TM4, TM5, and the ICL3 regions, which will then lead to the binding of a G protein heterotrimer (27).

1.3.4 Class F structure:

Class F only represents a small portion of the human GPCRs, characterized by a large extracellular domain rich in cysteine (28). Two binding sites have been discovered for this class – one in the transmembrane domain and one in the cysteine-rich domain. The smoothed receptor activated by cholesterol happens at the cysteine-rich domain, but its mechanism is not well understood due to the lack of a resolved structure.

1.4 GPCR Signaling

GPCRs are named after their binding partner, (G proteins) guanine nucleotide-binding proteins. These receptors signal through G protein-dependent signaling but can also signal independently through β-arrestin recruitment (29, 30). GPCR signaling begins with the interaction of a ligand with the receptor, which causes conformational changes in the receptor's structure. The G protein heterotrimer, consisting of the Gα, Gβ, and Gγ subunits, is then recruited to the receptor through the interaction of the distal C-terminus of the Gα (distal helix 5) with a crevice newly formed between TM3 and TM5 of GPCRs (DRY motif). Once the heterotrimer and the receptor are bound, the G protein undergoes conformational changes in the Guanosine diphosphate (GDP) binding pocket, resulting in the release of GDP and binding of Guanosine triphosphate (GTP) to the Gα subunit(31). This activates the G protein, causing the dissociation of the heterotrimer into Gα and Gβγ subunits. These subunits then propagate signals to effector proteins such as G protein-coupled inwardly rectifying potassium (GIRK) channels, voltage-gated calcium channels (VGCC), phosphodiesterase, phospholipase C, and adenylate cyclase (AC)(32). For example, AC could get stimulated by the alpha subunit, Gαs, leading to increased production of cAMP, or it could conversely be inhibited by Gαi/oi, leading to decreased cAMP production. G protein-dependant signaling stops when the intrinsic GTPase activity of the Gα subunits causes the hydrolysis of the GTP into GDP, and the reassembly of the heterotrimeric G protein occurs thereafter. Another fundamental mechanism of GPCR signaling and regulation is the recruitment of β-arrestins. These β-arrestins can adopt different conformations when bound to the receptor but generally involve interaction with the phosphorylated C-terminus of the receptors and ICL3 overlapping

the binding site of G proteins to a certain level (33–35). This exclusive interaction sterically inhibits the recruitment of G proteins, controlling signal transduction, a phenomenon called desensitization (36, 37). The C-terminus of the receptor is phosphorylated by different kinases, including, among others, G protein-receptor kinases (GRKs), PKA, and PKC, which are then recognized and sensed by β-arrestin. The activation of β-arrestin leads to its conformation rearrangement and interaction with various proteins involved in signal transduction or the internalization machinery(38, 39). G protein-independent signaling via β-arrestins could also lead to the inhibition of apoptosis, protein translation, along with other intracellular mechanisms. GPCR internalization could lead to either the recycling or degradation of the receptor (40, 41).

1.4.1 G protein-dependent signaling

As mentioned in the previous paragraph, there is more than one type of heterotrimeric G protein. They are classified according to their Gα subunit: G_s, $G_{i/o/z}$, $G_{q/11}$, and $G_{12/13}$; not all groups bind to the same GPCR and even send signals to the same effectors. The stimulatory Gα proteins (G_s) interact with adenylyl cyclase (AC) and increase the production of intracellular cAMP. Increased cAMP levels subsequently activate protein kinase A (PKA), which phosphorylates downstream targets and regulates cellular processes such as gene expression, ion channel activity, and neurotransmitter release. Conversely, the inhibitory Gα proteins ($G_{i/o/z}$) will inhibit AC, reducing cAMP production. $G_{q/11}$ proteins interact with and stimulate phospholipase C (PLC), leading to the hydrolysis of phosphatidylinositol 4,5-bisphosphate (PIP2) into inositol

trisphosphate (IP3) and diacylglycerol (DAG). IP3 releases calcium from intracellular stores, while DAG activates protein kinase C (PKC), which modulates various cellular functions, including neurotransmission, cell growth, and differentiation. Lastly, the $G_{12/13}$ proteins are mainly responsible for pathways involved in the regulation of cell morphology and motility through the regulation of guanine nucleotide exchange factors (GEFs) for the Rho small GTPase.

The α-GTP subunit and the βγ complex can independently modulate downstream signaling pathways. The βγ complex interacts with various effector proteins, including ion channels, enzymes, and other signaling molecules. These interactions can regulate multiple signaling pathways and cellular processes, such as ion channel activity, adenylyl cyclase regulation, phospholipase C (PLC) activity, ion fluxes regulation, and cellular proliferation and differentiation modulation. The βγ complex can also participate in feedback mechanisms to regulate GPCR signaling. It can modulate the activity of the GPCR itself through interactions with specific regions of the receptor, affecting its desensitization, internalization, or resensitization processes. Furthermore, the βγ complex can interact with other signaling proteins, such as kinases and scaffolding proteins, to form protein-protein complexes that coordinate and amplify downstream signaling events. These interactions contribute to the integration and modulation of GPCR signaling within cellular signaling networks. The β and γ subunits of heterotrimeric G proteins exist as multiple isoforms encoded by different genes. In mammals, multiple isoforms of both β (e.g., β1-β5) and γ (e.g., γ1-γ12) subunits have been identified. Each isoform can have distinct expression patterns, cellular localization, and functional properties, contributing to the diversity of

βγ complexes. For example, γ3 is found only in the brain (42). Understanding the variety of βγ complexes and their interactions with effectors and regulatory proteins is crucial for comprehending the complexity of G protein-mediated signaling networks. It highlights the ability of G protein signaling to modulate a wide range of cellular processes and responses in a context-dependent manner. Further research is needed to fully characterize the functional implications of βγ complex diversity and its contributions to physiological and pathological processes.

The interaction between GPCR and G proteins exhibits a certain level of promiscuity. The specificity of GPCR-G protein interactions is primarily determined by the coupling selectivity, which refers to the preference of a GPCR for a particular G protein subtype. Different GPCRs can exhibit varying degrees of coupling selectivity, with some showing a strong preference for a specific G protein subtype, while others can couple with multiple G protein subtypes (43, 44). The promiscuity of GPCR-G protein interactions provides a mechanism for fine-tuning and integrating cellular signaling. It allows for the generation of diverse cellular responses and enables GPCRs to respond to a wide range of extracellular stimuli. The ability of GPCRs to activate multiple G protein subtypes also contributes to the complexity of signaling networks. It provides opportunities for therapeutic intervention by targeting specific GPCR-G protein interactions.

It's worth noting that while promiscuous interactions occur, there are also instances of preferential coupling between specific GPCRs and G protein subtypes. This selectivity can be important for maintaining specificity and fidelity in signaling pathways. Further

research is needed to fully understand the molecular determinants and functional implications of promiscuous and selective GPCR-G protein interactions.

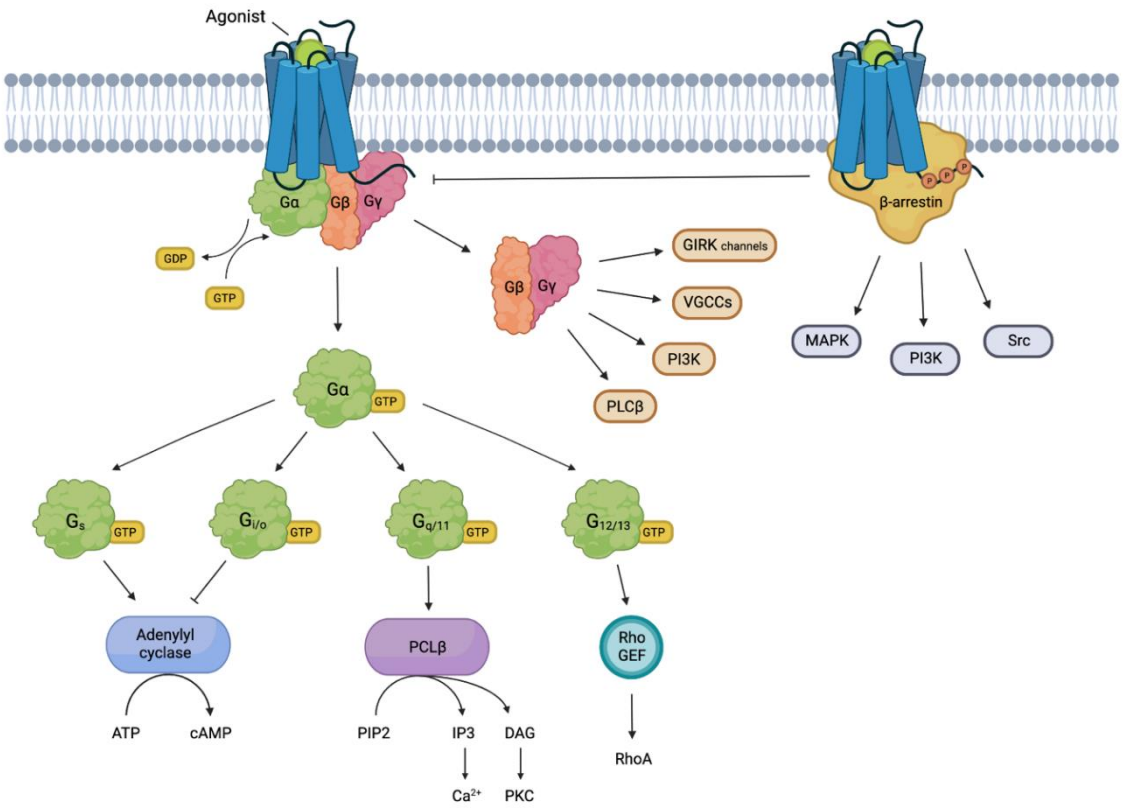
Agonist
Gα
Gβ
Gγ
GDP
GTP
β-arrestin
GIRK channels
VGCCs
PI3K
PLCβ
MAPK
PI3K
Src
Gα GTP
Gs GTP
Gi/o GTP
Gq/11 GTP
G12/13 GTP
Adenylyl cyclase
ATP
cAMP
PCLβ
PIP2
IP3
DAG
Ca2+
PKC
Rho GEF
RhoA

Figure 3 Pathways Involved in GPCR Signaling. The binding of an agonist to a GPCR activates G-protein-dependent and -independent pathways that modulate cellular signaling. The dissociation of the heterotrimeric G protein and the recruitment of β-arrestin allows for the activation of a variety of downstream effectors and messengers. G protein signaling is terminated through the recruitment of β-arrestin as well. The signaling of GPCRs involves a highly-regulated network, and only some examples of the pathways involved are highlighted. Figure made on Biorender

1.4.2 β-arrestin signaling pathway

Proteins known as β-Arrestins were initially thought only to desensitize GPCRs, but we now understand that they play numerous roles in various cell functions (45). These adapter proteins were named β-Arrestins due to their sequence similarity to visual arrestin (arrestin-1), which is responsible for arresting the rhodopsin signal in the retina. Like arrestin-1, β-Arrestins were discovered due to their ability to desensitize G protein-dependent signaling of the β2 adrenergic receptor following agonist stimulation (45). Two isoforms of β-Arrestins, β-arrestin1 and β-arrestin2, share 78% sequence homology and are encoded by arrestin-2 and arrestin-3 genes, respectively (46, 47). The other arrestins, visual arrestin (arrestin-1) and cone arrestin (arrestin-4), are only expressed in the eye. α-Arrestins are another group of arrestins that share structural similarities with β-Arrestins and are involved in receptor endocytosis, but they were discovered more recently (48, 49). While both β-Arrestins can interact with GPCRs, the level of interaction varies depending on the receptors, with some receptors being β-Arrestin1 biased and others being β-Arrestin2-biased (50, 51). It is now understood that β-Arrestins play a crucial role in arresting signals and are responsible for receptor recycling, receptor transactivation, MAPK signaling, and more (52). Although the two isoforms are similar, they have key differences, such as β-Arrestin1 accumulating everywhere in the cells, which is not the case for β-Arrestin2 only accumulating in the cytoplasm (53). Both β-Arrestins do not necessary share the same signaling pathways and may interact differently depending on the receptor. For example, a journal article published on angiotensin II type 1 receptor (AT1R) showed that a knockdown of β-Arrestin2 leads to a decrease in ERK signaling, while a knockdown of β-Arrestin1 increases ERK signaling (54). Similar knockdown effects

could be observed for other receptors, such as type 1 parathyroid hormone receptor (PTH1R), which leads to a decrease in ERK1/2 signaling (55) Other factors, such as the presence of signaling partners like GRK, could also influence β-Arrestins. For instance, the recruitment of β-Arrestin2 and internalization of the mu-opioid receptor were significantly reduced following GRK knockout (56).

1.4.3 Biased agonism/functional selectivity

GPCRs play a vital role in cell signaling and physiological responses. They were previously believed to activate only a single signaling pathway upon activation via ligand binding, leading to a uniform cellular response. A recent finding has challenged this belief, revealing that ligands can selectively activate specific signaling pathways, leading to different outcomes. This effect is known as biased agonism/functional selectivity and has significant implications for therapeutic development and drug discovery (57). Biased agonism refers to the ability of ligands to activate distinct downstream signaling pathways while exhibiting different efficacy or potency (58). This selective activation can lead to unique pharmacological effects and therapeutic outcomes, creating opportunities to develop drugs with improved efficacy and reduced side effects. The complex conformational dynamics and allosteric modulation of GPCRs are the molecular basis of biased agonism. Ligands can bind to different regions of the receptor and stabilize unique receptor conformations, resulting in the preferential recruitment of specific downstream effectors. The receptor conformational landscape and its coupling to different signaling proteins contribute to the biased agonistic properties of ligands (59,

60)Several techniques have been developed to characterize and quantify biased agonism, enabling the identification and characterization of biased agonists and facilitating the design of more selective drugs with desired functional profiles (61). This approach holds promise for a wide range of therapeutic areas, including cardiovascular diseases, neurological disorders, and cancer (57, 62). A comprehensive understanding of the underlying molecular mechanisms and the interplay between different signaling pathways is essential to comprehend the significance of biased agonism fully. Extensive research efforts have been dedicated to elucidating the structural determinants of biased agonism, exploring the receptor-dependent and ligand-dependent mechanisms, and uncovering the crosstalk and communication between signaling pathways (63–65).

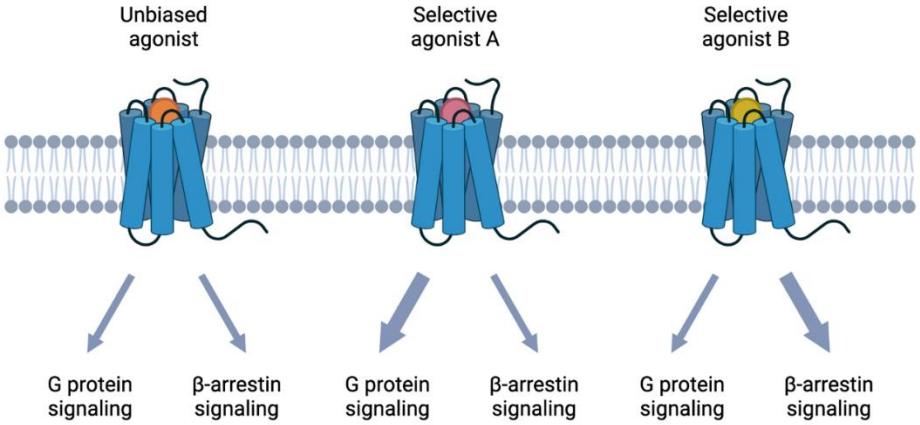
Unbiased agonist
Selective agonist A
Selective agonist B
G protein signaling
β-arrestin signaling
G protein signaling
β-arrestin signaling
G protein signaling
β-arrestin signaling

Figure 4 Bias signaling at GPCRs. One component of functional selectivity is the ligand-dependent preferential receptor activation of one over other pathways in a given cellular system and relative to a reference ligand. An unbiased agonist activates both G protein and β-arrestin signaling pathways to a similar potency and efficacy, while G protein-biased and β-arrestin-biased agonists favor one pathway over the other, leading to distinct cellular responses. Figure made on Biorender

1.5 Pain and opioid crisis

Everybody in their lives is expected to face pain. Pain is a common experience indicating something is wrong in our bodies (66). While pain can help us address the problem, it could also persist and significantly impact the overall health of an individual. Pain management, especially chronic pain, is challenging for health professionals and has contributed to the opioid crisis (67). This crisis had a devastating effect on the communities, families, and individuals. Everybody knows what pain is, but it is a very complex condition involving psychological and physiological aspects. Physiologically, pain is a sensory experience that identifies harmful stimuli and carries the signal to the central nervous system (CNS) via nerves expressing receptors known as nociceptors (68).

Acute pain usually results from an injury or tissue damage and serves as a way of telling humans the need for urgent attention. On the other hand, chronic pain is a long process lasting usually more than six months and is sometimes a core medical condition (69). Chronic pain is harder to understand fully and significantly affects a person's physical and mental well-being. This effect on a person could lead to, not surprisingly, a decrease in productivity, functionality, and quality of life (70). The opioid crisis emerged due to the misuse and over-prescription of opioid medications, such as hydrocodone, oxycodone, and morphine. While opioids can effectively treat acute pain or palliative care, their long-term use in managing chronic pain has raised concerns. In the late 1990s, pharmaceutical companies reassured healthcare providers those opioids had no addictive effects, leading to a surge in opioid prescriptions (71). Unfortunately, this surge resulted in an increase in opioid misuse, addiction, and overdose deaths. Opioids are highly addictive due to their euphoric

effects, which can lead to recreational use or the development of opioid use disorder (UOD). The consequences of the opioid crisis have been devastating, with almost half a million people in the United States dying from opioid overdoses between 1999 and 2019, according to the Centers for Disease Control and Prevention (CDC) (72). Opioid misuse has also contributed to increased blood infections, such as HIV and hepatitis C, due to sharing needles among users. Healthcare providers must approach pain management comprehensively and individually to prevent further harm to individuals and communities and avoid the potential misuse and overuse of opioids (73).

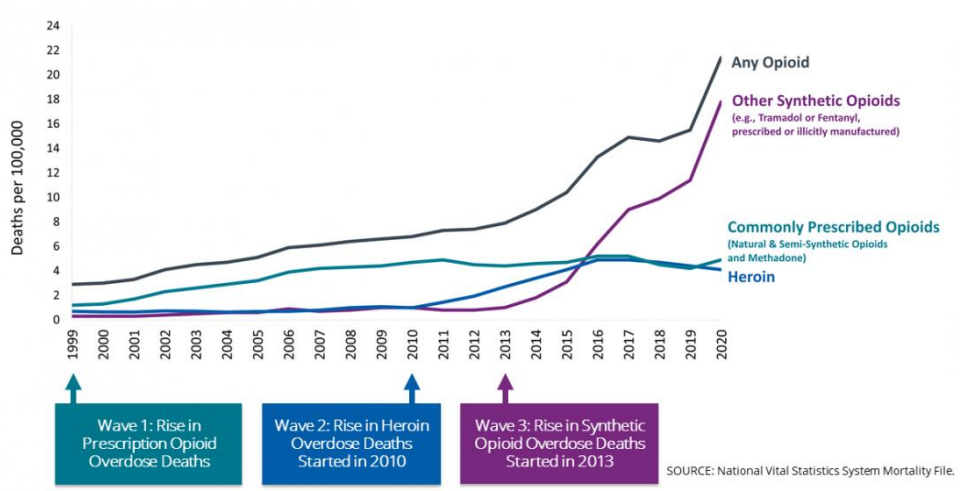
Deaths per 100,000
24
22
20
18
16
14
12
10
8
6
4
2
0
1999
2000
2001
2002
2003
2004
2005
2006
2007
2008
2009
2010
2011
2012
2013
2014
2015
2016
2017
2018
2019
2020
Any Opioid
Other Synthetic Opioids
(e.g., Tramadol or Fentanyl, prescribed or illicitly manufactured)
Commonly Prescribed Opioids
(Natural & Semi-Synthetic Opioids and Methadone)
Heroin
Wave 1: Rise in Prescription Opioid Overdose Deaths
Wave 2: Rise in Heroin Overdose Deaths Started in 2010
Wave 3: Rise in Synthetic Opioid Overdose Deaths Started in 2013
SOURCE: National Vital Statistics System Mortality File.

Figure 5 The State of the Opioid Crisis. Since 1999, the number of opioid-related deaths has increased in North America. Coming in waves due to different driving factors, the opioid crisis has become one of the worst public health crises that has ever been seen. Currently, synthetic opioids have been the main driver of overdose deaths, especially as they coincide with the increased production of illicitly manufactured drugs laced with fentanyl. The image is taken from the Centers of Disease and Control Prevention.

1.5.1 Opioid receptors

Opioids are among the most commonly prescribed and abused medications in the world (74). As a result of their actions on the nervous system, these drugs led to the discovery of their receptors in the late 1970s. They work by activating the three opioid receptors referred to as mu-opioid receptor (MOP), kappa-opioid receptor (KOP), and delta-opioid receptor (DOP), which are all members of the GPCR family (75–77). As a matter of fact, these receptors are predominantly expressed in the central nervous system, but they can also be found in peripheral neurons, the gastrointestinal and respiratory tracts, as well as immune cells. Among the primary functions of each of the receptors are to control the perception of pain, however, other outcomes have also been found for each receptor. For example, the mu-opioid receptor (MOP) receptor is primarily involved in central pain management; the letter m in mu signifies morphine, as the receptor is the target of morphinan-based painkillers, including oxycodone, fentanyl, morphine, and even codeine.

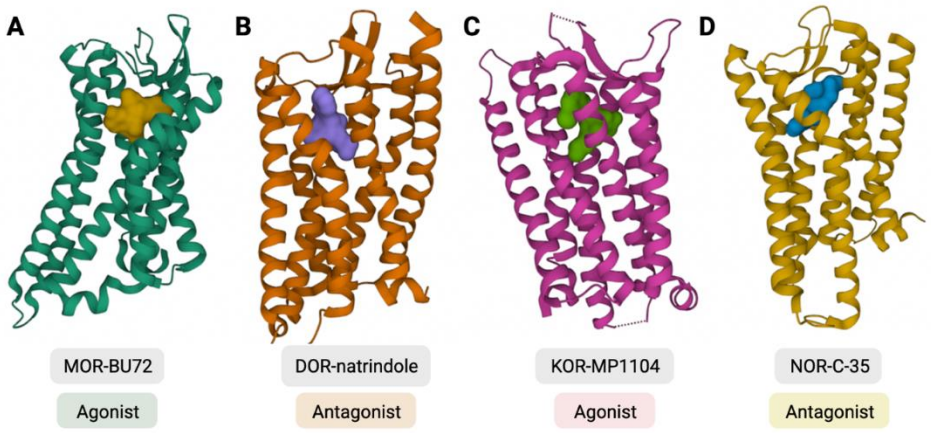
A
B
C
D
MOR-BU72
Agonist
DOR-natrindole
Antagonist
KOR-MP1104
Agonist
NOR-C-35
Antagonist

Figure 6 Resolved Crystal Structures of Opioid Receptors. The different opioid receptors, including their bound ligands, are shown. (A) MOR-BU72 (PDB ID: 5C1M); (B) DOR-Naltrindole (PDB ID: 4EJ4); (C) KOR-MP1104 (PDB ID: 6B73); (D) NOR-C-35 (PDB ID: 5DHG). The cartoon representation of the different receptors is shown, while the molecular surface of ligands is displayed. Nanobodies were used to stabilize some structures but were omitted in this figure used after the permission of creator Angelica Venes.

1.5.2 Mu-opioid receptor

The mu-opioid receptor (MOR) is crucial in controlling pain perception and reward pathways in the central nervous system (78). As a member of the GPCR superfamily, the MOR plays a vital role in mediating the effects of both endogenous opioids, such as endorphins, and exogenous opioids, such as morphine and fentanyl. Understanding the MOR's structure, function, and signaling mechanisms is essential to comprehend pain modulation, addiction, and developing targeted therapies. The mu-opioid receptor is coded by the OPRM1 gene, located on chromosome 6 in humans, with four exons spanning approximately 60 kilobases. The receptor protein consists of seven transmembrane helices (TMHs), connected by three extracellular and three intracellular loops. The extracellular N-terminus contains glycosylation sites, while the intracellular C-terminus plays a crucial role in receptor desensitization and internalization. The MOR is activated when endogenous or exogenous ligands bind to the receptor, triggering a cascade of intracellular events. Endogenous opioids, such as beta-endorphins and enkephalins, bind to the MOR with high affinity, modulating pain perception and emotional responses. Exogenous opioids, such as morphine and other opioid analgesics, also bind to the MOR, leading to analgesia, euphoria, and potential addiction (79). The MOR couples with G proteins after the binding of a ligand, initiating downstream signaling pathways. The primary signaling pathways associated with MOR activation include the inhibition of adenylyl cyclase via G inhibitory proteins, resulting in decreased levels of cyclic adenosine monophosphate (cAMP), and the activation of potassium channels, leading to hyperpolarization. These signaling events contribute to the analgesic effects of opioids and, unfortunately, their potential for abuse (29). Activation of the MOR in the CNS modulates pain perception by inhibiting

the transmission of pain signals through various mechanisms, including inhibition of neurotransmitter release, modulation of neuronal excitability, and modulation of descending pain pathways. The analgesic effects of opioids mediated by the MOR have been extensively studied and are the basis for their clinical use in pain management (80). Although opioids provide effective pain relief, activating the MOR also triggers reward pathways, leading to the potential for addiction. Prolonged opioid use can lead to tolerance, dependence, and withdrawal symptoms upon cessation. The mu-opioid receptor's role in reward pathways and addiction has contributed to the opioid crisis, with increased rates of opioid misuse, overdose deaths, and societal burden (81).

1.5.3 Opioid interactomes.

The latest drug discoveries for GPCRs are focused on analyzing their affinity/efficacy for G protein signaling and β-arrestin2 recruitment. This is because most miniaturized and high-throughput assays (HTS) have been developed to examine these two signaling pathways. However, the activation of GPCRs triggers many more pathways, often referred to as a pluridimensional GPCR signaling network, which can account for the physiological outcome of receptor activation. Currently, the understanding of the signaling networks activated by opioid receptors is limited to a few events, such as Gαi/o subfamily activation and arrestin recruitment. While some proteins are known to interact with opioid receptors, there is still a significant knowledge gap to fill (82, 83). For example, in the case of mu-opioid receptors or delta-opioid receptors, several proteins regulate trafficking and surface

expression. These interactions include Calnexin (84) and GASP (85), as well as signaling properties such as Calmodulin (86), RGS4 (87, 88), and β-arrestin, a non-canonical GPCR interactor that controls receptor desensitization and endocytosis. Notably, none of these proteins, except beta-arrestin and RGS 4, have been validated in terms of proximal interaction or using orthologous assays. Some groups, including our lab, have attempted to address this question by examining the GPCR's interactome using conventional proteomics approaches such as yeast-two-hybrid, mass spectrometry, or bioID. However, these approaches generate many potential hits with high rates of false positives, and it can be challenging to validate their interaction. GPCRs have very complex biochemical features, making it difficult to apply existing proteomics technologies to them. When extracted from their natural environment, they can result in misfolded and non-functional receptors, leading to numerous unwanted and artefactual interactions. Some GPCR interactors identified are associated with organelle structures, such as Golgi(89), endoplasmic reticulum(90, 91), and endosomes. They are also found with proteins in an intracellularly stacked arrangement following overexpression, and those interactions do not imply receptor functional state, a key element toward developing functional selective therapeutics.

1.6 Most common protein-protein assay

1.6.1 Presto-Tango

Understanding GPCR signaling and ligand pharmacology is crucial for creating effective therapeutics. In recent years, the Presto-Tango assay has become a powerful tool for studying GPCR signaling, ligand pharmacology, and drug discovery.

This versatile technique uses tango-optimized engineered GPCRs and β-arrestin recruitment to examine receptor activation. When a ligand binds, the GPCR containing the TEV cutting site (TEVcs) and the transcriptase activator (tTA) undergoes conformational changes that result in β-arrestin, fused with the TEV219, recruitment. This will then lead to the cleavage of the TEVcs and liberate the tTA, which enters the nucleus of cells and increases production of the luciferase gene reporter. The reporter interacts with the luciferase substrate, D-luciferin, leading to a luminescence emission. This assay provides valuable insights into ligand-receptor interactions and downstream signaling events, making it helpful in analyzing ligand pharmacology, including potency, efficacy, and signaling pathway selectivity (92). It can also identify new ligands and screen compound libraries for drug discovery in a high-throughput manner (93, 94).

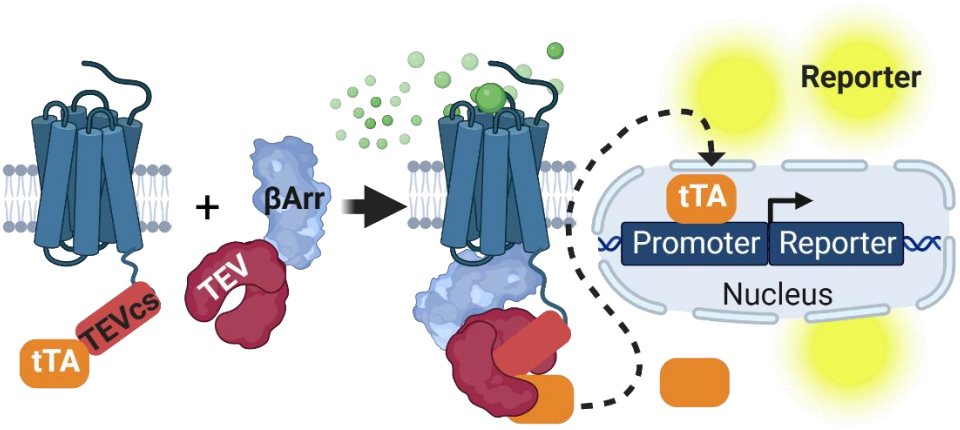
Reporter
tTA
Promoter
Reporter
Nucleus
βArr
TEV
TEVcs
tTA

Figure 7 Principle of the Tango 2.0 Assay. The recruitment of the β-arrestins upon receptor activation is monitored by tagging β-arrestin with TEV219 and receptor with TEV cutting site (TEVcs) and the transcriptase activator (tTA). This method was developed to study protein-protein interactions based on proximity. The proximity of the two proteins of interest will lead to the cleavage of the TEVcs by the TEV219 and liberate the tTA leading to an increased production of the reporter that will interact in the presence of the luciferase substrate, D-luciferin. The Tango signal is quantified via a plate reader by looking at luminescence.

1.6.2 BRET

Understanding protein-protein interactions is crucial for unraveling cellular signaling pathways and developing effective therapeutics. Bioluminescence Resonance Energy Transfer (BRET) assay has emerged as a compelling technique for studying these interactions in live cells (95). This technique is also used to study GPCRs (96). The BRET assay allows the investigation of protein-protein interactions in a physiological context (97). It utilizes the energy transfer between a bioluminescent donor, such as Renilla luciferases (Rluc) fused to one of the proteins of interest, and a fluorescent acceptor, such as GFP, fused to the binding partner to detect proximity-based interactions. Upon proximity, energy is transferred from the excited donor to the acceptor, leading to a measurable signal. This assay has many variants going from same cell expression with changes in acceptors or even split-BRET where the donor and acceptor are expressed in separate cells (98, 99). It enables the characterization of interactions between receptors and signaling proteins, the study of protein complex assembly and disassembly, and the analysis of protein conformational changes. In the case of GPCRs, it could be used to look at the recruitment of β-arrestins following receptor activation or even G protein signaling. The BRET assay has some advantages, like live cell imaging, real-time monitoring of interactions, and quantitative protein-protein interaction. Still, they are also some disadvantages, modification of the protein of interest by adding a large tag, difficulty in separating donor to acceptor signal leading to the optimisation of the assay with the BRET2 using GFP2 instead of YFP as the acceptor(100), and addressing the potential artifacts per example auto-fluorescence, inner-filter effects, etc. (101). Nonetheless, the BRET assay holds

significant promise for advancing the understanding of cellular pathways and is very useful in developing new therapeutics.

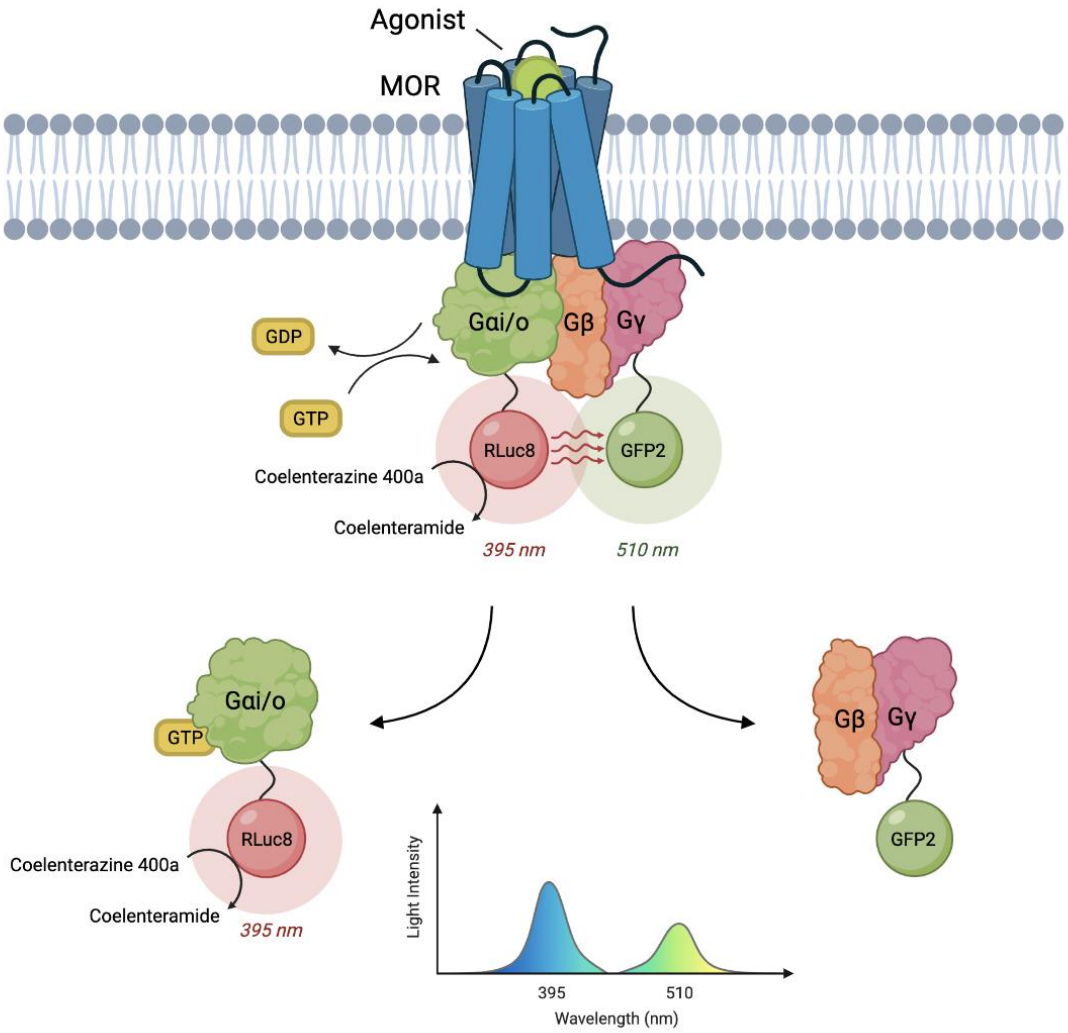
Agonist
MOR
Gαi/o
Gβ
Gγ
GDP
GTP
RLuc8
GFP2
Coelenterazine 400a
Coelenteramide
395 nm
510 nm
Gαi/o
GTP
RLuc8
Coelenterazine 400a
Coelenteramide
395 nm
Gβ
Gγ
GFP2
Light Intensity
395
510
Wavelength (nm)

Figure 8 Principle of the TRUPATH BRET2 Assay. The dissociation of the heterotrimeric G protein upon receptor activation is monitored by tagging Gα with RLuc8 and Gγ with GFP2. RLuc8 acts as the luciferase donor to facilitate resonance energy transfer to the fluorophore acceptor GFP2. These advanced biosensors were developed to study protein-protein interactions based on proximity. In the presence of the luciferase substrate, coelenterazine 400a, RLuc8 emits light at a wavelength of approximately 395 nm, which subsequently excites GFP2 to emit a fluorescent signal at 510 nm to indicate the close interaction between the two proteins of interest. The BRET signal is quantified by the ratio of the emissions of GFP2 to those of RLuc8. Figure made on Biorender

1.6.3 NanoBit

Studying protein-protein interactions is crucial in understanding complex cellular signaling processes. The NanoBiT assay is a highly versatile and sensitive tool for investigating live cell interactions (102). This assay uses a split NanoLuciferase (NanoLuc) system, which includes a large subunit (LgBiT) fused to one binding partner and a small subunit (SmBiT) fused to the other. It can detect and measure interactions between proteins of interest by bringing NanoLuc subunits into proximity, thereby reconstituting the functional enzyme and generating a luminescent signal. The NanoBiT assay can be used in various experimental designs, such as homogeneous solution-based assays or cellular systems, making it highly flexible (103). It allows for the characterization of interactions between receptors and signaling proteins, the study of protein complex dynamics, and the identification of novel interaction partners. The NanoBiT assay has several advantages, including a high signal-to-noise ratio and compatibility with live-cell imaging. However, similar to BRET, optimization is needed (101)The NanoBiT assay offers a significant understanding of cellular signaling pathways, including GPCRs, and holds immense potential for accelerating drug discovery and development (104).

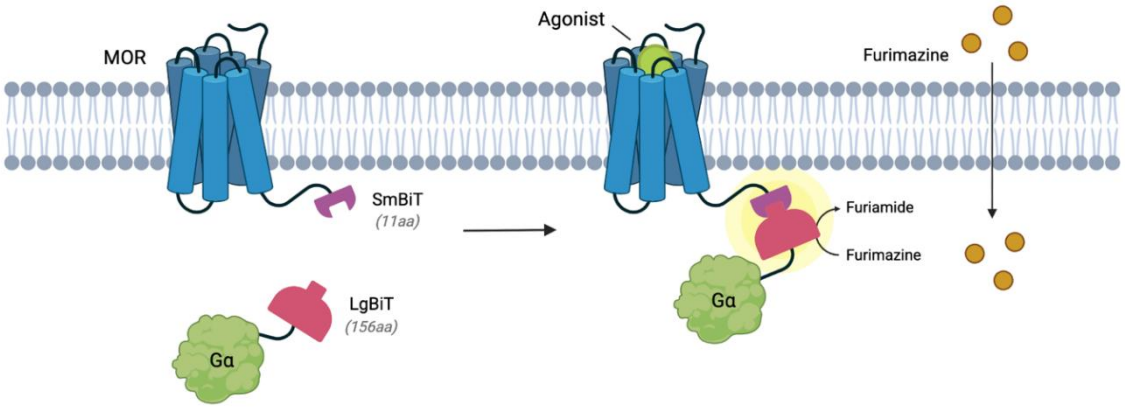
MOR
SmBiT
(11aa)
LgBiT
(156aa)
Gα
Agonist
Furimazine
Furiamide
Furimazine
Gα

Figure 9 Monitoring G Protein Coupling to the MOR via the NanoBiT Assay. To monitor the real-time interaction of the Gα subunit to the MOR, both the receptor and the Gα protein were tagged with SmBiT and LgBiT, respectively. The structural complementation of SmBiT and LgBiT is the basis of the NanoLuc Binary Technology (NanoBiT) system. Upon receptor stimulation by an agonist, the Gα protein is recruited to the receptor that facilitates the interaction of SmBiT and LgBiT, forming a complete NanoLuc luciferase enzyme. A luminescent signal in the presence of the furimazine substrate follows. Figure made on Biorender

1.7 Nanobodies

Considering the limitations above, adopting short peptide or epitope tags offers a reasonable possibility to probe PPIs. Less than 20 residues in length, epitope tags (e.g., HA, Flag, Myc, and V5) are commonplace in protein purification and localization/detection, such as microscopy, but less so for monitoring dynamic interactions(105). However, although fluorophores (e.g., GFP, mCherry) and other polypeptides (e.g., MBP, GST) are popularly used for probing recombinant proteins in a cellular context, including live cell imaging, reporter assays, and resonance energy transfer, the smaller size of epitope tags could be preferable for these purposes, as the fusion of bulkier fluorophores and polypeptides could interfere with the native behavior and functions of the protein of interest, especially interactions that are particularly proximity- or location-dependent(106). Besides avoiding cross-reactions within the native proteome, epitope tags obviate the need for custom antibody generation for every protein of interest and give rise to the possibility of multiplexing orthogonal peptide tags within the same experiment(105, 107).

Given the indispensability of these peptides, antibodies have continually been developed to recognize existing and newly developed epitope tags. Antibodies have proven to be very powerful tools in various cell biology research fields, going from western blot to vaccines; the possibilities are endless (108). Despite their huge ability to help scientific research, their large size prevents them from being used in living cell studies (109, 110). These limitations led to an improvement in engineering and the creation of intrabodies. Intrabodies are known for retaining important proprieties like recognition and neutralization with similar levels of affinity and specificity. The

advantage of this engineering is that their biophysical proprieties are different, allowing them to bind their specific targets expressed within the same living cells (111). However, it also comes with some drawbacks, as the single-chain variable fragments (scFvs) are very unstable in the intracellular environment (112–114). Another challenge that occurs and causes difficulty in the expression of intrabodies is the reducing environment of the cytoplasm, leading to blocking the formation of the disulfide bond (115, 116).

A major advance was the discovery and development of single variable domain (VHH) or nanobody (Nb). The VHH domains of camelid heavy chain antibodies have been shaped by more than 50 million years of evolution for high solubility and stability, independent of a partner VL domain. As recombinant proteins, VHH are designated single-domain antibodies or nanobodies in reference to their small size in the nanometer range (117). Despite of the outstanding track record of camelid nanobodies, there are three major restrictions linked to immunizations. First, the target space is limited to comparatively stable and immunogenic proteins. Second, it is very difficult to favor target conformations with non-covalent ligands because they dissociate from the protein shortly after injection. Third, immunizations require access to animal facilities, which makes it difficult and expensive for many researchers to implement binder generation on a routine basis in their own labs.

Synthetic nanobody (Nb) libraries are emerging as an attractive alternative to animal immunization for the selection of stable, high-affinity Nbs. Pure in vitro binder selection methods can overcome these drawbacks of immunization because they allow for full control over the binder selection process.

These libraries use a consensus framework derived from Llama Nbs combined with a designed variation of the complementarity-determining loops (CDRs) that comprise the highly variable antigen-binding interface of the VHH (118).

They have several important advantages such as their small size, high solubility, and stability. Remarkably, despite their monomeric binding region composed only of three hypervariable loops, Nbs can achieve affinities in the nanomolar and subnanomolar orders, just as clasical antibodies. Their modularity allows the easy generation of multivalent constructs for many different applications.

Due to their beneficial properties and accessibility to various cell compartments, Nbs applied as intrabodies have turned out to be highly suitable intracellular binding molecules(119–121). Having the ability to specifically visualize and/or modulate endogenous targets within living cells, intrabodies provide distinct advantages compared to other technologies such as fluorescent fusion proteins, conditional gene expression, RNA interference and chemical or genetic knockouts. Nevertheless, when it comes to intracellular applications it has to be considered that Nbs, like any other antibody-derived binding molecule, comprise evolutionary conserved disulfide bonds. While the endoplasmic reticulum (ER) and mitochondria provide naturally suitable compartments for Nbs due to their (at least partially) oxidative environment, the reducing milieu of the cytosol strongly impairs formation of disulfide bonds. This can massively affect correct paratope formation and overall folding. Consequently, only Nbs whose functionalities do not rely on the formation of disulfide bonds are suitable candidates for successful application as intrabodies (122, 123).

1.7.1 Nanobody in GPCRs' studies

1.7.1.1 Nanobody in structural biology

Nanobodies have been widely used to stabilize the active states of many GPCRs, including the β2- adrenergic (β2AR), M2-muscarinic (M2R), μ-opioid (MOR), k-opioid (KOR)(124), and angiotensin II type 1 (AT1R) receptors. The β2-adrenergic receptor (β2AR), a GPCR, is extensively studied due to its involvement in numerous physiological processes and relevance to drug discovery (21). GPCRs interact with G proteins and initiate intracellular cascades. However, studying their conformational changes and signaling partner interactions is challenging due to their flexibility and membrane-bound nature. Nanobodies are versatile tools for capturing and stabilizing GPCR conformational states (125). Nanobodies are a type of single-domain antibodies derived from camelids or sharks. They exhibit high affinity and specificity for their target proteins, making them excellent candidates for structural studies (126). They have shown their ability to facilitate X-ray crystallography by assisting with crystal formation and enhancing the complexity of protein structures(127). Researchers used nanobodies to stabilize β2AR-G protein complex for studying the interaction between GPCRs and G proteins in signal transduction (128). These nanobodies have provided valuable insights into receptor-G protein coupling and activation by capturing distinct conformational states of the complex. Nanobodies targeting the G protein component have been instrumental in obtaining high-quality crystal structures of β2AR-G protein complexes, revealing intricate details of the conformational changes and specific interactions between the receptor and the G protein upon GPCR activation. The ability to crystallize GPCR structures has revealed

their dynamic nature and aided in designing better therapeutics targeting GPCR-mediated pathways. Other nanobodies have also been known to significantly impact the field. Nanobody 6 (Nb6) and Nanobody 39 (Nb39) have a particularly strong affinity and selectivity toward opioid receptors (129). Nb6 targets an allosteric site in the intracellular loop 3 between TM5 and TM6 and stabilizes a ligand-independent inactive state. On the other hand, Nb39 stabilizes the active state of KOR(130). Nb6 and Nb39 have been used by many researchers as a helpful tool for x-ray crystallography and cryo-electron microscopy, due to the ability of the Nbs to form a more stable complex with GPCRs that consequently gives important information about GPCR activation, ligand binding, and allosteric modulation (131–133).

1.7.1.2 Nanobody as intracellular allosteric modulator of GPCR

Apart from the recognition and stabilization of specific conformations, nanobodies also act as allosteric effectors and can affect both ligand binding affinity and functional activity. For example, stabilization of an active and inactive conformation and dramatic alterations in ligand affinity at the β2AR by allosteric nanobodies were recently reported(134). For instance, Nb39 and Nb6 have unique binding properties that enable them to target specific conformational epitopes on opioid receptors, providing insights into opioid receptor activation dynamics and facilitating the stabilization of various receptor states. This capability is particularly significant in decoding the nuanced interactions between GPCRs and their downstream signaling partners. The use of Nb39 and Nb6 is crucial in exploring the structure of opioid receptors and has played a role in crystallizing GPCR-nanobody complexes, thereby enabling the

acquisition of high-resolution structures (130, 133). These structures provide a better understanding of the intricacies of ligand binding sites, allosteric pockets, and the complex mechanisms underlying GPCR activation. Nb39 is adaptable to cryo-electron microscopy, which has facilitated the visualization of opioid receptor complexes in environments closely resembling their natural states, affording a deeper understanding of their functional states. Nb39's modular nature enables fusion with diverse tags or reporter molecules, facilitating real-time monitoring of GPCR dynamics and interactions. This capability is essential in understanding phenomena such as ligand-receptor interactions, biased signaling, and allosteric modulation (135, 136). Nb39's genetic manipulability also holds promise for engineering innovative tools for GPCR-targeted therapeutics, with its small size and robust stability making it an asset for drug delivery and precision targeting.

1.7.2 Nanobody as intracellular biosensor

State-specific nanobodies have also been widely applied as conformational biosensors to monitor GPCR dynamics both in vitro and in vivo(137–140). A big part of the nanobody field in GPCR studies is mainly focused on specific Nb-GPCR biosensors such as Nb80 with β2AR(141), Nb.At110i1 with AT1R(142), Nb6 and Nb39 for opioid receptors. But other nanobodies like Nb33-eGFP (143) or even our own NbV5 (144)currently used as biosensors and are showing some promising results. Therefore, combining nanobodies with the current assays established in GPCR studies is a beneficial tool full of promises to increase the understanding of the

GPCR field and ultimately contribute to helping develop safer therapeutics with limited side effects(145).

To visualize native cell structures and dynamic processes within living cells, imaging probes must not influence their target structures or intracellular processes. Thus, transiently binding intrabodies have become universal and versatile tools for live-cell imaging. Studies suggested that, especially, physiochemical parameters have an important influence on the development of cytoplasmic stable intrabodies. The first intrabody developed were single chain antibody fragments (scFvs) fused to peptide-tags, conferring a strong negative charge and low isoelectric point in order to generate so-called ultra-stable cytoplasmic antibodies (STANDs). In their study, the authors demonstrated how fusion of scFvs to negatively charged s3Flag and HA peptide-tags induces a significantly increased stability of aggregation-prone cytoplasmic intrabodies(146). Notably, many Nbs are already strongly charged, showing either a positive or negative isoelectric point (pI) and therefore are less prone to aggregate at the most neutral pH of the cytoplasm (147).

1.8 Significances of our system (libraryV5)

Considering that shorter epitopes might have only a minor impact on native protein folding, function, and protein–protein interactions, extensive efforts have been undertaken to identify Nbs specifically recognizing small peptide-tags. Although most Nbs preferably address conformational epitopes (148, 149), more recently, a handful of Nbs recognizing linear epitopes were identified, mostly as byproducts from screening campaigns against full-sized proteins. Some of these Nbs have been

exploited as novel capture and detection systems. For purification of proteins comprising the small EPEA-tag (also known as C-tag)(150), Myc-tag or BC2- (Spot-) tag (151, 152), Nbs were converted into affinity matrices such as the CaptureSelect™ C-tag affinity matrix (**www.thermofisher.com**), the Myc-trap© or Spot-trap® resin (**www.chromotek.com**), respectively. Notably, besides their functionality to capture and detect peptide-tags, Nbs against the ALFA-tag(136), Moon-tag (153, 154) and Pep-tag (155) have also been successfully applied as intrabodies. However, most of these nanobodies were used to visualize antigens in living cells. Current assays used to study protein-protein interactions all require the fusion of large tags (TEV, GFP_2, LgBiT) to the proteins of interest to perform Tango, BRET or NanoBiT experiments. Using a nanobody as a carrier of the large tags and fusing a small peptide to the protein of interest could be a better alternative because the protein of interest can stay in a more native state (156).

Functional characterization of the human genome requires tools for systematically modulating gene expression in both loss- and gain-of-function experiments. With the overarching goal of studying GPCR's proximal interactome at a genome-wide level, we have thus undertaken to develop a suitable platform where a nanobody carrying a specialized tracker could recognize any protein exogenously expressed. The ONLY public genome-scale expression library of human ORFs was developed by a consortium led by the Broad Institute of Harvard and MIT and Center for Cancer Systems Biology (CCSB), generating a resource called ORFeome(157). Utilizing the hORFeome V8.1 collection, the entire library was shuttled into pLX304-Blast-V5 to create the CCSB-Broad Lentiviral Expression Library or pLX307-Puro-V5 to create the Mission TRC LentiORF library. These two libraries are the only genome-wide

expression libraries validated for high-throughput screening encoding a C-terminal peptide tag, the V5-epitope tag (158).

In order to exploit this resource to study the opioid receptors' interactome, we thus undertook to develop and optimize the ibodyV5, a nanobody recognizing the universal V5-tag (159–161). which serves as the foundation of our toolkit comprising intracellular nanobody-based biosensors.

1.9 Hypotheses and Aims

We hypothesize that yet-to-be-uncovered signaling pathways are responsible for the heterogeneity of drug action *in vivo*, which cannot be explained by *in vitro* profiling based on G protein, second messengers (such as cAMP), and β-arrestin recruitment. We also hypothesize that this toolkit could be more powerful as it better represents proteins of interest in their native state. We also hypothesize that this tool could be more powerful as it better represents proteins of interest in their native state.

Aim 1. Generation of a high-affinity intrabody directed against the V5-peptide tag. To this end, we will use genetic tools and structural biology to develop and optimize an anti-V5 nanobody-based intrabody.

Aim 2. Optimization and validation of our NbV5 in different assays. We will integrate the intrabody into different PPIs assays like NanoBiT, BRET, TANGO and microscopy for this aim**.**

Aim 3. Using NbV5 to study the precoupling of G protein with an inactive GPCR. To do this, we will look at all the GPCRs tagged with V5 from our library and look at the basal level of G protein tagged with LgBiT using our NbV5-SmBiT.

CHAPTER II: MATERIALS AND METHODS

2.1 Cell culture

Human embryonic kidney 293T (HEK293T) and HT1080 cells were obtained from the American Type Culture Collection (ATCC) and maintained in Dulbecco's modified Eagle's medium (DMEM) supplemented with 5% fetal bovine serum (Fisher Scientific), 5% bovine calf serum (Fisher Scientific) and 1X Pen-Strep (100 U/ml penicillin, and 100 µg/ml streptomycin) (Fisher Scientific).

HEK293T cells stably expressing MOR-SmBiT (MOR-SmBiT/HEK293T) were generated by transduction with lentivirus particles, which had been produced in HEK293T cells by transiently co-transfecting the lentiviral packaging plasmid psPAX2 (Addgene #12260), a lentiviral vector encoding µ-OR-SmBiT (pLenti-Blast Addgene #17451), and the envelope plasmid pCMV-VSV-G (gift from Marceline Côté) at a 1:1:1 ratio using PEI transfection reagent. The following day, media was changed, and the supernatant was harvested at 48h post transfection. Cells were then transduced with lentivirus in standard growth media containing 5 µg/ml polybrene and the next day, selected with blasticidin at 5µg/m. All cells were cultured at 37°C in a humidified atmosphere containing 5% CO_2.

2.2 Plasmids and cloning

All plasmid DNA used in this publication were fully sequenced and are available upon request or through Addgene repository.

Plasmid encoding ɣ-Actin-V5 was extracted from the MISSION TRC3 Human LentiORF Puromycin library (MilliporeSigma).

V5-βArrestin1, V5-βArrestin2, βArrestin1-V5, βArrestin2-V5, βArrestin2-ALFA, ALFA-βArrestin2, βArrestin1-ALFA and ALFA-βArrestin1 were amplified by PCR, including the V5 tag within the primer, and subsequently cloned into pcDNA3.1$^+$ at the HindIII-XbaI restriction sites.

GαoA with internal V5-tag at position 92 was synthesized by IDT (Integrated DNA Technologies) and cloned at HindIII-XbaI sites in pcDNA3.1$^+$.

BRET^2 constructs: AT_1R-RLuc8, μ-OR-RLuc8, NbV5-GFP2, GFP2-NbV5, βArrestin2-GFP2, βArrestin2-ALFA-GFP2 were amplified by PCR and cloned in pcDNA3.1$^+$ using NEB HiFi DNA Assembly (New England Biolabs). Gβ3 and Gγ2-GFP2 were generously gifted by Dr. Asuka Inoue (TOHOKU University).

NanoBiT constructs: μ-OR-SmBiT and AT_1R-SmBiT were amplified by PCR by including the SmBiT tag within the primer preceded by a $(GGGS)_{2x}$ linker. NbV5-LgBiT, LgBiT-NbV5, NbALFA-LgBiT and LgBiT-NbALFA were amplified by PCR and cloned in pcDNA3.1$^+$ using NEB HiFi DNA Assembly (New England Biolabs).

Gγ2-SmBiT was generously gifted by Dr. Asuka Inoue (TOHOKU University).

TANGO constructs: μ-OR-TANGO and AT_1R-TANGO are from the original PRESTO-TANGO library (162–164). Aforementioned receptors fused to the TEV219 or TEV219 S153N mutant were cloned by PCR at restriction sites HindIII-BamHI in pcDNA3.1$^+$-X-TEV219 vector. The S153N mutant was generated by site-directed mutagenesis.

Microscopy constructs: NbV5-eGFP was generated by PCR amplification of NbV5 and cloned into pEGFP-N1 (Clontech) at the HindIII-BamHI sites.

2.3 Nanobody development

To identify nanobodies that bind to a linear target and that could be expressed from inside the cell (as intrabodies), phage display selection was conducted with the Nali-H1 synthetic library (165) using a His-Halo protein fused with three successive V5-tags (Halo-3xV5). The naïve library was first depleted using another antigen fused in the same Halo vector and selected on magnetic streptavidin beads with the biotinylated Halo-3xV5. With the first round presenting a complexity of $3x10^6$ colonies, the DNA extracted from the first round were used to construct a Yeast-Two-Hybrid prey library by PCR and Gap repair. The VHH selected after one round of phage display against V5 tag-Biotin were cloned into the pP9 yeast prey vector, which is derived from the original pGADGH plasmid; the library had $2.6x10^5$ independent clones in yeast. A single V5 tag, as well as two tandem V5 tags, were cloned into pB27 as a C- terminal fusion to LexA (LexA-V5); pB27 is derived from the original pBTM116 plasmid (166). The constructs were verified by sequencing the insert and used as baits to screen the V5-specific VHH library For the screen, clones were vetted using a mating approach with YHGX13 (Y187 ade2-101:loxP-kanMX-loxP, matα) and L40ΔGal4 (mata) yeast strains as previously described(166). Moreover, the library has been screened at saturation by cell-to-cell mating (166). A total of 264 His+ colonies were selected on a medium lacking tryptophan, leucine and histidine supplemented with 0.5 mM 3-AT, obtaining 52 different VHH with redundancies from 1 to 37.

2.4 Protein purification

The NbA1 was cloned into the expression vector pET26b (+) (Novagen) at NcoI-XhoI restriction sites to generate the pelB leader-NbA1-His_6 construct. The plasmid was

transformed in SHuffle T7 Competent E. coli (New England BioLabs), and the NbA1 was subsequently purified from the periplasm of SHuffle T7 cells. Bacteria were then grown at 30°C in Terrific Broth and, after reaching an OD600 of ~0.6-0.8, were induced with 1mM IPTG (Isopropyl β-d-1-thiogalactopyranoside, ThermoFisher) at 25°C for approximately 16 hours. Bacteria were then pelleted and resuspended in a solution of lysis buffer (0.5 M sucrose, 0.2 M Tris pH 8, 0.5 mM EDTA) and water at a ratio of 1:2 to create an osmotic shock. The lysate was then frozen and thawed for more efficient purification. Followingly, the mixture was stirred for 45 minutes at 4 °C and brought to a concentration of 150 mM NaCl, 2 mM $MgCl_2$, and 20 mM imidazole and centrifuged at 20,000xg for 30 min at 4 °C. The supernatant was then filtered through a 0,22 µm filter. After filtration, the supernatant was added to a gravity column containing 4 mL of Ni-NTA (Qiagen). Beads were washed with a high salt buffer (20 mM HEPES pH 7.5, 500 mM NaCl, 20 mM Imidazole) and washed three times with low salt buffer (20 mM HEPES pH7.5, 100 mM NaCl, 20 mM imidazole). The nanobodies were then eluted (20 mM HEPES pH 7.5, 100 mM NaCl, 400 mM imidazole) and dialyzed into physiological buffer solution (10 mM HEPES pH 7.4, 140 mM KCl, 10 mM NaCl) and purified using FPLC (Fast protein liquid chromatography, AKTA GE) on an S75 prep size-exclusion column.

2.5 Crystallization, data collection and structure determination

Purified NbA1 (30mg/mL) was incubated with the V5 peptide in a 1:3 ratio (protein: peptide). The protein complex was crystallized via the sitting drop vapour diffusion method at 4°C with a mother liquor composed of Bis-Tris pH 6.5, 19% (w/v) PEG 3350 and 20% (v/v) ethylene glycol. The crystals were flash-frozen in liquid nitrogen, and a

full data set was collected using a Rigaku MicroMax-007HF equipped with a copper anode. Images were collected using an R-Axis IV++ detector (Rigaku) and processed using Structure Studio (Rigaku). The structure was solved by molecular replacement using the structure of NbALFA (PDB 6I2G) as search model and Phaser (136). Following several rounds of NbA1 building and refinement using COOT and Phenix, respectively, V5 was built in the positive Fourier map. The model was completed by adding the molecules and truncating side chains for which no electronic density could be observed. Ramachandran statistics: Non-glycine Ramachandran outliers; 0%, Non-glycine Ramachandran favored; 100%,Molprobity score : 1.65 . Statistics of data collection and refinement are summarized in Table1. All structural figures were prepared in PyMOL.

2.6 Isothermal titration calorimetry (ITC)

ITC experiments were performed on a VP-ITC calorimeter (MicroCal, Northampton, MA) by injecting the V5-peptide (521 µM) into the cell containing the NbV5 (38.7 µM) in HBS buffer solution (10 mM HEPES pH 7.4, 140 mM KCl, 10 mM NaCl) with or without 5 mM DTT. The assay was performed at 19°C and analyzed using the Origin software (OriginLab Corporation, Northampton, MA).

2.7 Nanobody maturation

To optimize the NbA1 sequence and potentially increase the affinity of the antibody towards V5, Rosetta single-state design protocol was performed using the Rosetta Software Suite on the crystal structure of the NbA1 complex. The structure of NbA1 was prepared for antibody affinity maturation for Rosetta by manually editing the PDB file in PyMOL. PyMOL command prompts were used to delete the unwanted water

molecules and all non-essential ligands and chains. An extra processing step was also performed to remove any protein atoms that are not involved in the antibody-antigen interface; chains were also renamed and reordered to help differentiate the antibody residues from the antigen residues. Next, a resfile (python script) was generated to identify the residues that were within a distance of specified residues that define the NbA1 protein interface. The side-chain conformations were optimized using the repacking and relaxing feature in Rosetta protein design, which was performed to minimize backbone phi-phi angles to relieve small clashes between sidechains. The relaxed model was then used to generate ten designed models through RosettaScripts XML file, which contains a design protocol that uses a single round of fixed backbone design. As a control, the same protocol was repeated to generate ten control models without designing any residues. These control models were generated to compare the scores and the binding energies of the designed models to the native sequence during the analysis stage. The designed sequences were then analyzed by looking at the score, binding energy, and the binding density of the models. The analysis of the metrics was plotted using RosettaScripts which plots the score and the binding energy of the deigned models against the control models. Subsequently, specific mutations were identified that resulted in the improvement of the NbA1 complex based on corresponding findings from functional assay experiments (as shown in Fig. 10). Finally, a sequence logo was generated from the designed models in order to determine which mutations were made and their frequencies.

2.8 BRET^2 assay

HEK293T cells were plated in 6-well plates at $1.2x10^6$ cells and subsequently transfected with $BRET^2$ constructs (at ratios indicated in the Figure legends) at a total of 3 µg of DNA per well. Transfected cells were detached and seeded on PLL-coated white 96-well assay plates (ThermoFisher). The following day, spent medium was removed and replaced with 60 µL of 1X HBSS buffer, followed by the addition of 10 µL of Coelenterazine 400a (Nanolight Technologies) at 50 µM to each well, for a final concentration of 5 µM. After incubating the plates away from light for 8 minutes, 30 µL of serial dilutions of agonists at 3X concentration was added. Plates were subsequently read 4 times after 2 minutes, 10 minutes, 20 minutes, and 30 minutes using the Hidex Sense Beta Plus microplate reader (Gamble Technologies) with 405 nm (RLuc8-Coelenterazine 400a) and 500 nm (GFP2) emission filters, at 1 second/well integration times. Figures shown in the manuscript account for the reads after 20-minute incubations with agonist (and correspondingly, approximately 30-minute incubations with Coelenterazine 400a). Data were extracted using the integrated software and subjected to non-linear least-squares regression analysis using the sigmoidal dose-response function provided in GraphPad Prism 9.0. Data of 3 or 4 independent experiments (N=3 or 4) performed in quadruplicate are presented as $BRET^2$ ratio (acceptor/donor) as indicated in figure legends.

2.9 NanoBiT assay

µ-OR-SmBiT/HEK293T and HEK293T cells were plated in 6-well plates at $1.0x10^6$ cells and then transfected with the NanoBiT constructs the next day (ratio and constructs in Figure legends) at a total of 3 µg of DNA per well. Transfected cells were detached and seeded on PLL-coated white 384-well assay plates (ThermoFisher) in

starvation media (DMEM, 1% FBS, 1x Pen-Strep), The next day, media was removed and replaced with 20µL of 1X HBSS buffer containing 5 µM furimazine and incubated for a total of 10 minutes at room temperature before reading on Fluorescent Imaging Plate Reader (FLIPR) Tetra system (Molecular Devices). Baseline measurements were initially read before drugs were added into their respective wells (concentration and different drugs in Figure legends). The subsequent changes in relative luminescence signals (RLU) were recorded over time. Data were extracted using the integrated ScreenWorks software and subjected to non-linear least-squares regression analysis using the sigmoidal dose-response function provided in GraphPad Prism 9.0. Data of 3 or 4 independent experiments (N=3 or 4) performed in quadruplicate are presented as Relative Luminescence Units (RLU) or normalized as indicated in figure legends.

2.10 TANGO assay

HTTL (HEK293T stably expressing a luciferase reporter gene under the TRE-Tight promoter) cells, an in-house developed reporter cell line (to be published), were seeded in 6-well plates at $1.2x10^6$ cells and were transfected with Tango-ized constructs using the PEI precipitation method. Twenty hours later, the transfected cells were plated in in DMEM supplemented with 1% dialyzed FBS into PLL coated 384-well white clear bottom cell culture plates at a density of 20,000 cells/well in a total volume of 40 µL for 5 hours to ensure proper attachment of cells. Agonist solutions, previously prepared at 3X concentration in sterilized assay buffer (20 mM HEPES, 1× Hanks' balanced salt solution (HBSS), pH 7.40), were added to the cells at 20 µL per well. Following overnight incubation, media was removed and 20 µL per well of

homemade luciferase detection reagent (108 mM Tris–HCl; 42 mM Tris-Base, 75 mM NaCl, 3 mM $MgCl_2$, 5 mM Dithiothreitol (DTT), 0.2 mM Coenzyme A, 0.14 mg/ml D-Luciferin, 1.1 mM ATP, 0.25% v/v Triton X-100, 2 mM Sodium hydrosulfite) was added to all wells. After 10 minutes of incubation in the dark at room temperature, plates were read using the Hidex Sense Beta Plus microplate reader (Gamble Technologies). Data were subjected to non-linear least-squares regression analysis using the sigmoidal dose-response function provided in GraphPad Prism 9.0. Data of 3 or 4 independent experiments (n=3 or 4) performed in quadruplicate are presented as Relative Luminescence Units (RLU) or normalized as indicated in figure legends.

2.11 Immunofluorescence

HT1080 were seeded in a chambered coverslip with 8 individual wells and high walls in complete medium to obtain a 50% confluency the following day. The next day, cells were transiently cotransfected using JetPRIME (Polyplus Transfection) with ɣ-actin-V5/pLX307 or pcDNA3 and NbV5-eGFP/pcDNA3.1+. Twenty-four hours post-transfection, cells were fixed with 4% paraformaldehyde, washed and then counterstained with Hoechst 33342 stain solution. Cells were imaged on a Zeiss Axio Observer D1 fluorescence microscope at 100X, and the images were analyzed using ImageJ software.

CHAPTER III: RESULTS

In our platform, two proteins interact with each other and are referred to as "bait" and "prey." The bait is a membrane receptor from the G protein-coupled receptor (GPCR) family, and in the case of GPCRs, it can only be fused to the C-terminal. The prey protein can be any V5-tagged protein, with the tag placed at the C- or N-termini or within the protein sequence. We used β-arrestin-1 and β-arrestin-2, well-established GPCR interactors, as the prey to demonstrate this concept. The anti-V5 intrabody acts as a bridge between the V5-tagged prey protein and the bait receptor, which carries the other functional moiety. This system allows for the reconstitution of a functional cell-based assay with minimal interference with the prey protein's function and the native complex formation.

Generation of a nanobody against the V5-Tag (work done in collaboration with Hybrigenics) – A group of selective nanobodies capable of recognizing the V5-tag has been identified and chosen using the Hybribody platform. This approach combines synthetic VHHs phage-display screening and yeast two-hybrid (Y2H) techniques. The CDRs were integrated into humanized scaffolds to create the synthetic library NaLi-H1 (165). This method is advantageous as it enriches stable and soluble intracellular-targeting nanobodies. The process is illustrated in (Fig.10A-B). In the initial phase, peptide phage display was conducted against a purified HaloTag protein with a duplicate V5-tag. The VHHs selected after one round of phage display were then cloned into yeast prey vector to perform yeast-two hybrid screening (166, 167). In total, 52 different VHHs with redundancies ranging from 1 to 37 were obtained. The first 20 clones with the most redundancies were selected, and VHHs

were cloned into pcDNA3.1+ fused at the C-terminus with the TEV219. Each clone was assessed using the TANGO-based assay with the mu-opioid receptor (μ-OR) and Angiotensin II receptor type 1 (AT1R) and the β-arrestin-2 carrying either an N- or C-terminal V5-tag (V5-β-arrestin-2 and β-arrestin-2-V5, respectively). The nanobody-based TANGO assay's overall schematic is depicted in (Fig.13A). Each clone was independently tested using an increasing concentration of the μ-OR agonist DAMGO and AT1R agonist angiotensin II, as previously described (162–164). From these preliminary findings, only one clone, referred to as NbA1, showed a robust response with β-arrestin-2-V5 but a ineffective response towards V5-β-arrestin-2. It's worth noting that codon optimization for human expression of the original nanobody resulted in a 3-fold increase in expression and was selected for further experiments in human cells (Fig.10C-D).

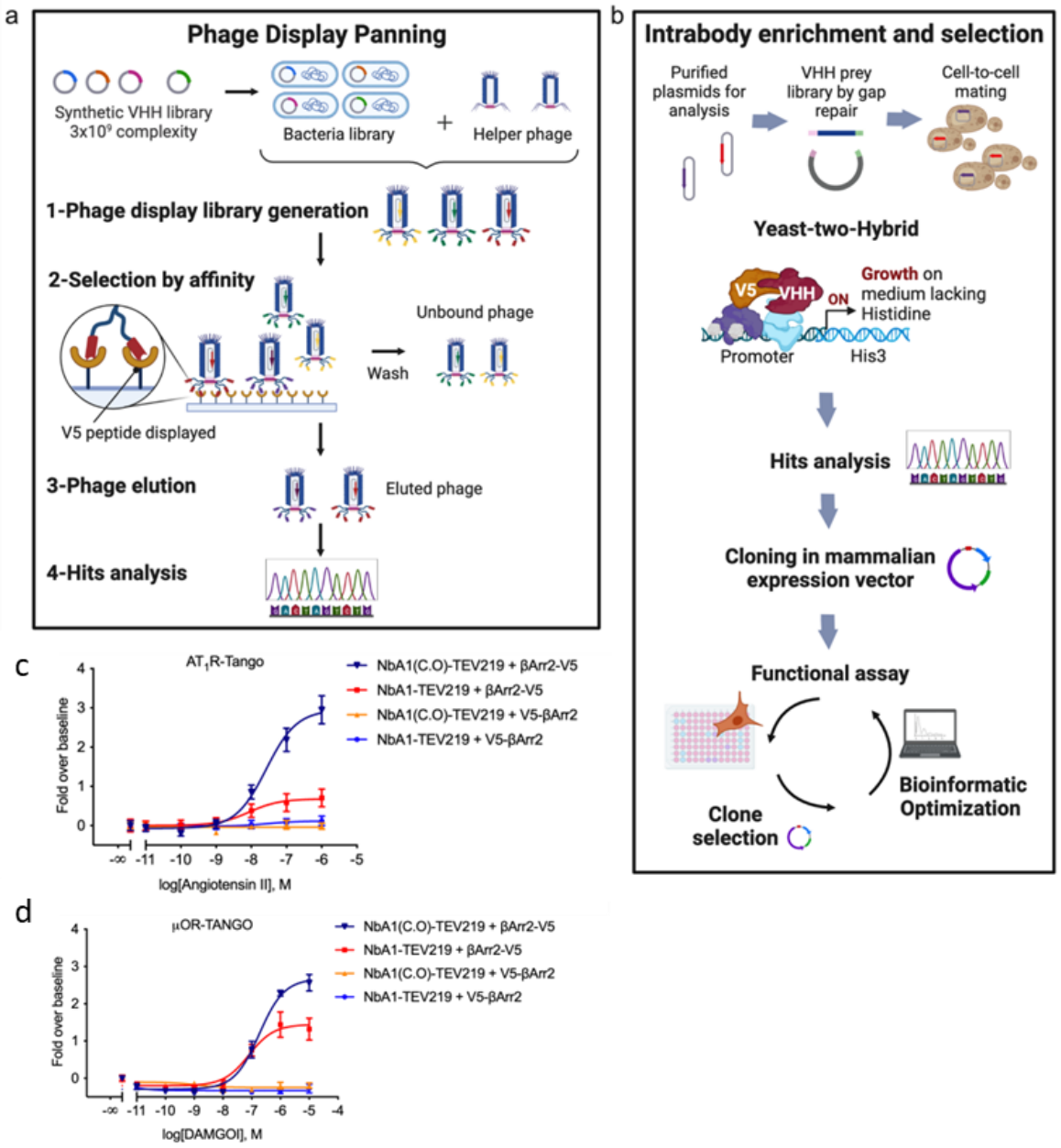
a
Phage Display Panning
Synthetic VHH library
3x10⁹ complexity
Bacteria library
+
Helper phage
1-Phage display library generation
2-Selection by affinity
Unbound phage
Wash
V5 peptide displayed
3-Phage elution
Eluted phage
4-Hits analysis
b
Intrabody enrichment and selection
Purified plasmids for analysis
VHH prey library by gap repair
Cell-to-cell mating
Yeast-two-Hybrid
V5
VHH
ON
Growth on medium lacking Histidine
Promoter
His3
Hits analysis
Cloning in mammalian expression vector
Functional assay
Bioinformatic Optimization
Clone selection
c
AT1R-Tango
NbA1(C.O)-TEV219 + βArr2-V5
NbA1-TEV219 + βArr2-V5
NbA1(C.O)-TEV219 + V5-βArr2
NbA1-TEV219 + V5-βArr2
Fold over baseline
log[Angiotensin II], M
d
μOR-TANGO
NbA1(C.O)-TEV219 + βArr2-V5
NbA1-TEV219 + βArr2-V5
NbA1(C.O)-TEV219 + V5-βArr2
NbA1-TEV219 + V5-βArr2
Fold over baseline
log[DAMGOI], M

Figure 10 Overview of the selection of a synthetic nanobody interacting with the V5-tag. A Schematic of the phage-display panning for the enrichment of nanobodies interacting with the V5-peptide tag. **B,** Schematic of the yeast-two-hybrid screening (Y2H) for the enrichment of nanobodies interacting with the V5-peptide tag in an intracellular environment (intrabody). The AT_1R-TANGO (**C**) and μ-OR-TANGO (**D**) were co-transfected with β-arrestin2 carrying a C- or N-terminal V5-peptide tag along with the NbA1(C.O)-TEV219 or NbA1-TEV219 and fusion protein. Dose-response agonist treatments demonstrate the recruitment of β-arrestin in all configurations tested. Dose-response curves were built using XY analysis and fitted using non-linear regression with the 3-parameters dose-response stimulation function. All error bars represent SD (n = 3 technical replicates) (C.O = codon optimized).

Crystal structure of the NbA1 – To improve the activity of NbA1 towards N-terminally tagged β-arrestin-2, a computer-aided affinity maturation approach was chosen. The first step was to solve the V5-bound structure of NbA1 at a resolution of 2Å (Table 1). The crystal structure, done with the help of Dr. Couture's group, showed that NbA1 folds conventionally as a V-shape IgG fold connected by a disulfide bond (168) (Fig.11A-B). The paratope responsible for V5 peptide interaction is mainly mediated by the CDR2 and CDR3 regions, which is typical for nanobodies (169) (Fig.11A-B). The V5 peptide interacts with NbA1 through several polar and hydrophobic contacts and is oriented at 90 degrees to the central axis. The V5-tag has no secondary structures, and 11 out of the 14 residues of the tag interact directly with NbA1 (Fig.11B). Data suggest that hydrophobic residues play a significant role in the interaction, indicating a strong contribution of entropic forces by the Nb:V5 interfaces (Fig. 11C). Nanobodies have greater paratope diversity compared to classical Ab VH domains, as highlighted by a recognition mode that is different from the ALFA-tag. The ALFA-tag involves contacts with all three CDRs and is oriented parallel to the central axis. Lastly, three residues (Gln57, Gly58, Asp59) within the CDR2 loop could not be modeled (Fig. 11A).

NbA1:V5	
Data collection	
Space group	P1
Cell dimensions	
a, *b*, *c* (Å)	45.4, 45.4, 70.6
α,β,γ (°)	90.0, 90.0, 97.9
Resolution (Å)	24.59 – 2.01 (2.08 – 2.01)*
R_{sym} or R_{merge}	0.034 (0.070)
$I / \sigma I$	24.2 (11.6)
Completeness (%)	95.1 (92.1)
Redundancy	2.6 (2.6)
Refinement	
Resolution (Å)	24.59 – 2.01
No. reflections	35510
R_{work} / R_{free}	19.1/23.8
No. atoms	
Protein (A/B/D/G)	926/936/928/925
V5 (E/C/F/H)	c
Water	288
B-factors (Å^2)	
Protein (E/B/C/D)	30.9/30.8/30.5/30.6
V5	28.0/28.7/29.1/29.0
Water	30.1
R.m.s. deviations	
Bond lengths (Å)	0.009
Bond angles (°)	1.136

*Values in parentheses are for the highest-resolution shell.

Table 1 Data collection and refinement statistics for NbA1 in complex with the V5 peptide.

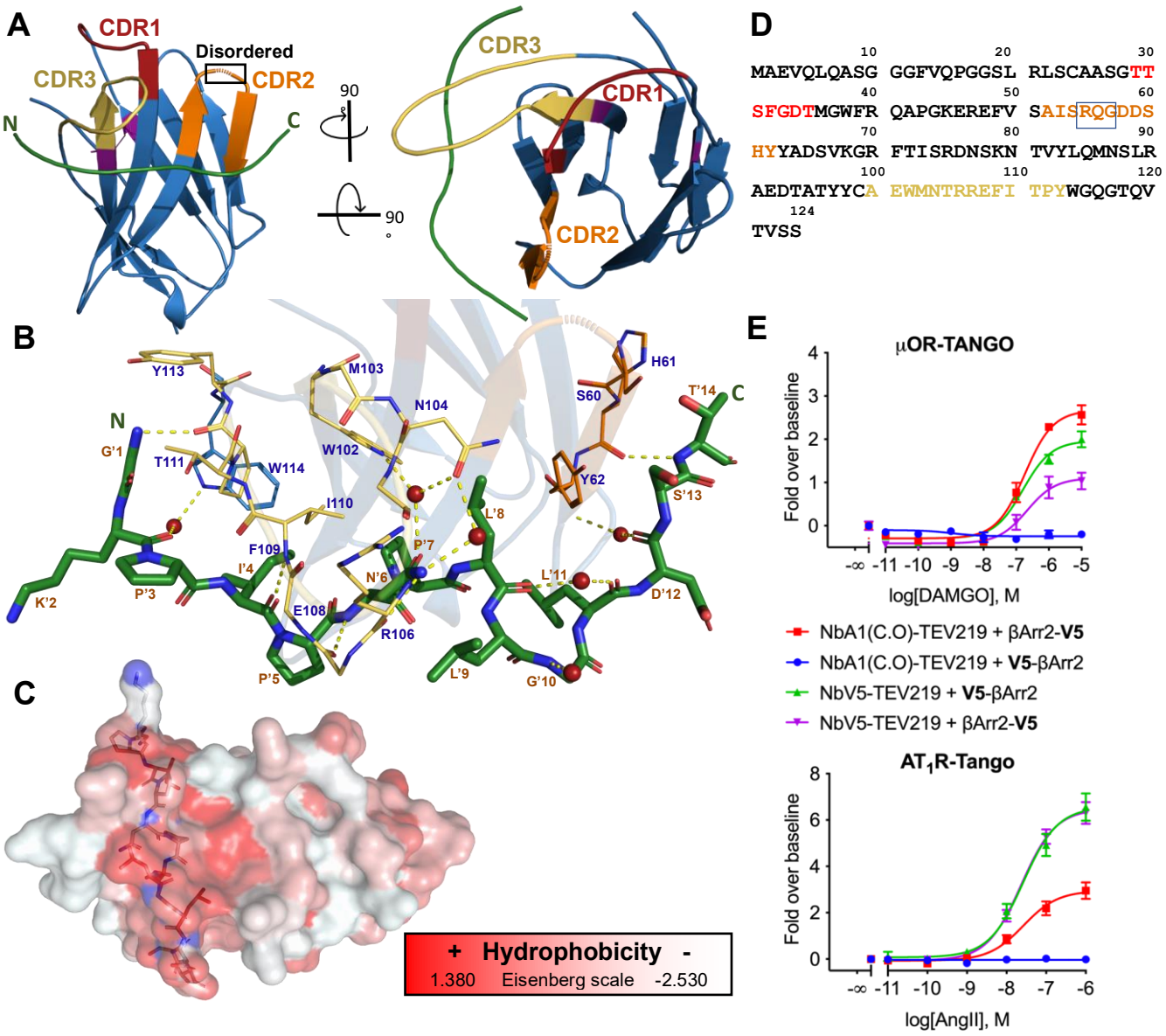
A
CDR1
Disordered
CDR3
CDR2
N
C
90
90
CDR3
CDR1
CDR2
D
10 20 30
MAEVQLQASG GGFVQPGGSL RLSCAASGTT
40 50 60
SFGDTMGWFR QAPGKEREFV SAISRQGDDS
70 80 90
HYYADSVKGR FTISRDNSKN TVYLQMNSLR
100 110 120
AEDTATYYCA EWMNTRREFI TPYWGQGTQV
124
TVSS
B
Y113
M103
N104
H61
S60
T'14
C
N
G'1
T111
W102
W114
Y62
S'13
I110
L'8
F109
P'7
I'4
N'6
L'11
K'2
P'3
D'12
E108
R106
P'5
L'9
G'10
C
+ Hydrophobicity -
1.380 Eisenberg scale -2.530
E
μOR-TANGO
Fold over baseline
log[DAMGO], M
NbA1(C.O)-TEV219 + βArr2-V5
NbA1(C.O)-TEV219 + V5-βArr2
NbV5-TEV219 + V5-βArr2
NbV5-TEV219 + βArr2-V5
AT1R-Tango
Fold over baseline
log[AngII], M

Figure 11 Structure of the NbA1 bound to the V5 peptide.
a, Overview of the NbA1-V5 peptide complex shown as cartoon representation. NbA1 is colored in blue with CDRs 1-3 colored in red, orange, and yellow, respectively. Three residues from the CDR2 were not resolved in the refined structure. **b,** Close-up view of the polar interactions within the complex including water-bridged interaction. The V5-peptide (green) is shown as stick representation with the N-terminal on the left. Interacting residues from the paratope are labeled in blue while the peptide labels are green and marked with a prime symbol. H-bonds are shown as yellow-dashed lines and water molecules as red spheres. **c,** The NbA1-V5 peptide complex shown as surface representation and colored using the color_h script based on the Eisenberg hydrophobicity scale 64. **d,** Sequence of NbA1 with CDRs 1-3 colored in red, orange, and yellow, respectively. The square highlights the RQG tripeptide that is disordered in the CDR2 loop. **e,** the initial assessment revealed that the nanobody was not well expressed in HEK293 and codon optimization (NbA1(C.O)) increased its expression and consequently its functional activity. The AT1R-TANGO and μ-OR-TANGO were co-transfected with β-arrestin1 or β-arrestin2 carrying a C- or N-terminal V5-peptide tag along with either the NbA1-TEV219, NbA1(C.O)-TEV219 or NbV5-TEV219 fusion protein. Dose-response agonist treatments demonstrate the difference between the NbA1 and NbV5 nanobodies. The NbV5 recognizes the N- or C-terminally V5-tagged β-arrestin2 with similar logistic parameters (potency and efficacy) while the original NbA1 clone only recognizes the C-terminally tagged β-arrestin2 (β-arrestin2-V5). Dose-response curves were built using XY analysis for non-linear regression curve and the 3-parameters dose-response stimulation function. All error bars represent SD (n = 3 technical replicates).

Maturation of the NbA1 – Our approach aims to aid in the study of protein-protein interactions through the use of a versatile nanobody-based sensor. Although NbA1 is functional, it exhibits a preference for the C-terminally tagged β-arrestin-2. This partiality may be due to the lack of interactions with the last two residues of V5. In silico affinity maturation was conducted using Rosetta modeling software to improve affinity. The relaxed model produced five designed mutants that were tested (Fig. 12A-B). AD-F showed promise compared to BD-F, with only one amino-acid difference in position 60 having a lysine for AD-F compared to a serine for BD-F. Ten mutants with degenerated mutations were synthesized and tested in a TANGO assay. Based on the functional evaluation, it was found that two mutations (delta59 and S60K) resulted in better activity compared to NbA1, particularly for the N-terminal V5-tagged arrestin. Consequently, an optimized nanobody, called NbV5, was created with only those two mutations. The maturated NbV5 exhibited a significant improvement in overall behavior in our functional TANGO assay (Fig.12C) and was selected for future development. Our biosensor platform was initially characterized with GPCRs, which allowed for the regulation of interaction using an agonist, thus providing a better approach to measuring the efficiency of our biosensor approach. Subsequent demonstrations were conducted using two divergent GPCRs, the angiotensin II receptor (AT1R) and the mu-opioid receptor (μ-OR), which are widely used receptors in our lab, to characterize the NbV5-based biosensors.

a

```
NbV5A1          MAEVQLQASGGGFVQPGGSLRLSCAASGTTSFGDTMGWFRQAPGKEREFVSAISRQGDDS   60
NbV5A-DF        MAEVQLQASGGGFVQPGGSLRLSCAASGTTSFGDTMGWFRQAPGKEPEFVSAISRQGDDK   60
NbV5B-DF        MAEVQLQASGGGFVQPGGSLRLSCAASGTTSFGDTMGWFRQAPGKEPEFVSAISRQGDDD   60
                ************************************************ ************.

NbV5A1          HYYADSVKGRFTISRDNSKNTVYLQMNSLRAEDTATYYCAEWMNTRREFITPYWGQGTQV   120
NbV5A-DF        QYYADSVKGRFTISRDNSKNTVYLQMNSLRAEDTATYYCAEWMNTNDEYIVPYWGQGTQV   120
NbV5B-DF        QYYADSVKGRFTISRDNSKNTVYLQMNSLRAEDTATYYCAEWMNTNDEYIVPYWGQGTQV   120
                :************************************************. *:*.*********

NbV5A1          TVSS        124
NbV5A-DF        TVSS        124
NbV5B-DF        TVSS        124
```

b

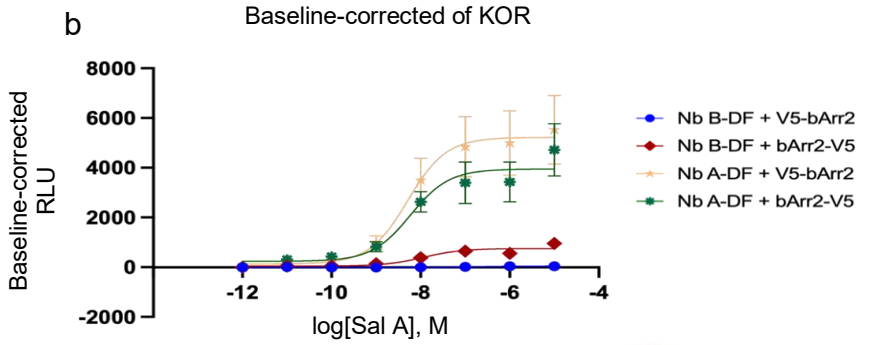

c

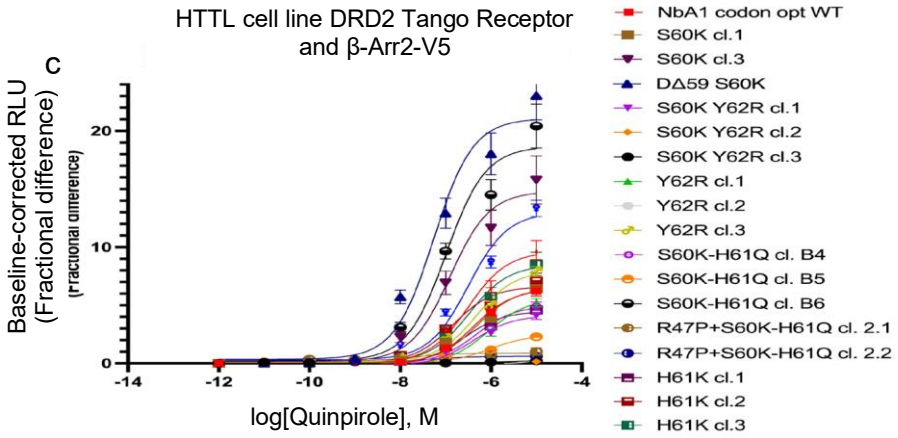

Figure 12 Effect of mutations on NbA1.
A, sequence of two mutants obtained via maturation of the NbA1 focused on the three CDRs with only one amino acid difference at position 60. **B**, The Nb B-DF and A-DF were fused with the TEV219 protease were transfected in HEK293T cells. Dose-response agonist treatments demonstrate the recruitment of β-arrestin in all configurations tested, and dose-response curves were built using XY analysis and fitted using non-linear regression and the 3-parameters dose-response stimulation function. All error bars represent SD (n = 3 technical replicates). **C**, Mutants targeting the position 60 fused with TEV219 were transfected in HEK293T cells. Dose-response agonist treatments demonstrate the recruitment of β-arrestin in all configurations tested, and dose-response curves were built using XY analysis for non-linear regression curve and the 3-parameters dose-response stimulation function. All error bars represent SD (n = 3 technical replicates).

TANGO – We used the protease-dependent TANGO assay as our primary method to evaluate our nanobody in the tripartite system. TANGO was chosen due to its high sensitivity and permissibility. Our nanobody was further characterized at the μ-OR and AT1R, showing a dose-response curve with both β-arrestin-1 and -2, as well as in both configurations with respect to the position of the V5-tag (Fig.13). It is worth mentioning that the EC50 is comparable to our updated TANGO assay with the TEV219 directly fused at the C-terminus of the β-arrestins (170). These findings support the suitability of our NbV5-based biosensors for use with the TANGO-based assay.

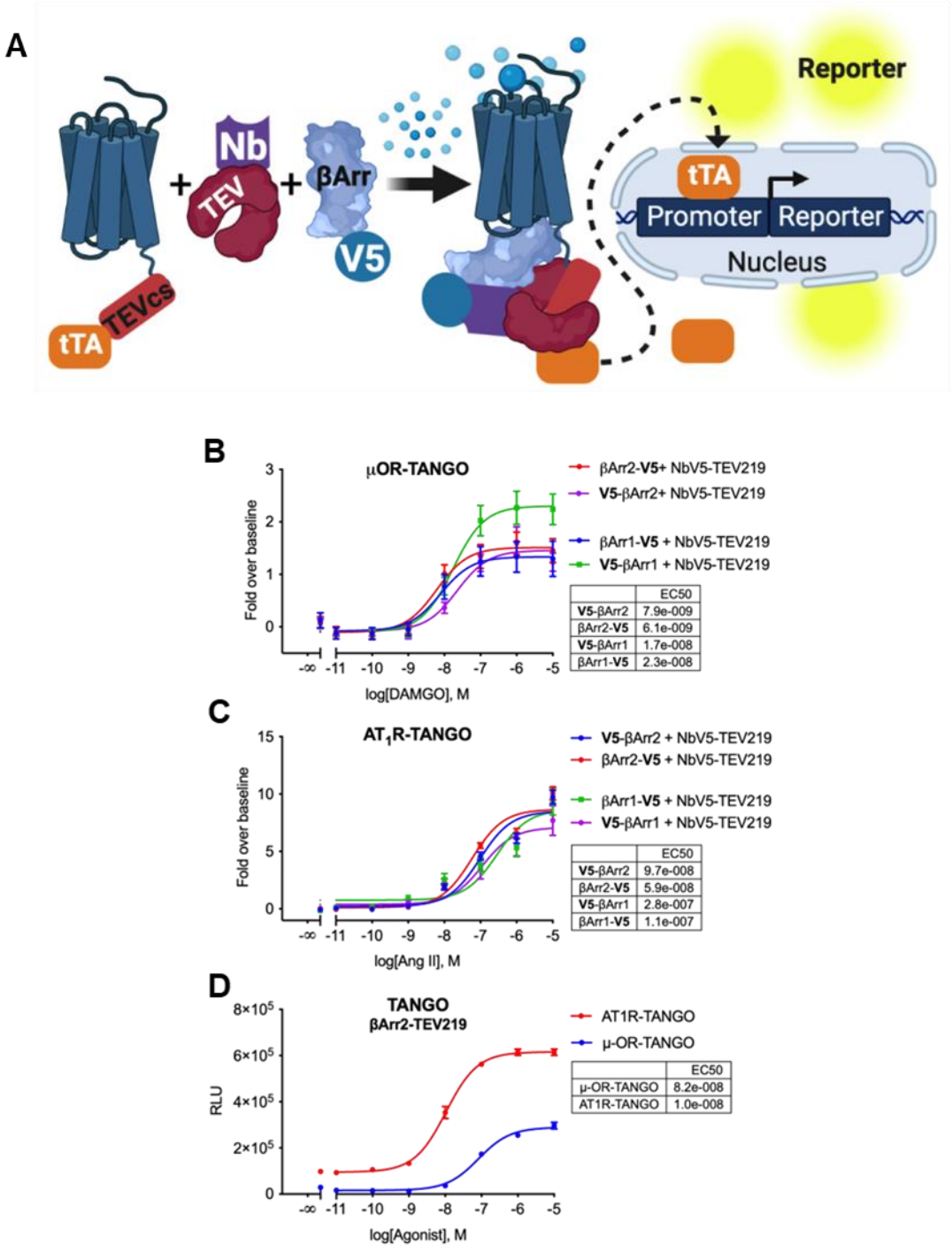
A
Reporter
Nb
TEV
βArr
V5
tTA
TEVcs
tTA
Promoter
Reporter
Nucleus
B
μOR-TANGO
Fold over baseline
log[DAMGO], M
βArr2-V5+ NbV5-TEV219
V5-βArr2+ NbV5-TEV219
βArr1-V5 + NbV5-TEV219
V5-βArr1 + NbV5-TEV219
EC50
V5-βArr2 7.9e-009
βArr2-V5 6.1e-009
V5-βArr1 1.7e-008
βArr1-V5 2.3e-008
C
AT1R-TANGO
Fold over baseline
log[Ang II], M
V5-βArr2 + NbV5-TEV219
βArr2-V5 + NbV5-TEV219
βArr1-V5 + NbV5-TEV219
V5-βArr1 + NbV5-TEV219
EC50
V5-βArr2 9.7e-008
βArr2-V5 5.9e-008
V5-βArr1 2.8e-007
βArr1-V5 1.1e-007
D
TANGO
βArr2-TEV219
RLU
log[Agonist], M
AT1R-TANGO
μ-OR-TANGO
EC50
μ-OR-TANGO 8.2e-008
AT1R-TANGO 1.0e-008

Figure 13 NbV5 as a versatile nanobody-based biosensor: application in protease-dependent cell-based assay (TANGO).

A, Schematic of the protease-dependent cell-based assay (TANGO) used to assay the anti-V5 nanobodies. The original NbA1 clone selected from the Y2H screening was fused with the TEV219 protease and cloned into a eukaryotic expression vector. The initial assessment revealed that the nanobody was not well expressed in HEK293, and codon optimization (NbA1(C.O)) increased its expression and consequently its functional activity. The μ-OR-TANGO (**B**) and AT_1R-TANGO (**C**) were co-transfected with β-arrestin1 or β-arrestin2 carrying a C- or N-terminal V5-peptide tag along with the NbV5-TEV219 fusion protein. Dose-response agonist treatments demonstrate the recruitment of β-arrestin in all configurations tested. (**D**) The μ-OR-TANGO and AT_1R-TANGO were co-transfected with β-arrestin2-TEV219 and stimulated with agonists showing that EC50 obtained using the original TANGO is similar to the NbV5-adapted TANGO. Dose-response curves were built using XY analysis and fitted using the non-linear regression and the 3-parameters dose-response stimulation function. All error bars represent SD (n = 3 technical replicates).

BRET – In our NbV5-based biosensor toolkit, we adapted the BRET functional assay, which proved to be a common approach. To ensure accurate results, we compared the β-arrestin-1 and β-arrestin-2 fused at the N- or C-terminus with the V5-tag. We also included the ALFA-tag as a reference, which has been previously characterized and works well with all tag placements (N-term, C-term, and internal) illustrating that all configurations produced strong signals (Fig. 14). However, the NbV5-GFP2 with a C-terminal tag gave a better BRET2 ratio, while the NbALFA showed less impact. The NbALFA's binding mode is at a 90-degree angle compared to NbV5, which could explain this observation. Notably, the tag placement on the prey protein did not significantly affect the tested receptor-β-arrestin coupling. Specifically, for AT1R, both β-arrestin isoforms were well recruited with a slight preference for β-arrestin-2 in this assay. Overall, our NbV5-based biosensors are ideal for use with BRET assays.

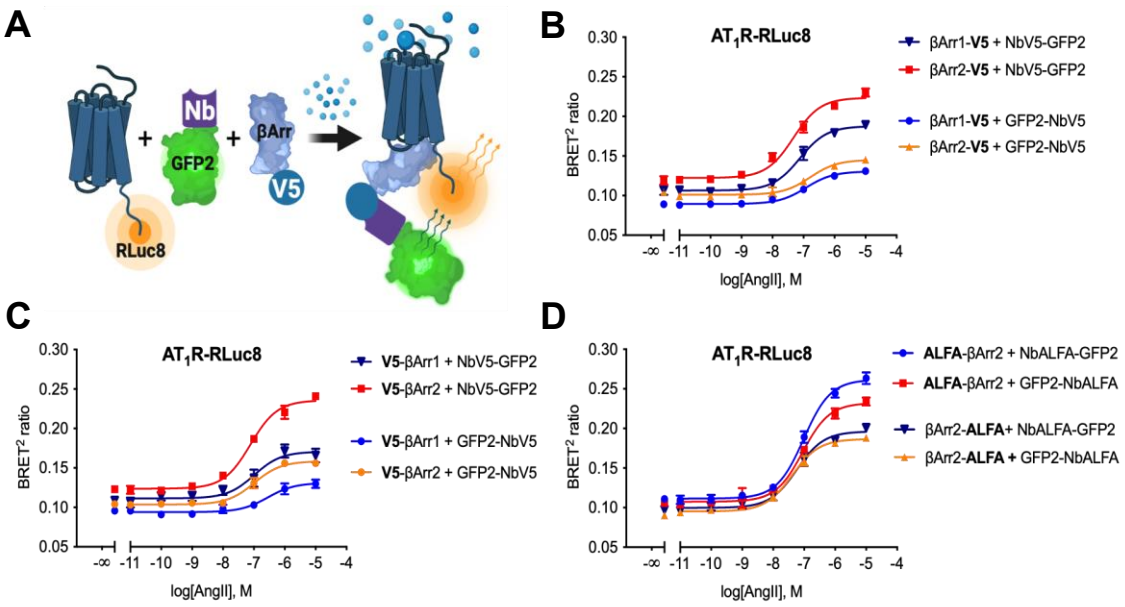
A
Nb
GFP2
βArr
V5
RLuc8
B
AT1R-RLuc8
BRET2 ratio
log[AngII], M
βArr1-V5 + NbV5-GFP2
βArr2-V5 + NbV5-GFP2
βArr1-V5 + GFP2-NbV5
βArr2-V5 + GFP2-NbV5
C
AT1R-RLuc8
BRET2 ratio
log[AngII], M
V5-βArr1 + NbV5-GFP2
V5-βArr2 + NbV5-GFP2
V5-βArr1 + GFP2-NbV5
V5-βArr2 + GFP2-NbV5
D
AT1R-RLuc8
BRET2 ratio
log[AngII], M
ALFA-βArr2 + NbALFA-GFP2
ALFA-βArr2 + GFP2-NbALFA
βArr2-ALFA+ NbALFA-GFP2
βArr2-ALFA + GFP2-NbALFA

Figure 14 NbV5 as a versatile nanobody-based biosensor: application in Bioluminescence Resonance Energy Transfer (BRET2).

A, Schematic of the BRET2 cell-based assay used to evaluate the NbV5. The recruitment of the β-arrestin-NbV5-GFP2 complex to the receptor fused to RLuc8 allows the energy transfer between the Renilla reniformis Luciferase mutant (RLuc8) and the green fluorescence protein mutant GFP2 in the presence of the RLuc8 substrate Coelenterazine 400a. **B-D,** NbV5-based detection of β-arrestin1 and β-arrestin2 recruitment at the AT1R-RLuc8. N- and C-terminally V5-tagged β-arrestins were tested as well as both N- and C-terminally GFP2-tagged NbV5. Dose-response curve treatment with angiotensin II reveals equivalent recruitment of β-arrestin1 and 2 at the AT1R. No major differences were observed between the N- and C-terminally V5-tagged β-arrestin, whereas the C-terminally GFP2-tagged NbV5 (NbV5-GFP2) showed better response. **D,** Similar results were obtained with the ultra-potent nanobody that recognizes the synthetic ALFA-tag (NbALFA). Dose-response curves were built using XY analysis and fitted using non-linear regression and the 3-parameters dose-response stimulation function. All error bars represent SD (n = 3 technical replicates).

NanoBiT – We have introduced our nanobody biosensors for the nanoluciferase binary complementation technique. We compared different configurations for β-arrestins (V5-β-arrestin and β-arrestin-V5) and nanobody fusions (Nbs-LgBiT and LgBiT-Nbs) (Fig. 15). The LgBiT-NbV5 produced a better response compared to NbV5-LgBiT, indicating the importance of testing both orientations for optimum response and sensitivity. Using NanoBiT, we found that β-arrestin-1 is preferred over β-arrestin-2 at the AT1 receptor (Fig.15B-D). Similar results were obtained with the ALFA-tag system, indicating that the tag system does not affect the results. For the μ-OR, we co-transfected the GPCR kinase 2 (GRK2), known to increase β-arrestins recruitment for this receptor (Fig.15-16). We found that β-arrestin-1 is favored over β-arrestin-2 for μ-OR and that the N-terminally V5-tag β-arrestins and N-terminal LgBiT-NbV5 are the optimal orientations for this receptor (Fig. 15E-G).

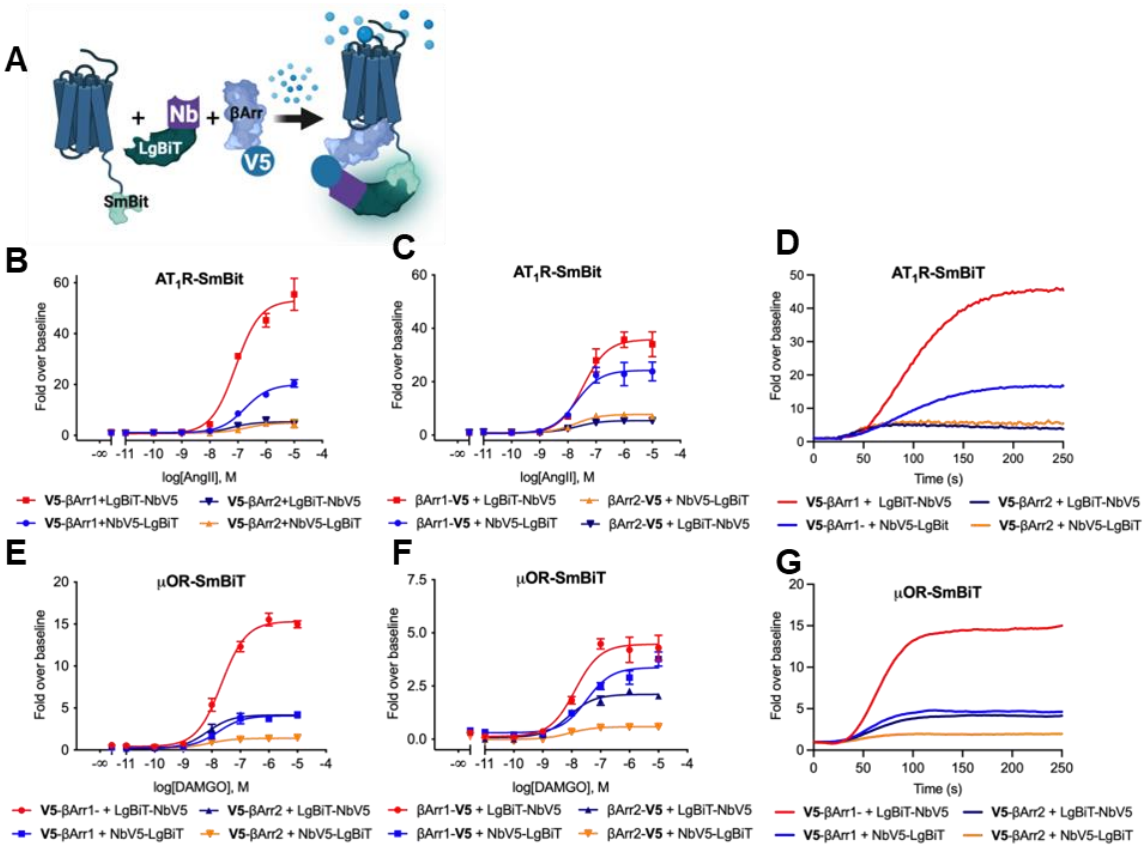
A
Nb
βArr
LgBiT
V5
SmBit
B
AT1R-SmBit
Fold over baseline
log[AngII], M
V5-βArr1+LgBiT-NbV5
V5-βArr2+LgBiT-NbV5
V5-βArr1+NbV5-LgBiT
V5-βArr2+NbV5-LgBiT
C
AT1R-SmBit
log[AngII], M
βArr1-V5 + LgBiT-NbV5
βArr2-V5 + NbV5-LgBiT
βArr1-V5 + NbV5-LgBiT
βArr2-V5 + LgBiT-NbV5
D
AT1R-SmBiT
Time (s)
V5-βArr1 + LgBiT-NbV5
V5-βArr2 + LgBiT-NbV5
V5-βArr1- + NbV5-LgBit
V5-βArr2 + NbV5-LgBiT
E
μOR-SmBiT
log[DAMGO], M
V5-βArr1- + LgBiT-NbV5
V5-βArr2 + LgBiT-NbV5
V5-βArr1 + NbV5-LgBiT
V5-βArr2 + NbV5-LgBiT
F
μOR-SmBiT
log[DAMGO], M
βArr1-V5 + LgBiT-NbV5
βArr2-V5 + LgBiT-NbV5
βArr1-V5 + NbV5-LgBiT
βArr2-V5 + NbV5-LgBiT
G
μOR-SmBiT
Time (s)
V5-βArr1- + LgBiT-NbV5
V5-βArr2 + LgBiT-NbV5
V5-βArr1 + NbV5-LgBiT
V5-βArr2 + NbV5-LgBiT
H
α
β
γ
V5
Nb
LgBiT
SmBit
I
μOR + GαoA-iV5 + Gβ3 + SmBiT-Gγ2
Baseline-corrected
log[DAMGO], M
NbV5-LgBiT
LgBiT-NbV5

Figure 15 NbV5 as a versatile nanobody-based biosensor: application in *Nano*luciferase *Bi*nary *T*echnology (NanoBiT).

A, Schematic of the NanoBiT cell-based assay used to evaluate the NbV5. NbV5-based detection of β-arrestin1 and β-arrestin2 recruitment at the AT_1R-SmBiT (**B,C,D**) and μ-OR-SmBiT (**E,F,G**) was assayed. N- and C-terminally V5-tagged β-arrestin was tested as well as both N- and C-terminally LgBiT-tagged NbV5. (**D,G**), Live kinetic traces at 1 μM agonist are shown in (**D**) for the AT1R and (**G**) for the μ-OR. The trace represents the mean of a quadruplicate experiment. **H**, Schematic of the NanoBiT cell-based assay used to assess the internal V5-tag. **I**, Functional recognition of an internal localized V5-tag was also assayed by NanoBiT by incorporating the V5-tag at position 92 of the GαoA (GαoA-iV5) and measuring the dissociation from the Gβ3 and SmBiT-Gɣ2 dimer upon μ-OR activation with DAMGO. (**B,C,E,F,I**), Dose-response curves were built using XY analysis and fitted using non-linear regression and the 3-parameters dose-response stimulation function. All error bars represent SD (n = 3 technical replicates).

We evaluated the ability of NbV5 to recognize an internally positioned V5-tag using the inhibitory G protein GαoA with the V5-tag inserted at position 92. It is well established that inhibitory G proteins tolerate insertion at this position, commonly used to insert a fluorescent protein or RLuc8 for BRET experiments (171) (Fig. 15H-I). We fused SmBiT at the N-terminus of the Gγ2 subunit and co-expressed it with Gβ3, assembling to make the obligatory Gβγ dimer, which interacts with the inactive GDP-bound GαoA. Once activated by the Gαi/o-coupled μ-OR, the activation of the G protein can be detected through the dissociation of the heterotrimer (Fig. 15H-I). Our Nb-based sensor allows the measurement of G protein activation by inserting the V5 sequence, which minimizes the possibility of affecting overall G protein regulation. We have found that internally-inserted NanoBiT complementary subunits are not well tolerated, which is an advantage of using our V5-tagged biosensors based on prior experiments performed in our laboratory.

In traditional assays, larger tags like GFP2, RLuc, or TEV219 are used and attached to the prey proteins. However, we sought to investigate the impact of a larger tag fusion to β-arrestin with the NbALFA:ALFA-tag system. Our assumption was that the rigidity of the ALFA-tag combined with including a proline before and after the tag would reduce its steric effect. The NanoBiT results (Fig. 15) differed from those obtained in BRET2 (Fig. 14) in various ways. We observed a preference for β-arrestin1 recruitment over β-arrestin2 and a significant positional effect depending on the tag location. To investigate the effect of adding GFP2 to β-arrestin and its recruitment at the receptor, we tested β-arrestin2-ALFA and β-arrestin2-ALFA-GFP2 at both AT1R and μ-OR. We also co-expressed the G protein-coupled receptor kinase 2 (GRK2) to

achieve reasonable recruitment at the μ-OR, since its expression levels are none in HEK293 cells (171). Our findings (Fig.16D-E) revealed that β-arrestin recruitment significantly increased at the μ-OR in the presence of GRK2, but the GFP2 tag had a strong detrimental effect compared to that observed with AT1R in (Fig. 16D-E). We concluded that the bulkiness of the tag has an unpredictable effect that depends on the bait:prey pair used and should be avoided as much as possible. Therefore, using a tag system such as NbV5:V5 should minimize the potential effect. The NanoBiT assay offers the ease of performing a live experiment, which can be used for endpoint assays on a microplate reader as in (Fig.16B-D), a real-time kinetic reader can reveal more information. With GPCRs, kinetic experiments and appropriate models should be favored to study signaling in non-equilibrium conditions (172). In (Fig. 16C-E), we conducted a live kinetics experiment that examined the recruitment of β-arrestin-ALFA versus β-arrestin-ALFA-GFP2 at the μ-OR and AT1R in the presence and absence of GRK2, using a single concentration of selective agonist. As previously reported, the expression of GRK2 has opposite effects at the AT1R and μ-OR (173), with an increase in efficacy and potency at μ-OR and a decrease in these parameters at AT1R. The endpoint experiment accurately represented the latter, but the live experiment revealed that GRK2 expression significantly increases the rate of β-arrestin recruitment at μ-OR, reaching a steady state that remains relatively stable over time.

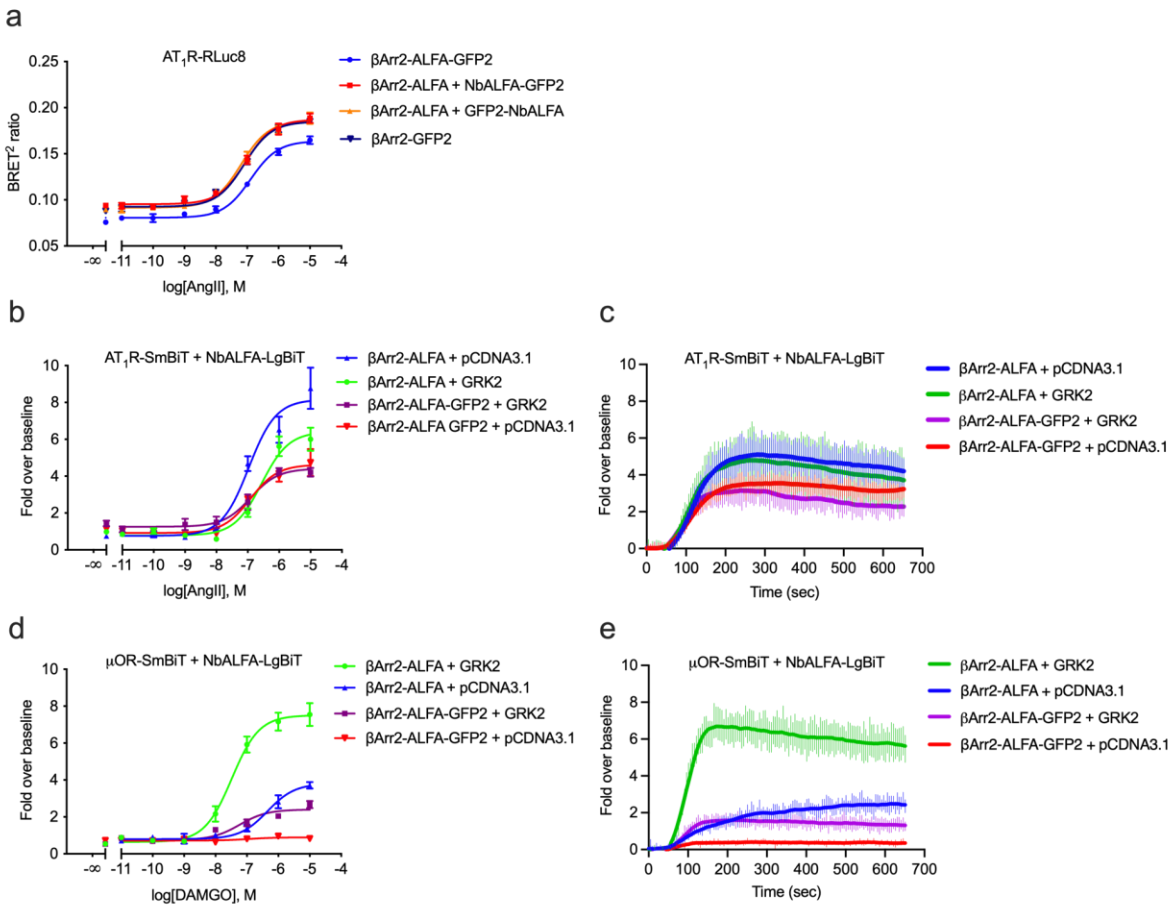
a
AT1R-RLuc8
βArr2-ALFA-GFP2
βArr2-ALFA + NbALFA-GFP2
βArr2-ALFA + GFP2-NbALFA
βArr2-GFP2
BRET2 ratio
log[AngII], M
b
AT1R-SmBiT + NbALFA-LgBiT
βArr2-ALFA + pCDNA3.1
βArr2-ALFA + GRK2
βArr2-ALFA-GFP2 + GRK2
βArr2-ALFA GFP2 + pCDNA3.1
Fold over baseline
log[AngII], M
c
AT1R-SmBiT + NbALFA-LgBiT
βArr2-ALFA + pCDNA3.1
βArr2-ALFA + GRK2
βArr2-ALFA-GFP2 + GRK2
βArr2-ALFA-GFP2 + pCDNA3.1
Fold over baseline
Time (sec)
d
μOR-SmBiT + NbALFA-LgBiT
βArr2-ALFA + GRK2
βArr2-ALFA + pCDNA3.1
βArr2-ALFA-GFP2 + GRK2
βArr2-ALFA-GFP2 + pCDNA3.1
Fold over baseline
log[DAMGO], M
e
μOR-SmBiT + NbALFA-LgBiT
βArr2-ALFA + GRK2
βArr2-ALFA + pCDNA3.1
βArr2-ALFA-GFP2 + GRK2
βArr2-ALFA-GFP2 + pCDNA3.1
Fold over baseline
Time (sec)

Figure 16 Effect of tag size on β-arrestin recruitment in BRET2 and NanoBiT assays.

To assess the effect of a larger tag on the activity of β-arrestin2 recruitment at the AT1R, β-arrestin2-ALFA was compared against β-arrestin2-ALFA-GFP2. **a,** NbALFA-based detection of β-arrestin2 recruitment at the AT1R-RLuc8 was assayed in BRET2, with no difference being observed in this configuration. NbALFA-based detection of β-arrestin2 recruitment was then assayed in NanoBiT at the AT1 (**b,c**) and μ-opioid (**d,e**) receptors in the presence and absence of GRK2. The addition of GFP2 tag decreases β-arrestin2 at AT1R but also abolishes the cooperative effect of GRK2. A similar observation was made for the μ-OR but with more amplified phenotype. GRK2 has a strong cooperative effect on β-arrestin2 recruitment at the μ-OR. GFP2 almost completely abolishes β-arrestin2 recruitment at the μ-OR in the absence of GRK2 and strongly reduces the efficacy and potency in the presence of GRK2. Live kinetic trace at 1 μM agonist are shown in (**c**) for the AT1R and (**e**) for the μ-OR. GRK2 expression increases the rate of β-arrestin2 recruitment at μ-OR while having modest or no effect at AT1R. Dose-response curves were built using XY analysis for non-linear regression curve and the 3-parameters dose-response stimulation function. All error bars represent SD (n = 3 technical replicates).

Nanobodies as fluorescence trackers for microscopy

Our next objective was to investigate the potential of using the NbV5 fused with a constitutive fluorescent protein, such as eGFP, as a genetically-encoded tracker. To achieve this, we co-expressed γ-actin, carrying a C-terminal V5 tag (γ-actin-V5), with the NbV5-eGFP fusion protein. As depicted in (Fig. 17), the NbV5-eGFP diffuses throughout the cell in the absence of γ-actin-V5 but associates with it in its presence. Notably, various actin-related structures, such as stress fibers and lamellipodia, can be observed, implying that the NbV5-eGFP can efficiently interact with dynamic proteins, such as γ-actin, without disrupting their natural localization. Consequently, the NbV5 can be utilized as a tool for tracking protein remodeling or trafficking in live-cell-based experiments.

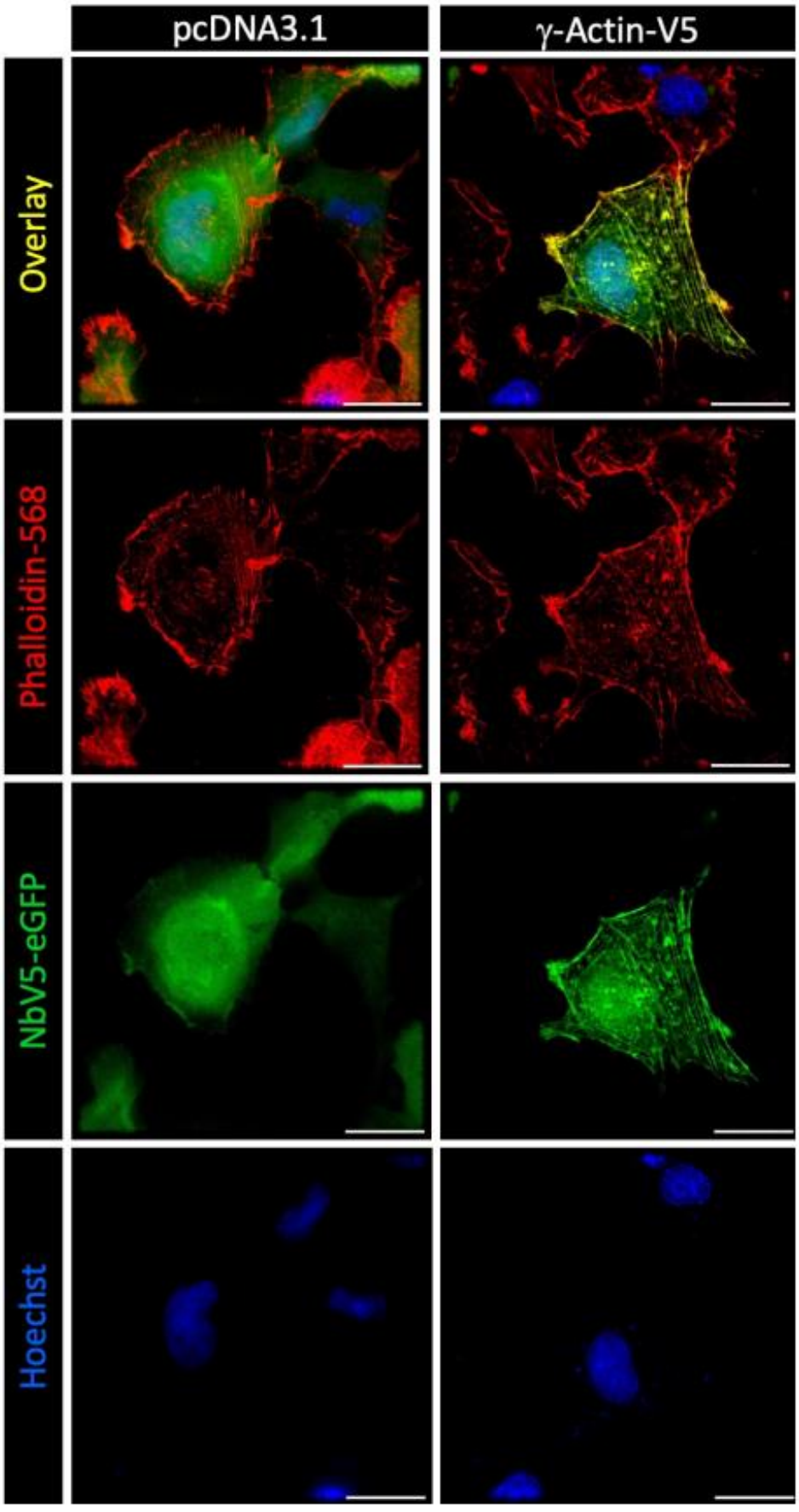
pcDNA3.1
γ-Actin-V5
Overlay
Phalloidin-568
NbV5-eGFP
Hoechst

Figure 17 NbV5-based detection of V5-tagged proteins by cell imaging.
Fluorescence imaging of HT1080 cells expressing NbV5-eGFP and ɣ-Actin-V5 or pcDNA3.1+ as a negative control. In the absence of ɣ-Actin-V5, NbV5-eGFP (green) is diffuse throughout the cell, while in the presence of ɣ-Actin-V5, NbV5-eGFP is enriched in actin-rich protrusions and structures. Cells were co-stained with the F-actin probe Alexa Fluor 568 phalloidin (red) and the blue DNA stain Hoechst. The overlay is shown on the top panel. Images are representative of 25 cells from three independent experiments. Scale bars are 25 µm.

CHAPTER IV: PRELIMINARY DATA

Nanobodies to study basal level interactions of G proteins.

The subsequent phase of our research involved the application of the nanobody within our laboratory's field of study. To validate its effectiveness, we sought to juxtapose it with the most recent data we had acquired (as depicted in Fig. 18A). The data indicated that the GαoA is present at the receptor in the inactive state using the G protein-LgBiT, a finding that was not observed with other G proteins. This observation was successfully replicated using the nanobody system (as shown in Fig. 18B), thereby reinforcing the potential utility of the nanobody in various studies. Currently, we are employing NbV5 to investigate the basal level of G proteins, a level that is comparable to that of the G protein-LgBiT. Our exploration of the concept of an inhibitory G protein (GαoA) associated with the inactive form of the receptor offers a fresh perspective in this field. We are eagerly anticipating the testing of over 400 GPCR-tagged V5 in the near future and have already begun testing a few receptors, with some promising results that we look forward to sharing soon. However, these findings have prompted us to question why GαoA is the sole G protein recruited to the inactive receptor, especially considering that many research groups are more focused on the difference between Gi and Go inhibitory proteins. GαoA and GαoB are products of alternative splicing and primarily differ in the C-terminus of the protein sequence (174). To gain a deeper understanding of the uniqueness of GαoA, we are currently conducting research in our laboratory to study the difference between GαoA and GαoB at the basal level, as previously described, but also by examining various pathways such as interactions with the GPCRs, interaction with GIRKs, and

others(175). Our objective is to comprehend the rationale behind their divergent interaction patterns, and we are also attempting to investigate this by creating mutants of these two intriguing G proteins. This endeavor will not only enhance our understanding of these proteins but also contribute significantly to the broader scientific community. In a more long-term view, the NbV5 will be used to interrogate the proximal interactome of the MOR, GαoA, and the MOR- GαoA complex using the genome-wide ORF library. This functional proteomics assay is under development but will use the NbV5 developed during my master's degree as the bridge between the V5-tag encoded protein from the library and the interrogated target (MOR, GαoA, MOR- GαoA).

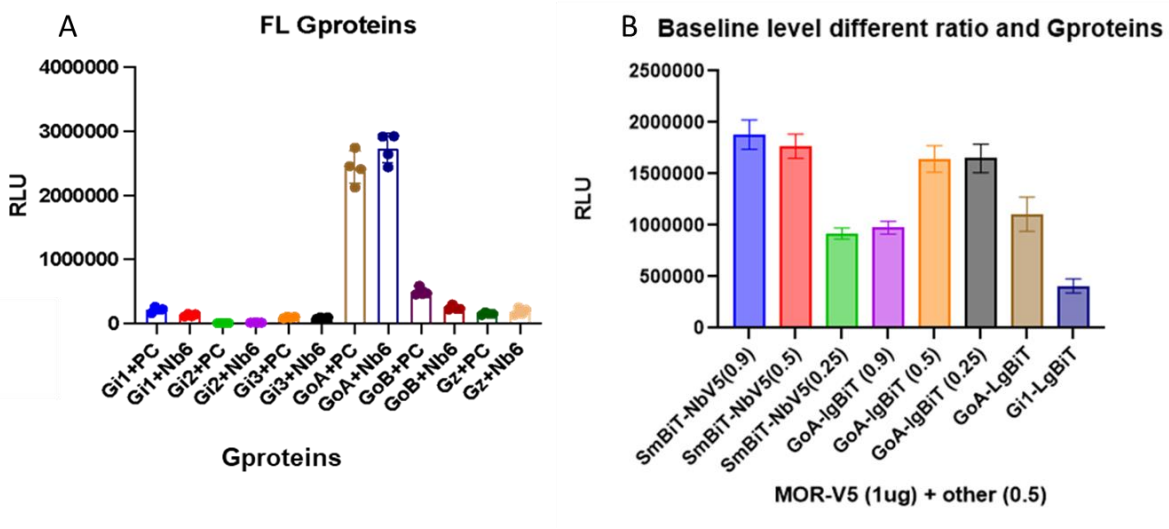
A
FL Gproteins
RLU
4000000
3000000
2000000
1000000
0
Gi1+PC
Gi1+Nb6
Gi2+PC
Gi2+Nb6
Gi3+PC
Gi3+Nb6
GoA+PC
GoA+Nb6
GoB+PC
GoB+Nb6
Gz+PC
Gz+Nb6
Gproteins
B
Baseline level different ratio and Gproteins
RLU
2500000
2000000
1500000
1000000
500000
0
SmBiT-NbV5(0.9)
SmBiT-NbV5(0.5)
SmBiT-NbV5(0.25)
GoA-lgBiT (0.9)
GoA-lgBiT (0.5)
GoA-lgBiT (0.25)
GoA-LgBiT
Gi1-LgBiT
MOR-V5 (1ug) + other (0.5)

Figure 18 Interaction level of G protein with the inactive receptor.
A, Baseline levels of interaction between Gproteins-LgBiT and μ-OR-SmBiT (**B**) NbV5-based detection of GoA-LgBiT recruitment at the μ-OR-V5 with the addition of NbV5-SmBiT. (**A-B**) The experiment was done via co-transfection of different plasmids and read on the Hidex reader for luminescence levels.

CHAPTER V: DISCUSSION

In this report, we discuss the creation and analysis of a V5-tag nanobody and a series of versatile, nanobody-based biosensors for intracellular use. The goal of our approach was to prevent the need for attaching a large, functionalized tag to a protein. Instead, we aimed to utilize a freely available genome-wide library of C-terminally V5-tagged ORFs. The V5-epitope is a well-established peptide tag that has been utilized for over three decades. At physiological pH, the 14-mer peptide has no net charge. Although it lacks any predicted secondary structures, it possesses a well-organized core because of the existence of three prolines. This intrinsic rigidity is believed to reduce the multidimensionality of the conformational landscape, thus minimizing the impact of environmentally-induced secondary structures and unpredictable behaviour in solution. Over time, various peptide tags have been developed, each with its own advantages and disadvantages. However, only a few tag systems have functional intrabodies that are fully characterized, as demonstrated in this study. The NbALFA:ALFAtag is the only well-characterized tag system currently available on the market, although it is worth noting that it is an artificial peptide tag. Although ALFA performs well, it is not an open-source resource, which may limit its further utilization. Additionally, the inflexible helical structure of the ALFA tag may potentially affect the local secondary structures inside cells. One could take advantage of having two distinct tag systems by implementing both tags simultaneously.

In the field of biotechnologies, it is common to require information about cellular components such as their abundance, localization, and dynamic interactions. This information is crucial for characterizing and validating potential drug targets, as well

as for understanding physiological and pathophysiological cellular processes(176). The creation of traceable proteins that can be monitored within cells is essential for both endpoint analysis and real-time diagnostics. This is especially important given the growing need for a more comprehensive understanding of cellular processes, and the potential to expand the use of intracellular tracers to a genome-wide or even (omics)-wide scale

Most nanobodies currently available were created through animal immunization, but there is significant potential in the development of synthetic in vitro platforms, as demonstrated here (165, 177). The Hybribody approach combines peptide phage-display and intracellular yeast-two-hybrid for further enrichment of potential intrabodies. Therefore, the selection of Nbs wherein the paratope folding does not rely on disulfide bonds is crucial for the discovery of potential intrabodies.

Through screening, a number of potential nanobodies were identified, with clone NbA1 proving to be the most effective as an intrabody. However, initial tests showed that all nanobodies had low expression levels, which was resolved by optimizing the codons for a human expression system. Based on the results of the TANGO cell-based assay, it was determined that NbA1 was not the most effective in recognizing the N-terminal V5-tag. As a result, the NbA1 was isolated from the periplasm of SHUFFLE bacteria, which are particularly adept at purifying proteins that contain disulfide bonds. The purified NbA1 was co-crystallized with the V5-tag and the resulting structure was utilized for computer-aided maturation to produce the final optimized NbV5, which exhibited improved functionality in vitro. The maturation process was limited to the three CDRs, and no mutations were identified that could significantly alter the binding energy. Based on the mutants tested in TANGO, it was

discovered that NbV5-AD-F had a similar impact as the codon-optimized version with a C-terminally attached V5-tag, but it was capable of interacting with the V5-tag on the N-terminal end. Additionally, it was observed that NbV5-BD-F, despite having the same sequence as AD-F except for a Lys at position 60, was unable to interact with the V5-tag on the N-terminal end due to its original Ser. After careful consideration, mutations were made on the region in question, resulting in extensive point mutation and ultimately leading to the creation of NbV5. The most notable improvement of NbV5, in comparison to NbA1, is its enhanced interaction with N-terminally positioned V5-tag. (Fig 12C). The two mutations were found to be juxtaposed wherein the Asp^{59} is removed and the Ser^{60} is mutated to Lys (ΔD^{59},$S^{60}K$) (Fig. 12C). It is possible that the removal of one residue in the vicinity of a disordered loop in the CDR2 and the presence of Lys^{60} could lead to the stabilization of this region. The formation of intramolecular H-bonds within the CDR2 loop by Lys^{60} may further enhance the stability of the region. (Fig. 11B).

After determining the appropriate method of interaction, we developed a comprehensive toolkit for use in commonly utilized cellular assays such as TANGO, BRET, and NanoBiT assays. However, we believe that our toolkit can be further expanded and that other assays can be modified to incorporate the NbV5:V5 system.

Our research has demonstrated the capability of our nanobiosensors to investigate the involvement of β-arrestin-1 and β-arrestin-2 in two widely known GPCRs: the μ-OR and the AT1R. The former is responsible for the effects of commonly prescribed painkillers such as morphine and fentanyl, while the latter plays a crucial role in regulating vasoconstriction. AT1R antagonists (ARBs) are prescribed for the management of hypertension, congestive heart failure, and diabetic

nephropathy. It has been observed that these two receptors have the ability to recruit β-arrestins, but there is conflicting information regarding the selectivity of isoforms and, most importantly, the inherent effectiveness of drugs. The measurement of the direct interaction between the receptor and its effector is a key aspect for the accurate determination of intrinsic drug efficacy and as such, the use of smaller tags should mitigate some distortions caused by larger functional tags. When examining AT1R, the impact of a bigger tag wasn't very significant. However, when comparing the effect of a larger tag on the μ-OR, it becomes evident that using NbV5 as a carrier for bigger tags is more advantageous.

One of the assays that has been successfully converted to be included in the NbV5-based toolkit is the TEV-dependent reporter method. This particular assay was chosen due to its high permissibility and sensitivity. However, it's worth noting that a potential limitation of TEV-dependent reporter methods is their catalysis kinetics. In 2020, Sanchez et al. reported the S153N TEV219 mutant with an increased catalytic rate (178). After conducting a test on the new mutant, we noticed a 3 to 4-fold rise in the total RLU produced. However, we did not detect any significant changes in the fold-over-baseline and EC50. While the S153N mutant enhances the dynamic range, it does not offer significant advantages in our system. Therefore, we decided to go ahead with the non-mutated TEV219. Next, we proceeded to modify two well-known PPI assays, BRET and NanoBiT, to work with the Nb V5 platform. It's important to mention that we observed a notable distinction between BRET and NanoBiT in terms of the specific recruitment of different β-arrestin isoforms at AT1R. It's worth noting that the NanoBiT assay reveals a preference for β-arrestin-1 compared to β-arrestin-2, whereas BRET2 and TANGO showed no difference.

It is unclear why this observation occurs. Based on the data presented in (Fig. 16), the size and orientation of the tag have a more significant impact on NanoBit than BRET2. This disparity can be explained by the fact that binary complementation, being an interaction assay, is unable to track spatial rearrangement. On the other hand, BRET2 is highly reliant on conformation, and its efficiency is contingent on the distance and spatial orientation necessary for dipole-dipole coupling. It is possible that the BRET2 signal measured reflects a combination of recruitment and conformational changes (multi-states), whereas NanoBit only detects newly recruited β-arrestin or a single conformational state of the complex.

Our team has tested the effectiveness of the Nanobody V5 in microscopy experiments involving γ-actin-V5. The results showed that it is a useful tool for tracking protein remodelling and trafficking in live-cell-based experiments. Currently, we are using NbV5 to study the basal level of G proteins, which is similar to the level of G protein-LgBiT. This opens up a new perspective in the field as we explore the concept of having an inhibitory G protein (GoA) associated with the inactive form of the receptor. We are excited to test over 400 GPCR-tagged V5 soon. Some receptors have already been tested and very interesting results are going to be shared in the near future. But these findings bring questions on why GoA is the only Gprotein recruited to the inactive receptor especially considering that a lot of research groups are not even making the distinction between GoA and GoB. Research to understand the uniqueness of GoA is currently performed in our lab.

As previously stated, the existence of a comprehensive open reading frame (ORF) library featuring a C-terminal V5-tag brings about promising opportunities for advancing mammalian functional proteomics. This particular approach offers

significant benefits over other proteomics assays as it is not restricted to endogenous proteins, can be executed in living human cells, and captures ligand-dependent interactomes. Our laboratory is presently investigating the potential of this approach to enhance binary protein-protein interaction (PPI) mapping. A similar library has recently been employed for genome-wide profiling of human HOX proteins interactome using bimolecular fluorescence complementation (BiFc) assay. This research demonstrated the power of this approach as a tool for illuminating the binary PPI interactome. We are optimistic that the NbV5:V5 system will make similar assays more feasible both economically and technically for the scientific community as a whole. Although this study employed G protein-coupled receptors (GPCRs) to characterize the toolkit, we have confidence that NbV5:V5 or NbALFA:ALFA systems could be utilized to study any receptor-protein or protein-protein interaction (179).

1. Fredriksson, R., Lagerström, M. C., Lundin, L. G., and Schiöth, H. B. (2003) The G-protein-coupled receptors in the human genome form five main families. Phylogenetic analysis, paralogon groups, and fingerprints. *Mol Pharmacol*. **63**, 1256–1272
2. Davenport, A. P., Alexander, S. P. H., Sharman, J. L., Pawson, A. J., Benson, H. E., Monaghan, A. E., Liew, W. C., Mpamhanga, C. P., Bonner, T. I., Neubig, R. R., Pin, J. P., Spedding, M., and Harmar, A. J. (2013) International Union of Basic and Clinical Pharmacology. LXXXVIII. G protein-coupled receptor list: recommendations for new pairings with cognate ligands. *Pharmacol Rev*. **65**, 967–986
3. Roth, B. L., and Kroeze, W. K. (2015) Integrated Approaches for Genome-wide Interrogation of the Druggable Non-olfactory G Protein-coupled Receptor Superfamily. *J Biol Chem*. **290**, 19471–19477
4. Schiöth, H. B., and Lagerström, M. C. (2008) Structural diversity of G protein-coupled receptors and significance for drug discovery. *Nat Rev Drug Discov*. **7**, 339–357
5. Fredriksson, R., and Schiöth, H. B. (2005) The repertoire of G-protein-coupled receptors in fully sequenced genomes. *Mol Pharmacol*. **67**, 1414–1425
6. Santos, R., Ursu, O., Gaulton, A., Bento, A. P., Donadi, R. S., Bologa, C. G., Karlsson, A., Al-Lazikani, B., Hersey, A., Oprea, T. I., and Overington, J. P. (2017) A comprehensive map of molecular drug targets. *Nat Rev Drug Discov*. **16**, 19–34
7. Insel, P. A., Sriram, K., Gorr, M. W., Wiley, S. Z., Michkov, A., Salmerón, C., and Chinn, A. M. (2019) GPCRomics: An Approach to Discover GPCR Drug Targets. *Trends Pharmacol Sci*. **40**, 378–387
8. Kolakowski, L. F. (1994) GCRDb: A G-protein-coupled receptor database. *Recept Channels*. **2**, 1–7
9. Fredriksson, R., Lagerström, M. C., Lundin, L. G., and Schiöth, H. B. (2003) The G-protein-coupled receptors in the human genome form five main families. Phylogenetic analysis, paralogon groups, and fingerprints. *Mol Pharmacol*. **63**, 1256–1272
10. Isberg, V., Mordalski, S., Munk, C., Rataj, K., Harpsøe, K., Hauser, A. S., Vroling, B., Bojarski, A. J., Vriend, G., and Gloriam, D. E. (2016) GPCRdb: an information system for G protein-coupled receptors. *Nucleic Acids Res*. **44**, D356–D364
11. Fredriksson, R., and Schiöth, H. B. (2005) The repertoire of G-protein-coupled receptors in fully sequenced genomes. *Mol Pharmacol*. **67**, 1414–1425
12. Schiöth, H. B., and Lagerström, M. C. (2008) Structural diversity of G protein-coupled receptors and significance for drug discovery. *Nat Rev Drug Discov*. **7**, 339–357
13. Foord, S. M., Bonner, T. I., Neubig, R. R., Rosser, E. M., Pin, J. P., Davenport, A. P., Spedding, M., and Harmar, A. J. (2005) International Union of Pharmacology. XLVI. G protein-coupled receptor list. *Pharmacol Rev*. **57**, 279–288
14. Huang, X. P., Karpiak, J., Kroeze, W. K., Zhu, H., Chen, X., Moy, S. S., Saddoris, K. A., Nikolova, V. D., Farrell, M. S., Wang, S., Mangano, T. J., Deshpande, D. A., Jiang, A., Penn, R. B., Jin, J., Koller, B. H., Kenakin, T., Shoichet, B. K., and Roth, B. L. (2015) Allosteric ligands for the pharmacologically dark receptors GPR68 and GPR65. *Nature*. **527**, 477–483

15. Santos, R., Ursu, O., Gaulton, A., Bento, A. P., Donadi, R. S., Bologa, C. G., Karlsson, A., Al-Lazikani, B., Hersey, A., Oprea, T. I., and Overington, J. P. (2017) A comprehensive map of molecular drug targets. *Nat Rev Drug Discov*. **16**, 19–34
16. Chen, Y., and Palczewski, K. (2016) Systems Pharmacology Links GPCRs with Retinal Degenerative Disorders. *Annu Rev Pharmacol Toxicol*. **56**, 273
17. Palczewski K, kumasaka T, hori T, behnke CA, motoshima H, fox BA, trong IL, teller DC, okada T, stenkamp RE, yamamoto M, and miyano M. (2000) Crystal structure of rhodopsin: a G protein-coupled receptor. 2000;289:739-745. *American journal of ophthalmologyPalczewski K,*(1) kumasaka T, hori T, behnke CA, motoshima H, fox BA, trong IL, teller DC, okada T, stenkamp RE, yamamoto M, miyano M. Science* . **130**, 865
18. Hanson, M. A., Brooun, A., Baker, K. A., Jaakola, V.-P., Roth, C., Chien, E. Y. T., Alexandrov, A., Velasquez, J., Davis, L., Griffith, M., Moy, K., Ganser-Pornillos, B. K., Hua, Y., Kuhn, P., Ellis, S., Yeager, M., and Stevens, R. C. (2007) Profiling of membrane protein variants in a baculovirus system by coupling cell-surface detection with small-scale parallel expression. *Protein Expr Purif*. **56**, 85–92
19. Chae, P. S., Rasmussen, S. G. F., Rana, R. R., Gotfryd, K., Chandra, R., Goren, M. A., Kruse, A. C., Nurva, S., Loland, C. J., Pierre, Y., Drew, D., Popot, J.-L., Picot, D., Fox, B. G., Guan, L., Gether, U., Byrne, B., Kobilka, B., and Gellman, S. H. (2010) Maltose-neopentyl glycol (MNG) amphiphiles for solubilization, stabilization and crystallization of membrane proteins. *Nat Methods*. **7**, 1003–8
20. Caffrey, M. (2011) Crystallizing membrane proteins for structure-function studies using lipidic mesophases. *Biochem Soc Trans*. **39**, 725–32
21. Rasmussen, S. G. F., DeVree, B. T., Zou, Y., Kruse, A. C., Chung, K. Y., Kobilka, T. S., Thian, F. S., Chae, P. S., Pardon, E., Calinski, D., Mathiesen, J. M., Shah, S. T. A., Lyons, J. A., Caffrey, M., Gellman, S. H., Steyaert, J., Skiniotis, G., Weis, W. I., Sunahara, R. K., and Kobilka, B. K. (2011) Crystal structure of the β2 adrenergic receptor-Gs protein complex. *Nature*. **477**, 549–55
22. Kang, Y., Zhou, X. E., Gao, X., He, Y., Liu, W., Ishchenko, A., Barty, A., White, T. A., Yefanov, O., Han, G. W., Xu, Q., de Waal, P. W., Ke, J., Tan, M. H. E., Zhang, C., Moeller, A., West, G. M., Pascal, B. D., Van Eps, N., Caro, L. N., Vishnivetskiy, S. A., Lee, R. J., Suino-Powell, K. M., Gu, X., Pal, K., Ma, J., Zhi, X., Boutet, S., Williams, G. J., Messerschmidt, M., Gati, C., Zatsepin, N. A., Wang, D., James, D., Basu, S., Roy-Chowdhury, S., Conrad, C. E., Coe, J., Liu, H., Lisova, S., Kupitz, C., Grotjohann, I., Fromme, R., Jiang, Y., Tan, M., Yang, H., Li, J., Wang, M., Zheng, Z., Li, D., Howe, N., Zhao, Y., Standfuss, J., Diederichs, K., Dong, Y., Potter, C. S., Carragher, B., Caffrey, M., Jiang, H., Chapman, H. N., Spence, J. C. H., Fromme, P., Weierstall, U., Ernst, O. P., Katritch, V., Gurevich, V. V, Griffin, P. R., Hubbell, W. L., Stevens, R. C., Cherezov, V., Melcher, K., and Xu, H. E. (2015) Crystal structure of rhodopsin bound to arrestin by femtosecond X-ray laser. *Nature*. **523**, 561–7
23. Katritch, V., Cherezov, V., and Stevens, R. C. (2013) Structure-function of the G protein-coupled receptor superfamily. *Annu Rev Pharmacol Toxicol*. **53**, 531–556
24. Zhou, Q., Yang, D., Wu, M., Guo, Y., Guo, W., Zhong, L., Cai, X., Dai, A., Jang, W., Shakhnovich, E., Liu, Z. J., Stevens, R. C., Lambert, N. A., Babu, M. M., Wang, M. W., and Zhao, S. (2019) Common activation mechanism of class A GPCRs. *Elife*. 10.7554/ELIFE.50279

25. Geng, Y., Bush, M., Mosyak, L., Wang, F., and Fan, Q. R. (2013) Structural mechanism of ligand activation in human GABA(B) receptor. *Nature*. **504**, 254–259
26. Koehl, A., Hu, H., Feng, D., Sun, B., Zhang, Y., Robertson, M. J., Chu, M., Kobilka, T. S., Laermans, T., Steyaert, J., Tarrasch, J., Dutta, S., Fonseca, R., Weis, W. I., Mathiesen, J. M., Skiniotis, G., and Kobilka, B. K. (2019) Structural insights into the activation of metabotropic glutamate receptors. *Nature*. **566**, 79–84
27. Papasergi-Scott, M. M., Robertson, M. J., Seven, A. B., Panova, O., Mathiesen, J. M., and Skiniotis, G. (2020) Structures of metabotropic GABAB receptor. *Nature*. **584**, 310–314
28. Mao, C., Shen, C., Li, C., Shen, D. D., Xu, C., Zhang, S., Zhou, R., Shen, Q., Chen, L. N., Jiang, Z., Liu, J., and Zhang, Y. (2020) Cryo-EM structures of inactive and active GABAB receptor. *Cell Res*. **30**, 564–573
29. Williams, J. T., Ingram, S. L., Henderson, G., Chavkin, C., von Zastrow, M., Schulz, S., Koch, T., Evans, C. J., and Christie, M. J. (2013) Regulation of μ-opioid receptors: desensitization, phosphorylation, internalization, and tolerance. *Pharmacol Rev*. **65**, 223–254
30. Hilger, D., Masureel, M., and Kobilka, B. K. (2018) Structure and dynamics of GPCR signaling complexes. *Nat Struct Mol Biol*. **25**, 4–12
31. Neer, E. J., Kim, S. Y., Ang, S. L., Bloch, D. B., Bloch, K. D., Kawahara, Y., Tolman, C., Lee, R., Logothetis, D., Kim, D., Seidman, J. G., and Clapham, D. E. (1988) Functions of G-protein subunits. *Cold Spring Harb Symp Quant Biol*. **53 Pt 1**, 241–246
32. Neer, E. J., and Clapham, D. E. (1988) Roles of G protein subunits in transmembrane signalling. *Nature*. **333**, 129–134
33. Mafi, A., Kim, S. K., and Goddard, W. A. (2020) Mechanism of β-arrestin recruitment by the μ-opioid G protein-coupled receptor. *Proc Natl Acad Sci U S A*. **117**, 16346–16355
34. Bohn, L. M., Lefkowitz, R. J., Gainetdinov, R. R., Peppel, K., Caron, M. G., and Lin, F. T. (1999) Enhanced morphine analgesia in mice lacking β-arrestin 2. *Science (1979)*. **286**, 2495–2498
35. Zhuang, Y., Wang, Y., He, B., He, X., Zhou, X. E., Guo, S., Rao, Q., Yang, J., Liu, J., Zhou, Q., Wang, X., Liu, M., Liu, W., Jiang, X., Yang, D., Jiang, H., Shen, J., Melcher, K., Chen, H., Jiang, Y., Cheng, X., Wang, M. W., Xie, X., and Xu, H. E. (2022) Molecular recognition of morphine and fentanyl by the human μ-opioid receptor. *Cell*. **185**, 4361-4375.e19
36. Luttrell, L. M., and Lefkowitz, R. J. (2002) The role of beta-arrestins in the termination and transduction of G-protein-coupled receptor signals. *J Cell Sci*. **115**, 455–465
37. Siuda, E. R., Carr, R., Rominger, D. H., and Violin, J. D. (2017) Biased mu-opioid receptor ligands: a promising new generation of pain therapeutics. *Curr Opin Pharmacol*. **32**, 77–84
38. Freedman, N. J., Liggett, S. B., Drachman, D. E., Pei, G., Caron, M. G., and Lefkowitz, R. J. (1995) Phosphorylation and desensitization of the human beta 1-adrenergic receptor. Involvement of G protein-coupled receptor kinases and cAMP-dependent protein kinase. *J Biol Chem*. **270**, 17953–17961

39. Pitcher, J., Caron, M. G., Lefkowitz, R. J., Lohse, M. J., and Codina, J. (1992) Desensitization of the isolated beta 2-adrenergic receptor by beta-adrenergic receptor kinase, cAMP-dependent protein kinase, and protein kinase C occurs via distinct molecular mechanisms. *Biochemistry*. **31**, 3193–3197
40. Donia, T., Abouda, M., Kelany, M., and Hessien, M. (2021) β-Arrestin inhibition induces autophagy, apoptosis, G0/G1 cell cycle arrest in agonist-activated V2R receptor in breast cancer cells. *Med Oncol*. 10.1007/S12032-021-01484-Z
41. Liu, J., Li, Q. X., Wang, X. J., Zhang, C., Duan, Y. Q., Wang, Z. Y., Zhang, Y., Yu, X., Li, N. J., Sun, J. P., and Yi, F. (2016) β-Arrestins promote podocyte injury by inhibition of autophagy in diabetic nephropathy. *Cell Death Dis*. 10.1038/CDDIS.2016.89
42. Dingus, J., and Hildebrandt, J. D. (2012) Synthesis and assembly of G protein βγ dimers: comparison of in vitro and in vivo studies. *Subcell Biochem*. **63**, 155–180
43. Gudermann, T., Kalkbrenner, F., and Schultz, G. (1996) Diversity and selectivity of receptor-G protein interaction. *Annu Rev Pharmacol Toxicol*. **36**, 429–459
44. Gudermann, T., Schöneberg, T., and Schultz, G. (1997) Functional and structural complexity of signal transduction via G- protein-coupled receptors. *Annu Rev Neurosci*. **20**, 399–427
45. Lohse, M. J., Benovic, J. L., Codina, J., Caron, M. G., and Lefkowitz, R. J. (1990) β-Arrestin: a Protein that Regulates β-adrenergic Receptor Function. *Science (1979)*. **248**, 1547–1550
46. Wilden, U., Wüst, E., Weyand, I., and Kühn, H. (1986) Rapid affinity purification of retinal arrestin (48 kDa protein) via its light-dependent binding to phosphorylated rhodopsin. *FEBS Lett*. **207**, 292–295
47. Attramadals, H., Arrizas, J. L., Aoki8, C., Dawsonqll, T. M., Codina, J., Kwatra$, M. M., Snyderq, S. H., Caron$, M. G., and Lefkowitzs $$, R. J. (1992) Beta-arrestin2, a novel member of the arrestin/beta-arrestin gene family. *J Biol Chem*. **267**, 17882–17890
48. Kahlhofer, J., Leon, S., Teis, D., and Schmidt, O. (2021) The α-arrestin family of ubiquitin ligase adaptors links metabolism with selective endocytosis. *Biol Cell*. **113**, 183–219
49. Patwari, P., and Lee, R. T. (2012) An Expanded Family of Arrestins Regulate Metabolism. *Trends in Endocrinology and Metabolism*. **23**, 216
50. Degraff, J. L., Gurevich, V. V., and Benovic, J. L. (2002) The third intracellular loop of alpha 2-adrenergic receptors determines subtype specificity of arrestin interaction. *J Biol Chem*. **277**, 43247–43252
51. Wang, Q., and Limbird, L. E. (2002) Regulated interactions of the α2A adrenergic receptor with spinophilin, 14-3-3ζ, and arrestin 3. *Journal of Biological Chemistry*. **277**, 50589–50596
52. Kang, D. S., Tian, X., and Benovic, J. L. (2014) Role of β-arrestins and arrestin domain-containing proteins in G protein-coupled receptor trafficking. *Curr Opin Cell Biol*. **27**, 63–71
53. Scott, M. G. H., Rouzic, E. Le, Périanin, A., Pierotti, V., Enslen, H., Benichou, S., Marullo, S., and Benmerah, A. (2002) Differential nucleocytoplasmic shuttling of beta-arrestins. Characterization of a leucine-rich nuclear export signal in beta-arrestin2. *J Biol Chem*. **277**, 37693–37701

54. Ahn, S., Wei, H., Garrison, T. R., and Lefkowitz, R. J. (2004) Reciprocal regulation of angiotensin receptor-activated extracellular signal-regulated kinases by beta-arrestins 1 and 2. *J Biol Chem*. **279**, 7807–7811
55. Gesty-Palmer, D., Chen, M., Reiter, E., Ahn, S., Nelson, C. D., Wang, S., Eckhardt, A. E., Cowan, C. L., Spurney, R. F., Luttrell, L. M., and Lefkowitz, R. J. (2006) Distinct beta-arrestin- and G protein-dependent pathways for parathyroid hormone receptor-stimulated ERK1/2 activation. *J Biol Chem*. **281**, 10856–10864
56. Tobin, A. B., Butcher, A. J., and Kong, K. C. (2008) Location, location, location...site-specific GPCR phosphorylation offers a mechanism for cell-type-specific signalling. *Trends Pharmacol Sci*. **29**, 413–420
57. Kenakin, T. (2019) Biased Receptor Signaling in Drug Discovery. *Pharmacol Rev*. **71**, 267–315
58. Violin, J. D., Crombie, A. L., Soergel, D. G., and Lark, M. W. (2014) Biased ligands at G-protein-coupled receptors: promise and progress. *Trends Pharmacol Sci*. **35**, 308–316
59. Urban, J. D., Clarke, W. P., Von Zastrow, M., Nichols, D. E., Kobilka, B., Weinstein, H., Javitch, J. A., Roth, B. L., Christopoulos, A., Sexton, P. M., Miller, K. J., Spedding, M., and Mailman, R. B. (2007) Functional selectivity and classical concepts of quantitative pharmacology. *J Pharmacol Exp Ther*. **320**, 1–13
60. Bock, A., Merten, N., Schrage, R., Dallanoce, C., Bätz, J., Klöckner, J., Schmitz, J., Matera, C., Simon, K., Kebig, A., Peters, L., Müller, A., Schrobang-Ley, J., Tränkle, C., Hoffmann, C., De Amici, M., Holzgrabe, U., Kostenis, E., and Mohr, K. (2016) Dynamic ligand binding of dualsteric (allosteric/orthosteric) molecular probes controls the graded activation of muscarinic acetylcholine receptors. *Nat Commun*. **3**, PC45–PC45
61. Rajagopal, S., Ahn, S., Rominger, D. H., Gowen-MacDonald, W., Lam, C. M., DeWire, S. M., Violin, J. D., and Lefkowitz, R. J. (2011) Quantifying ligand bias at seven-transmembrane receptors. *Mol Pharmacol*. **80**, 367–377
62. Schmid, C. L., Kennedy, N. M., Ross, N. C., Lovell, K. M., Yue, Z., Morgenweck, J., Cameron, M. D., Bannister, T. D., and Bohn, L. M. (2017) Bias Factor and Therapeutic Window Correlate to Predict Safer Opioid Analgesics. *Cell*. **171**, 1165.e13-1175.e13
63. Luttrell, L. M., Ferguson, S. S. G., Daaka, Y., Miller, W. E., Maudsley, S., Della Rocca, G. J., Lin, F. T., Kawakatsu, H., Owada, K., Luttrell, D. K., Caron, M. G., and Lefkowitz, R. J. (1999) Beta-arrestin-dependent formation of beta2 adrenergic receptor-Src protein kinase complexes. *Science*. **283**, 655–661
64. Shukla, A. K., Westfield, G. H., Xiao, K., Reis, R. I., Huang, L. Y., Tripathi-Shukla, P., Qian, J., Li, S., Blanc, A., Oleskie, A. N., Dosey, A. M., Su, M., Liang, C. R., Gu, L. L., Shan, J. M., Chen, X., Hanna, R., Choi, M., Yao, X. J., Klink, B. U., Kahsai, A. W., Sidhu, S. S., Koide, S., Penczek, P. A., Kossiakoff, A. A., Woods, V. L., Kobilka, B. K., Skiniotis, G., and Lefkowitz, R. J. (2014) Visualization of arrestin recruitment by a G-protein-coupled receptor. *Nature*. **512**, 218–222
65. Kelly, E., Bailey, C. P., and Henderson, G. (2008) Agonist-selective mechanisms of GPCR desensitization. *Br J Pharmacol*. **153**, S379
66. Woolf, C. J. (2010) What is this thing called pain? *J Clin Invest*. **120**, 3742–3744

67. Volkow, N. D., and Blanco, C. (2021) The changing opioid crisis: development, challenges and opportunities. *Mol Psychiatry*. **26**, 218–233
68. Taylor, S. S., Noor, N., Urits, I., Paladini, A., Sadhu, M. S., Gibb, C., Carlson, T., Myrcik, D., Varrassi, G., and Viswanath, O. (2021) Complex Regional Pain Syndrome: A Comprehensive Review. *Pain Ther*. **10**, 875–892
69. Bell, A. (2018) The neurobiology of acute pain. *Vet J*. **237**, 55–62
70. Glare, P., Aubrey, K. R., and Myles, P. S. (2019) Transition from acute to chronic pain after surgery. *The Lancet*. **393**, 1537–1546
71. Cohen, S. P., Vase, L., and Hooten, W. M. (2021) Chronic pain: an update on burden, best practices, and new advances. *The Lancet*. **397**, 2082–2097
72. Denham-Jones, L., Gaskell, L., Spence, N., and Pigott, T. (2022) A systematic review of the effectiveness of Pilates on pain, disability, physical function, and quality of life in older adults with chronic musculoskeletal conditions. *Musculoskeletal Care*. **20**, 10–30
73. Mattson, C. L., Tanz, L. J., Quinn, K., Kariisa, M., Patel, P., and Davis, N. L. (2022) Trends and Geographic Patterns in Drug and Synthetic Opioid Overdose Deaths — United States, 2013–2019. *MMWR Morb Mortal Wkly Rep*. **70**, 202–207
74. Corbett, A. D., Henderson, G., McKnight, A. T., and Paterson, S. J. (2006) 75 years of opioid research: the exciting but vain quest for the Holy Grail. *Br J Pharmacol*. 10.1038/SJ.BJP.0706435
75. Pasternak, G. W. (2014) Opioids and their receptors: Are we there yet? *Neuropharmacology*. **76 Pt B**, 198–203
76. Lapalu, S., Moisand, C., Butour, J. L., Mollereau, C., and Meunier, J. C. (1998) Different domains of the ORL1 and kappa-opioid receptors are involved in recognition of nociceptin and dynorphin A. *FEBS Lett*. **427**, 296–300
77. Lapalu, S., Moisand, C., Mazarguil, H., Cambois, G., Mollereau, C., and Meunier, J. C. (1997) Comparison of the structure-activity relationships of nociceptin and dynorphin A using chimeric peptides. *FEBS Lett*. **417**, 333–336
78. Pasternak, G. W. (2005) Molecular biology of opioid analgesia. *J Pain Symptom Manage*. **29**, 2
79. Koch, T., and Höllt, V. (2008) Role of receptor internalization in opioid tolerance and dependence. *Pharmacol Ther*. **117**, 199–206
80. Al-Hasani, R., and Bruchas, M. R. (2011) Molecular mechanisms of opioid receptor-dependent signaling and behavior. *Anesthesiology*. **115**, 1363–1381
81. Volkow, N. D., and McLellan, A. T. (2016) Opioid Abuse in Chronic Pain--Misconceptions and Mitigation Strategies. *N Engl J Med*. **374**, 1253–1263
82. Georgoussi, Z., Georganta, E.-M., and Milligan, G. (2012) The other side of opioid receptor signalling: regulation by protein-protein interaction. *Curr Drug Targets*. **13**, 80–102
83. Beaudry, H., Mercier-Blais, A. A., Delaygue, C., Lavoie, C., Parent, J. L., Neugebauer, W., and Gendron, L. (2015) Regulation of μ and δ opioid receptor functions: involvement of cyclin-dependent kinase 5. *Br J Pharmacol*. **172**, 2573–2587
84. Leskelä, T. T., Markkanen, P. M. H., Pietilä, E. M., Tuusa, J. T., and Petäjä-Repo, U. E. (2007) Opioid receptor pharmacological chaperones act by binding and stabilizing newly synthesized receptors in the endoplasmic reticulum. *J Biol Chem*. **282**, 23171–23183

85. Whistler, J. L., Enquist, J., Marley, A., Fong, J., Gladher, F., Tsuruda, P., Murray, S. R., and Von Zastrow, M. (2002) Modulation of postendocytic sorting of G protein-coupled receptors. *Science*. **297**, 615–620
86. Wang, D., Sadée, W., and Quillan, J. M. (1999) Calmodulin binding to G protein-coupling domain of opioid receptors. *J Biol Chem*. **274**, 22081–22088
87. Fourla, D. D., Papakonstantinou, M. P., Vrana, S. M., and Georgoussi, Z. (2012) Selective interactions of spinophilin with the C-terminal domains of the δ- and μ-opioid receptors and G proteins differentially modulate opioid receptor signaling. *Cell Signal*. **24**, 2315–2328
88. Leontiadis, L. J., Papakonstantinou, M. P., and Georgoussi, Z. (2009) Regulator of G protein signaling 4 confers selectivity to specific G proteins to modulate mu- and delta-opioid receptor signaling. *Cell Signal*. **21**, 1218–1228
89. Ulengin-Talkish, I., Parson, M. A. H., Jenkins, M. L., Roy, J., Shih, A. Z. L., St-Denis, N., Gulyas, G., Balla, T., Gingras, A. C., Várnai, P., Conibear, E., Burke, J. E., and Cyert, M. S. (2021) Palmitoylation targets the calcineurin phosphatase to the phosphatidylinositol 4-kinase complex at the plasma membrane. *Nat Commun*. 10.1038/S41467-021-26326-4
90. Gorkhali, R., Tian, L., Dong, B., Bagchi, P., Deng, X., Pawar, S., Duong, D., Fang, N., Seyfried, N., and Yang, J. (2021) Extracellular calcium alters calcium-sensing receptor network integrating intracellular calcium-signaling and related key pathway. *Sci Rep*. 10.1038/S41598-021-00067-2
91. Sharaf, A., Mensching, L., Keller, C., Rading, S., Scheffold, M., Palkowitsch, L., Djogo, N., Rezgaoui, M., Kestler, H. A., Moepps, B., Failla, A. V., and Karsak, M. (2019) Systematic Affinity Purification Coupled to Mass Spectrometry Identified p62 as Part of the Cannabinoid Receptor CB2 Interactome. *Front Mol Neurosci*. 10.3389/FNMOL.2019.00224
92. Namkung, Y., Le Gouill, C., Lukashova, V., Kobayashi, H., Hogue, M., Khoury, E., Song, M., Bouvier, M., and Laporte, S. A. (2016) Monitoring G protein-coupled receptor and β-arrestin trafficking in live cells using enhanced bystander BRET. *Nat Commun*. 10.1038/NCOMMS12178
93. Winpenny, D., Clark, M., and Cawkill, D. (2016) Biased ligand quantification in drug discovery: from theory to high throughput screening to identify new biased μ opioid receptor agonists. *Br J Pharmacol*. **173**, 1393–1403
94. Kroeze, W. K., Sassano, M. F., Huang, X. P., Lansu, K., McCorvy, J. D., Giguère, P. M., Sciaky, N., and Roth, B. L. (2015) PRESTO-Tango as an open-source resource for interrogation of the druggable human GPCRome. *Nat Struct Mol Biol*. **22**, 362–369
95. Galés, C., Rebois, R. V., Hogue, M., Trieu, P., Breit, A., Hébert, T. E., and Bouvier, M. (2005) Real-time monitoring of receptor and G-protein interactions in living cells. *Nature Methods 2005 2:3*. **2**, 177–184
96. Bouvier, M., Heveker, N., Jockers, R., Marullo, S., and Milligan, G. (2007) BRET analysis of GPCR oligomerization: newer does not mean better. *Nat Methods*. **4**, 3–4
97. Pfleger, K. D. G., Seeber, R. M., and Eidne, K. A. (2006) Bioluminescence resonance energy transfer (BRET) for the real-time detection of protein-protein interactions. *Nat Protoc*. **1**, 337–345

98. Kobayashi, H., Picard, L. P., Schönegge, A. M., and Bouvier, M. (2019) Bioluminescence resonance energy transfer–based imaging of protein–protein interactions in living cells. *Nature Protocols 2019 14:4*. **14**, 1084–1107
99. Kobayashi, H., and Bouvier, M. (2021) Bioluminescence Resonance Energy Transfer (BRET) Imaging in Living Cells: Image Acquisition and Quantification. *Methods Mol Biol*. **2274**, 305–314
100. Bertrand, L., Parent, S., Caron, M., Legault, M., Joly, E., Angers, S., Bouvier, M., Brown, M., Houle, B., and Ménard, L. (2002) The BRET2/arrestin assay in stable recombinant cells: a platform to screen for compounds that interact with G protein-coupled receptors (GPCRS). *J Recept Signal Transduct Res*. **22**, 533–541
101. Coussens, N. P., Auld, D., Roby, P., Walsh, J., Baell, J. B., Kales, S., Hadian, K., and Dahlin, J. L. (2020) Compound-Mediated Assay Interferences in Homogeneous Proximity Assays. *Assay Guidance Manual*. [online] https://www.ncbi.nlm.nih.gov/books/NBK553584/ (Accessed September 3, 2023)
102. Mo, X. L., and Fu, H. (2016) BRET: NanoLuc-Based Bioluminescence Resonance Energy Transfer Platform to Monitor Protein-Protein Interactions in Live Cells. *Methods Mol Biol*. **1439**, 263–271
103. Inoue, A., Raimondi, F., Kadji, F. M. N., Singh, G., Kishi, T., Uwamizu, A., Ono, Y., Shinjo, Y., Ishida, S., Arang, N., Kawakami, K., Gutkind, J. S., Aoki, J., and Russell, R. B. (2019) Illuminating G-Protein-Coupling Selectivity of GPCRs. *Cell*. **177**, 1933-1947.e25
104. Reyes-Alcaraz, A., Lucero Garcia-Rojas, E. Y., Merlinsky, E. A., Seong, J. Y., Bond, R. A., and McConnell, B. K. (2022) A NanoBiT assay to monitor membrane proteins trafficking for drug discovery and drug development. *Commun Biol*. 10.1038/S42003-022-03163-9
105. Kimple, M. E., Brill, A. L., and Pasker, R. L. (2013) Overview of affinity tags for protein purification. *Curr Protoc Protein Sci*. 10.1002/0471140864.PS0909S73
106. Küey, C., Larocque, G., Clarke, N. I., and Royle, S. J. (2019) Unintended perturbation of protein function using GFP nanobodies in human cells. *J Cell Sci*. 10.1242/JCS.234955
107. Zhao, X., Li, G., and Liang, S. (2013) Several affinity tags commonly used in chromatographic purification. *J Anal Methods Chem*. 10.1155/2013/581093
108. Brilhante-da-Silva, N., de Oliveira Sousa, R. M., Arruda, A., dos Santos, E. L., Marinho, A. C. M., Stabeli, R. G., Fernandes, C. F. C., and Pereira, S. dos S. (2021) Camelid Single-Domain Antibodies for the Development of Potent Diagnosis Platforms. *Mol Diagn Ther*. **25**, 439–456
109. Dingus, J. G., Tang, J. C. Y., Amamoto, R., Wallick, G. K., and Cepko, C. L. (2022) A general approach for stabilizing nanobodies for intracellular expression. *Elife*. 10.7554/ELIFE.68253
110. McMahon, C., Baier, A. S., Pascolutti, R., Wegrecki, M., Zheng, S., Ong, J. X., Erlandson, S. C., Hilger, D., Rasmussen, S. G. F., Ring, A. M., Manglik, A., and Kruse, A. C. (2018) Yeast surface display platform for rapid discovery of conformationally selective nanobodies. *Nat Struct Mol Biol*. **25**, 289–296
111. Marschall, A. L. J., Dübel, S., and Böldicke, T. (2015) Specific in vivo knockdown of protein function by intrabodies. *MAbs*. **7**, 1010–1035

112. Power, C. A., and Bates, A. (2019) David vs. Goliath: The Structure, Function, and Clinical Prospects of Antibody Fragments. *Antibodies (Basel)*. 10.3390/ANTIB8020028
113. Hudson, P. J., and Kortt, A. A. (1999) High avidity scFv multimers; diabodies and triabodies. *J Immunol Methods*. **231**, 177–189
114. Kabayama, H., Takeuchi, M., Tokushige, N., Muramatsu, S. ichi, Kabayama, M., Fukuda, M., Yamada, Y., and Mikoshiba, K. (2020) An ultra-stable cytoplasmic antibody engineered for in vivo applications. *Nat Commun*. 10.1038/S41467-019-13654-9
115. Kvam, E., Sierks, M. R., Shoemaker, C. B., and Messer, A. (2010) Physico-chemical determinants of soluble intrabody expression in mammalian cell cytoplasm. *Protein Eng Des Sel*. **23**, 489–498
116. Guglielmi, L., Denis, V., Vezzio-Vié, N., Bec, N., Dariavach, P., Larroque, C., and Martineau, P. (2011) Selection for intrabody solubility in mammalian cells using GFP fusions. *Protein Eng Des Sel*. **24**, 873–881
117. Goldman, E. R., Liu, J. L., Zabetakis, D., and Anderson, G. P. (2017) Enhancing Stability of Camelid and Shark Single Domain Antibodies: An Overview. *Front Immunol*. 10.3389/FIMMU.2017.00865
118. Flicker, S., Zettl, I., and Tillib, S. V. (2020) Nanobodies-Useful Tools for Allergy Treatment? *Front Immunol*. 10.3389/FIMMU.2020.576255
119. Traenkle, B., and Rothbauer, U. (2017) Under the Microscope: Single-Domain Antibodies for Live-Cell Imaging and Super-Resolution Microscopy. *Front Immunol*. 10.3389/FIMMU.2017.01030
120. Kaiser, P. D., Maier, J., Traenkle, B., Emele, F., and Rothbauer, U. (2014) Recent progress in generating intracellular functional antibody fragments to target and trace cellular components in living cells. *Biochim Biophys Acta*. **1844**, 1933–1942
121. Helma, J., Cardoso, M. C., Muyldermans, S., and Leonhardt, H. (2015) Nanobodies and recombinant binders in cell biology. *J Cell Biol*. **209**, 633–644
122. Cheloha, R. W., Fischer, F. A., Woodham, A. W., Daley, E., Suminski, N., Gardella, T. J., and Ploegh, H. L. (2020) Improved GPCR ligands from nanobody tethering. *Nat Commun*. 10.1038/S41467-020-15884-8
123. Wagner, T. R., and Rothbauer, U. (2020) Nanobodies Right in the Middle: Intrabodies as Toolbox to Visualize and Modulate Antigens in the Living Cell. *Biomolecules*. **10**, 1–19
124. Che, T., English, J., Krumm, B. E., Kim, K., Pardon, E., Olsen, R. H. J., Wang, S., Zhang, S., Diberto, J. F., Sciaky, N., Carroll, F. I., Steyaert, J., Wacker, D., and Roth, B. L. (2020) Nanobody-enabled monitoring of kappa opioid receptor states. *Nat Commun*. 10.1038/S41467-020-14889-7
125. Steyaert, J., and Kobilka, B. K. (2011) Nanobody stabilization of G protein-coupled receptor conformational states. *Curr Opin Struct Biol*. **21**, 567–572
126. Manglik, A., and Kobilka, B. (2014) The role of protein dynamics in GPCR function: insights from the β2AR and rhodopsin. *Curr Opin Cell Biol*. **27**, 136–143
127. Staus, D. P., Wingler, L. M., Strachan, R. T., Rasmussen, S. G. F., Pardon, E., Ahn, S., Steyaert, J., Kobilka, B. K., and Lefkowitz, R. J. (2014) Regulation of β2-adrenergic receptor function by conformationally selective single-domain intrabodies. *Mol Pharmacol*. **85**, 472–481

128. Westfield, G. H., Rasmussen, S. G. F., Su, M., Dutta, S., DeVree, B. T., Chung, K. Y., Calinski, D., Velez-Ruiz, G., Oleskie, A. N., Pardon, E., Chae, P. S., Liu, T., Li, S., Woods, V. L., Steyaert, J., Kobilka, B. K., Sunahara, R. K., and Skiniotis, G. (2011) Structural flexibility of the G alpha s alpha-helical domain in the beta2-adrenoceptor Gs complex. *Proc Natl Acad Sci U S A*. **108**, 16086–16091
129. Che, T., English, J., Krumm, B. E., Kim, K., Pardon, E., Olsen, R. H. J., Wang, S., Zhang, S., Diberto, J. F., Sciaky, N., Carroll, F. I., Steyaert, J., Wacker, D., and Roth, B. L. (2020) Nanobody-enabled monitoring of kappa opioid receptor states. *Nat Commun*. 10.1038/S41467-020-14889-7
130. Che, T., Majumdar, S., Zaidi, S. A., Ondachi, P., McCorvy, J. D., Wang, S., Mosier, P. D., Uprety, R., Vardy, E., Krumm, B. E., Han, G. W., Lee, M. Y., Pardon, E., Steyaert, J., Huang, X. P., Strachan, R. T., Tribo, A. R., Pasternak, G. W., Carroll, F. I., Stevens, R. C., Cherezov, V., Katritch, V., Wacker, D., and Roth, B. L. (2018) Structure of the Nanobody-Stabilized Active State of the Kappa Opioid Receptor. *Cell*. **172**, 55-67.e15
131. Zhang, L., Wang, L., Cao, S., Lv, H., Huang, J., Zhang, G., Tabynov, K., Zhao, Q., and Zhou, E. M. (2021) Nanobody Nb6 fused with porcine IgG Fc as the delivering tag to inhibit porcine reproductive and respiratory syndrome virus replication in porcine alveolar macrophages. *Vet Res*. 10.1186/S13567-020-00868-9
132. Livingston, K. E., Mahoney, J. P., Manglik, A., Sunahara, R. K., and Traynor, J. R. (2018) Measuring ligand efficacy at the mu-opioid receptor using a conformational biosensor. *Elife*. 10.7554/ELIFE.32499
133. Che, T., English, J., Krumm, B. E., Kim, K., Pardon, E., Olsen, R. H. J., Wang, S., Zhang, S., Diberto, J. F., Sciaky, N., Carroll, F. I., Steyaert, J., Wacker, D., and Roth, B. L. (2020) Nanobody-enabled monitoring of kappa opioid receptor states. *Nat Commun*. 10.1038/S41467-020-14889-7
134. Staus, D. P., Strachan, R. T., Manglik, A., Pani, B., Kahsai, A. W., Kim, T. H., Wingler, L. M., Ahn, S., Chatterjee, A., Masoudi, A., Kruse, A. C., Pardon, E., Steyaert, J., Weis, W. I., Prosser, R. S., Kobilka, B. K., Costa, T., and Lefkowitz, R. J. (2016) Allosteric nanobodies reveal the dynamic range and diverse mechanisms of G-protein-coupled receptor activation. *Nature*. **535**, 448–452
135. Vasudevan, L., and Stove, C. P. (2020) A novel nanobody-based bio-assay using functional complementation of a split nanoluciferase to monitor Mu- opioid receptor activation. *Anal Bioanal Chem*. **412**, 8015–8022
136. Götzke, H., Kilisch, M., Martínez-Carranza, M., Sograte-Idrissi, S., Rajavel, A., Schlichthaerle, T., Engels, N., Jungmann, R., Stenmark, P., Opazo, F., and Frey, S. (2019) The ALFA-tag is a highly versatile tool for nanobody-based bioscience applications. *Nat Commun*. 10.1038/S41467-019-12301-7
137. Stoeber, M., Jullié, D., Lobingier, B. T., Laeremans, T., Steyaert, J., Schiller, P. W., Manglik, A., and von Zastrow, M. (2018) A Genetically Encoded Biosensor Reveals Location Bias of Opioid Drug Action. *Neuron*. **98**, 963-976.e5
138. Livingston, K. E., Mahoney, J. P., Manglik, A., Sunahara, R. K., and Traynor, J. R. (2018) Measuring ligand efficacy at the mu-opioid receptor using a conformational biosensor. *Elife*. 10.7554/ELIFE.32499
139. Staus, D. P., Wingler, L. M., Strachan, R. T., Rasmussen, S. G. F., Pardon, E., Ahn, S., Steyaert, J., Kobilka, B. K., and Lefkowitz, R. J. (2014) Regulation of β2-adrenergic

receptor function by conformationally selective single-domain intrabodies. *Mol Pharmacol*. **85**, 472–481
140. Irannejad, R., Tomshine, J. C., Tomshine, J. R., Chevalier, M., Mahoney, J. P., Steyaert, J., Rasmussen, S. G. F., Sunahara, R. K., El-Samad, H., Huang, B., and Von Zastrow, M. (2013) Conformational biosensors reveal GPCR signalling from endosomes. *Nature*. **495**, 534–538
141. Rasmussen, S. G. F., Choi, H. J., Fung, J. J., Pardon, E., Casarosa, P., Chae, P. S., Devree, B. T., Rosenbaum, D. M., Thian, F. S., Kobilka, T. S., Schnapp, A., Konetzki, I., Sunahara, R. K., Gellman, S. H., Pautsch, A., Steyaert, J., Weis, W. I., and Kobilka, B. K. (2011) Structure of a nanobody-stabilized active state of the β(2) adrenoceptor. *Nature*. **469**, 175–181
142. Wingler, L. M., McMahon, C., Staus, D. P., Lefkowitz, R. J., and Kruse, A. C. (2019) Distinctive Activation Mechanism for Angiotensin Receptor Revealed by a Synthetic Nanobody. *Cell*. **176**, 479-490.e12
143. Stoeber, M., Jullié, D., Lobingier, B. T., Laeremans, T., Steyaert, J., Schiller, P. W., Manglik, A., and von Zastrow, M. (2018) A Genetically Encoded Biosensor Reveals Location Bias of Opioid Drug Action. *Neuron*. **98**, 963-976.e5
144. Zeghal, M., Matte, K., Venes, A., Patel, S., Laroche, G., Sarvan, S., Joshi, M., Rain, J.-C., Couture, J.-F., and Giguère, P. M. (2023) Development of a V5-tag-directed nanobody and its implementation as an intracellular biosensor of GPCR signaling. *J Biol Chem*. **299**, 105107
145. Olson, K. M., Campbell, A., Alt, A., and Traynor, J. R. (2022) Finding the Perfect Fit: Conformational Biosensors to Determine the Efficacy of GPCR Ligands. *ACS Pharmacol Transl Sci*. **5**, 694–709
146. Kabayama, H., Takeuchi, M., Tokushige, N., Muramatsu, S. ichi, Kabayama, M., Fukuda, M., Yamada, Y., and Mikoshiba, K. (2020) An ultra-stable cytoplasmic antibody engineered for in vivo applications. *Nat Commun*. 10.1038/S41467-019-13654-9
147. Li, T., Bourgeois, J. P., Celli, S., Glacial, F., Le Sourd, A. M., Mecheri, S., Weksler, B., Romero, I., Couraud, P. O., Rougeon, F., and Lafaye, P. (2012) Cell-penetrating anti-GFAP VHH and corresponding fluorescent fusion protein VHH-GFP spontaneously cross the blood-brain barrier and specifically recognize astrocytes: application to brain imaging. *FASEB J*. **26**, 3969–3979
148. Pardon, E., Laeremans, T., Triest, S., Rasmussen, S. G. F., Wohlkönig, A., Ruf, A., Muyldermans, S., Hol, W. G. J., Kobilka, B. K., and Steyaert, J. (2014) A general protocol for the generation of Nanobodies for structural biology. *Nat Protoc*. **9**, 674–693
149. De Genst, E., Silence, K., Decanniere, K., Conrath, K., Loris, R., Kinne, J., Muyldermans, S., and Wyns, L. (2006) Molecular basis for the preferential cleft recognition by dromedary heavy-chain antibodies. *Proc Natl Acad Sci U S A*. **103**, 4586–4591
150. De Genst, E. J., Guilliams, T., Wellens, J., Day, E. M., Waudby, C. A., Meehan, S., Dumoulin, M., Hsu, S. T. D., Cremades, N., Verschueren, K. H. G., Pardon, E., Wyns, L., Steyaert, J., Christodoulou, J., and Dobson, C. M. (2010) Structure and properties of a complex of α-synuclein and a single-domain camelid antibody. *J Mol Biol*. **402**, 326–343

151. Braun, M. B., Traenkle, B., Koch, P. A., Emele, F., Weiss, F., Poetz, O., Stehle, T., and Rothbauer, U. (2016) Peptides in headlock--a novel high-affinity and versatile peptide-binding nanobody for proteomics and microscopy. *Sci Rep*. 10.1038/SREP19211
152. Virant, D., Traenkle, B., Maier, J., Kaiser, P. D., Bodenhöfer, M., Schmees, C., Vojnovic, I., Pisak-Lukáts, B., Endesfelder, U., and Rothbauer, U. (2018) A peptide tag-specific nanobody enables high-quality labeling for dSTORM imaging. *Nat Commun*. 10.1038/S41467-018-03191-2
153. Boersma, S., Khuperkar, D., Verhagen, B. M. P., Sonneveld, S., Grimm, J. B., Lavis, L. D., and Tanenbaum, M. E. (2019) Multi-Color Single-Molecule Imaging Uncovers Extensive Heterogeneity in mRNA Decoding. *Cell*. **178**, 458-472.e19
154. Lutje Hulsik, D., Liu, Y. ying, Strokappe, N. M., Battella, S., El Khattabi, M., McCoy, L. E., Sabin, C., Hinz, A., Hock, M., Macheboeuf, P., Bonvin, A. M. J. J., Langedijk, J. P. M., Davis, D., Forsman Quigley, A., Aasa-Chapman, M. M. I., Seaman, M. S., Ramos, A., Poignard, P., Favier, A., Simorre, J. P., Weiss, R. A., Verrips, C. T., Weissenhorn, W., and Rutten, L. (2013) A gp41 MPER-specific llama VHH requires a hydrophobic CDR3 for neutralization but not for antigen recognition. *PLoS Pathog*. 10.1371/JOURNAL.PPAT.1003202
155. Traenkle, B., Segan, S., Fagbadebo, F. O., Kaiser, P. D., and Rothbauer, U. (2020) A novel epitope tagging system to visualize and monitor antigens in live cells with chromobodies. *Sci Rep*. 10.1038/S41598-020-71091-X
156. Küey, C., Larocque, G., Clarke, N. I., and Royle, S. J. (2019) Unintended perturbation of protein function using GFP nanobodies in human cells. *J Cell Sci*. 10.1242/JCS.234955
157. Yang, X., Boehm, J. S., Yang, X., Salehi-Ashtiani, K., Hao, T., Shen, Y., Lubonja, R., Thomas, S. R., Alkan, O., Bhimdi, T., Green, T. M., Johannessen, C. M., Silver, S. J., Nguyen, C., Murray, R. R., Hieronymus, H., Balcha, D., Fan, C., Lin, C., Ghamsari, L., Vidal, M., Hahn, W. C., Hill, D. E., and Root, D. E. (2011) A public genome-scale lentiviral expression library of human ORFs. *Nat Methods*. **8**, 659–661
158. Yang, X., Boehm, J. S., Yang, X., Salehi-Ashtiani, K., Hao, T., Shen, Y., Lubonja, R., Thomas, S. R., Alkan, O., Bhimdi, T., Green, T. M., Johannessen, C. M., Silver, S. J., Nguyen, C., Murray, R. R., Hieronymus, H., Balcha, D., Fan, C., Lin, C., Ghamsari, L., Vidal, M., Hahn, W. C., Hill, D. E., and Root, D. E. (2011) A public genome-scale lentiviral expression library of human ORFs. *Nat Methods*. **8**, 659–661
159. Hanke, T., and Randall, R. E. (1995) Variable domain sequences of mAb with high affinity for a linear oligopeptide. *Immunogenetics*. **42**, 442–443
160. Randall, R. E., Young, D. F., Goswami, K. K., and Russell, W. C. (1987) Isolation and characterization of monoclonal antibodies to simian virus 5 and their use in revealing antigenic differences between human, canine and simian isolates. *J Gen Virol*. **68 (Pt 11)**, 2769–2780
161. Hanke, T., Szawlowski, P., and Randall, R. E. (1992) Construction of solid matrix-antibody-antigen complexes containing simian immunodeficiency virus p27 using tag-specific monoclonal antibody and tag-linked antigen. *J Gen Virol*. **73 (Pt 3)**, 653–660

162. Kroeze, W. K., Sassano, M. F., Huang, X. P., Lansu, K., McCorvy, J. D., Giguère, P. M., Sciaky, N., and Roth, B. L. (2015) PRESTO-Tango as an open-source resource for interrogation of the druggable human GPCRome. *Nat Struct Mol Biol*. **22**, 362–369
163. Laroche, G., and Giguère, P. M. (2019) Measurement of β-Arrestin Recruitment at GPCRs Using the Tango Assay. *Methods Mol Biol*. **1947**, 257–267
164. Zeghal, M., Laroche, G., and Giguère, P. M. (2020) Parallel Interrogation of β-Arrestin2 Recruitment for Ligand Screening on a GPCR-Wide Scale using PRESTO-Tango Assay. *J Vis Exp*. 10.3791/60823
165. Moutel, S., Bery, N., Bernard, V., Keller, L., Lemesre, E., De Marco, A., Ligat, L., Rain, J. C., Favre, G., Olichon, A., and Perez, F. (2016) NaLi-H1: A universal synthetic library of humanized nanobodies providing highly functional antibodies and intrabodies. *Elife*. 10.7554/ELIFE.16228
166. Fromont-Racine, M., Rain, J. C., and Legrain, P. (1997) Toward a functional analysis of the yeast genome through exhaustive two-hybrid screens. *Nat Genet*. **16**, 277–282
167. Bartel, P. L., and Fields, S. (1995) Analyzing protein-protein interactions using two-hybrid system. *Methods Enzymol*. **254**, 241–263
168. Miura, N., Miyamoto, K., Ohtani, Y., Yaginuma, K., Aburaya, S., Kitagawa, Y., Aoki, W., and Ueda, M. (2019) Domain swapping of complementarity-determining region in nanobodies produced by Pichia pastoris. *AMB Express*. 10.1186/S13568-019-0833-2
169. Mitchell, L. S., and Colwell, L. J. (2018) Analysis of nanobody paratopes reveals greater diversity than classical antibodies. *Protein Eng Des Sel*. **31**, 267–275
170. Zeghal, M., Laroche, G., Freitas, J. D., Wang, R., and Giguère, P. M. (2023) Profiling of basal and ligand-dependent GPCR activities by means of a polyvalent cell-based high-throughput platform. *Nat Commun*. 10.1038/S41467-023-39132-X
171. Nickolls, S. A., Humphreys, S., Clark, M., and McMurray, G. (2013) Co-expression of GRK2 reveals a novel conformational state of the μ-opioid receptor. *PLoS One*. 10.1371/JOURNAL.PONE.0083691
172. Culhane, K. J., Gupte, T. M., Madhugiri, I., Gadgil, C. J., and Sivaramakrishnan, S. (2022) Kinetic model of GPCR-G protein interactions reveals allokairic modulation of signaling. *Nat Commun*. 10.1038/S41467-022-28789-5
173. Drube, J., Haider, R. S., Matthees, E. S. F., Reichel, M., Zeiner, J., Fritzwanker, S., Ziegler, C., Barz, S., Klement, L., Filor, J., Weitzel, V., Kliewer, A., Miess-Tanneberg, E., Kostenis, E., Schulz, S., and Hoffmann, C. (2022) GPCR kinase knockout cells reveal the impact of individual GRKs on arrestin binding and GPCR regulation. *Nat Commun*. 10.1038/S41467-022-28152-8
174. Strathmann, M., Wilkie, T. M., and Simon, M. I. (1990) Alternative splicing produces transcripts encoding two forms of the alpha subunit of GTP-binding protein Go. *Proc Natl Acad Sci U S A*. **87**, 6477–6481
175. Tateyama, M., and Kubo, Y. (2018) Gi/o-coupled muscarinic receptors co-localize with GIRK channel for efficient channel activation. *PLoS One*. 10.1371/JOURNAL.PONE.0204447
176. Wagner, T. R., and Rothbauer, U. (2020) Nanobodies Right in the Middle: Intrabodies as Toolbox to Visualize and Modulate Antigens in the Living Cell. *Biomolecules*. **10**, 1–19

177. McMahon, C., Baier, A. S., Pascolutti, R., Wegrecki, M., Zheng, S., Ong, J. X., Erlandson, S. C., Hilger, D., Rasmussen, S. G. F., Ring, A. M., Manglik, A., and Kruse, A. C. (2018) Yeast surface display platform for rapid discovery of conformationally selective nanobodies. *Nat Struct Mol Biol*. **25**, 289–296
178. Sanchez, M. I., and Ting, A. Y. (2020) Directed evolution improves the catalytic efficiency of TEV protease. *Nat Methods*. **17**, 167–174
179. Jia, Y., Reboulet, J., Gillet, B., Hughes, S., Forcet, C., Tribollet, V., Hajj Sleiman, N., Kundlacz, C., Vanacker, J. M., Bleicher, F., and Merabet, S. (2023) A Live Cell Protein Complementation Assay for ORFeome-Wide Probing of Human HOX Interactomes. *Cells*. 10.3390/CELLS12010200